

UNIVERSITY OF CRETE
DEPARTMENT OF MATERIALS SCIENCE
AND TECHNOLOGY



“Design and study of peptide composite biomaterials”

PhD thesis:

Emmanouil Kasotakis

Supervisor: Assoc. Prof. Mitraki Anna

February 2012

Abstract

The present PhD thesis is focused on the ‘Design and study of peptide composite biomaterials’. Self-assembling peptides are supramolecular entities that spontaneously form from elementary building blocks, held together with non-covalent interactions. Introduction of biological self-assembly principles in the field of biomaterial and nanoscale engineering, is relatively recent and many avenues still remain to be explored. A major advantage in the assembly of biological materials is their self-assembly from building blocks, under non-aggressive conditions such as ambient temperatures and aqueous environments, and the good interface that exists between organic and inorganic phases. Another important feature in biological materials and especially proteins is the possibility of tailor-made modifications that can be enabled at the sequence level in order to confer functionalities on the self-assembled scaffolds. These modifications cover a wide range and can include change of amino acids, incorporation of non-natural amino acids, and chemical modifications.

The present thesis is focused on self-assembling octapeptides, made up from building blocks found in natural proteins. The aim of the project is to investigate minimal amino acid modifications for designing peptides that maintain their self-assembling ability intact and are able to anchor inorganic materials on their surface.

The first part focuses on templating silica on the surface of the fibrils and the role of serine (Ser (S)) residues is investigated in the templating of silica precursors. In the second part two-dimensional films are constructed and through thiolated peptides, quantum dot nanoparticles are deposited on the surface of the films. The third part reports the laser photocrosslinking of the formed assemblies, mediated by the introduction of crosslinkable aromatic residues. The final chapter focuses on a different self-assembling system and describes the synthesis of peptide-porphyrin hybrid materials with photoelectronic properties.

Overall the thesis reports how a single self-assembling building block can be modified by rational choice of amino acids in order to be targeted for different functionalities.

Περίληψη

Η παρούσα Διδακτορική Διατριβή εστιάζεται στην «Σύνθεση και μελέτη σύνθετων πεπτιδικών βιοϋλικών». Τα αυτο-οργανωμένα πεπτίδια είναι υπερμοριακές δομές οι οποίες αυτο-οργανώνονται αυθόρμητα από μικρούς ‘δομικούς λίθους’ οι οποίοι συνδέονται με μη ομοιοπολικές αλληλεπιδράσεις. Η εισαγωγή των αυτο-οργανωμένων βιολογικών αρχών στο πεδίο της μηχανικής των βιοϋλικών και της νανοδομής, είναι σχετικά πρόσφατη και πολλές κατευθύνσεις μένουν να μελετηθούν. Μεγάλο πλεονέκτημα στην οργάνωση των βιολογικών υλικών αποτελεί η αυτο-οργάνωση τους από ‘δομικούς λίθους’ υπό φυσιολογικές συνθήκες θερμοκρασίας και υδάτινου περιβάλλοντος καθώς επίσης και η ακριβής αλληλεπίδραση που υπάρχει μεταξύ οργανικών και ανόργανων φάσεων. Ένα πολύ σημαντικό χαρακτηριστικό στα βιολογικά υλικά και ειδικά στις πρωτεΐνες είναι η δυνατότητα της τροποποίησης τους σε επίπεδο αλληλουχίας με σκοπό την ενσωμάτωση λειτουργιών στις αυτο-οργανωμένες δομές. Αυτές οι αλλαγές καλύπτουν ένα μεγάλο εύρος και περιλαμβάνουν αλλαγές στα αμινοξέα, εισαγωγή μη-φυσικών αμινοξέων και χημικές τροποποιήσεις.

Η παρούσα διατριβή εστιάζει στην αυτο-οργάνωση οκτα-πεπτιδίων, κατασκευασμένα με ‘δομικούς λίθους’ που προέρχονται από φυσικές πρωτεΐνες. Σκοπός της εργασίας είναι να διερευνήσει τις ελάχιστες αμινοξικές αλλαγές που χρειάζονται για τον σχεδιασμό πεπτιδίων που κρατούν την ιδιότητα αυτό-οργάνωσης ανέπαφη και είναι ικανά να προσδέσουν ανόργανα υλικά στην επιφάνειά τους.

Το πρώτο μέρος της εργασίας στοχεύει στην πρόσδεση βιοπυριτίας στην επιφάνεια των ινών και επίσης διερευνείται ο ρόλος του κατάλοιπου της Σερίνης (Ser, S) στην πρόσδεση πυριτικών προδρόμων. Στο δεύτερο μέρος κατασκευάζονται υμένα δυο διαστάσεων και μέσω πεπτιδίων που περιέχουν θειόλες, γίνεται εναπόθεση κβαντικών νανοσωματιδίων στην επιφάνεια των υμενίων. Στο τρίτο μέρος γίνεται αναφορά στην διασύνδεση αυτο-οργανωμένων δομών μέσω πηγής φωτός Laser, διαμέσου εισαγωγής αρωματικών αμινοξέων. Στο τελευταίο μέρος περιγράφουμε ένα διαφορετικό αυτό-οργανωμένο σύστημα και μελετάμε την σύνθεση υβριδικών υλικών από πεπτίδια-πορφυρίνες με φωτοηλεκτρονικές ιδιότητες

Γενικά η μελέτη αναδεικνύει πως ένας αυτό-οργανώμενος δομικός λίθος με προεπιλεγμένη σειρά αμινοξέων μπορεί να στοχεύσει σε διαφορετικές λειτουργίες.

Acknowledgments

First and foremost, I need to thank my supervisor Assoc. Prof. Anna Mitraki, at the Materials Science and Technology Department, for her advice, support and encouragement not only to perform this dissertation but also to find the motivation and strength to complete it. She not only gave me all the freedom to travel, attend conferences and initiate collaborations in foreign laboratories but also taught me to perceive and correct my own mistakes and helped me to grow up as a scientist.

I wish to thank my three-member committee members Assoc. Prof. Electra Gizeli at the Biology Department and Assoc. Prof. George Kioseoglou at the Materials Science and Technology Department for their guidance throughout and their advice about my dissertation. I would also like to thank Dr. Maite Paternostre, Researcher at Commissariat à l'Energie Atomique (CEA, France), Assoc. Prof. Maria Vamvakaki the Materials Science Department, Dr. Alexandros Lappas, Principal Researcher, at the Institute of Electronic Structure & Laser, Foundation for Research & Technology – Hellas, and Assoc. Prof. Konstantinos Demadis at the Department of Chemistry, for accepting to be part of my thesis Committee.

I would like to thank the Department of Biology, the Department of Materials Science and Technology and the Institute of Electronic Structure & Laser Foundation for Research & Technology - Hellas for their hospitality and the freedom to carry out research at their facility.

Special thanks go to Assist. Prof. Maria Chatzinikolaidou, MSc Chrystalleni Hadjicharalambous, MSc Ariadni Prigipaki, MSc Konstantina Terzaki, Vaggelis Georgilis and Lia Anagnostopoulou for being very good friends and colleagues and for the endless fun at stressful times in the laboratory.

The support staff of the Electron Microscopy Facility “Vassilis Galanopoulos”, Alexandra Siakouli, Aleka Manousaki, Sevasti Papadogiorgaki and Stefanos Papadakis is warmly acknowledged for their expertise, help, and for teaching me the operation of Scanning Electron Microscope and Transmission Electron Microscope. I would also like to thank Professor Pantelis Trikalitis for spending a lot of time teaching me the use of the High Resolution Electron Microscope.

I also wish to thank my collaborators for their exchange of ideas, suggestions and very good working environment:

In the two-dimensional Quantum dot assembly study, Dr. Athanasia Kostopoulou and Dr. Miguel Spuch-Calvar at the IESL-FORTH, Professor Nikos Pelekanos and Dr. Rahul Jayaprakash at the Materials Science and Technology Department and Ms. Androulidaki Maria at the IESL-FORTH.

In the cross-linking of the self-assembling peptides study, Dr. Alexandros Selimis and MSc. Maria Sygletou at the IESL-FORTH.

In the hybrid peptide-porphyrin self-assembling study, Professor Athanasios Coutsolelos, Dr. Georgios Charalambidis, and Dr. Theodore Lazarides at the Department of Chemistry in the University of Crete.

In the Molecular Dynamics Simulation studies, Professor Georgios Archontis and Dr. Phanourios Tamamis at the Department of Physics of the University of Cyprus.

The accomplishment of this work would not be possible without the financial support of the European Commission (BeNatural project - NMP4-CT-2006-033256), coordinated by the University of Crete.

Special thanks to my colleagues and best friends Dr. Jana Alonso, Dr. Sergio Galan Bartual, Professor Mark J. van Raaij, Dr. Jaime Castillo-Leon, Professor Winnie Svendsen, Dr. Ioana Luciu, Dr. Georgina Kaklamani, Dr. Emmanouil Stratakis, Dr. Hara Simitzi, Dr. Maria Massaouti, Dr. Dimitra Achilleos, Dr. Maria Abrazi, Dr. George Dialynas, Dr. George Koutsodontis, Dr. Simos Tsintzos, Dr. Fotis Kalaitzakis, Dr. Raluka Buiculescu and Dr. Dinca Valentina for their scientific guidance, hospitality and for the fun moments together.

The friends that through all these years shared with me funny, lovely and cooking moments are: Ioanna, Nektarios, Nikos, Kostas, Manos, Giannis, Katerina, Noni, Lena, Maria, Maria-Cristina, Katrien, Tom, Belen, Isaac, Carmela, George, Alkistis, Stefania and Maria. Noni. Without your support and valuable efforts this work would not have been completed on time and I wish the very best to all of you.

Finally I would like to recognize the entrustment and love of my parents that support me all these years with their teaching, my brother George with his girlfriend Georgia and my sister Anna that we stay together as a family and we smile to all the good and difficult moments.

This PhD thesis is devoted to my grandmothers Aristea Melesanaki and Popi Kasotaki that passed away during the years of my thesis.

Table of Contents

CHAPTER 1 INTRODUCTION.....	14
1.1 Top Down – Bottom Up	14
1.2 Biological composite materials	17
CHAPTER 2 SELF-ASSEMBLY AND APPLICATIONS	19
2.1 Self-assembling peptides corresponding to natural sequences	19
2.2 Self-assembling peptides corresponding to non-natural sequences	21
2.3 Biological composite materials from self-assembled proteins/peptides and inorganic compounds	23
2.3.1 Natural self-assembling proteins	23
2.3.2 Self-assembling peptides	25
CHAPTER 3 ADENOVIRUS FIBER AS A SELF-ASSEMBLY SYSTEM	28
CHAPTER 4 RATIONALE OF THESIS PROJECT	34
CHAPTER 5 TECHNIQUES	36
5.1 Transmission Electron Microscopy (TEM)	36
5.2 Energy-Dispersive X-ray Spectroscopy (EDS)	38
5.3 Photoluminescence Spectroscopy (PL).....	39
5.4 Mass Spectrometry (MS) - Matrix-Assisted Laser Desorption – Ionization (MALDI)	40
5.5 Dityrosine formation through Laser-Induced Fluorescence (LIF)	41
5.6 Experimental contributions - collaborations	42
CHAPTER 6 SILICA NANOPARTICLE TEMPLATING BY THE SELF-ASSEMBLED PEPTIDE FIBRILS	43
6.1 Background and state of the art	43

6.1.1	Family of Silaffin proteins	43
6.1.2	Family of Silicatein proteins	45
6.1.3	De novo designed self-assembling peptides that template biosilica	47
6.2	Methodology	48
6.2.1	In vitro silification protocol	48
6.3	Results and Discussion	49
6.4	Conclusions	60
CHAPTER 7 2D SELF-ASSEMBLY OF PEPTIDE FIBRIL FILMS TEMPLATED WITH QUANTUM		
DOTS 63		
7.1	Background and state of the art	63
7.1.1	Synthesis of quantum dot nanoparticles	65
7.1.2	Core-shell Quantum dots	66
7.1.3	Templating of quantum dots on natural proteins.....	67
7.1.4	1D, 2D & 3D Assembly of quantum dots.....	68
7.2	Methodology	70
7.2.1	Peptide two dimensional (2D) film formation	70
7.2.2	Synthesis of TOPO-Capped CdSe/ZnS quantum dots.....	70
7.2.3	ZnS coating of the CdSe quantum dots.....	71
7.2.4	Templating of 2D self-assembled fibril films with Qdots	71
7.2.5	Transmission electron Microscopy (TEM) analysis	71
7.2.6	Optical characterization	72
7.3	Results and Discussion	73
7.4	Conclusions	83
CHAPTER 8 CROSS-LINKING OF SELF-ASSEMBLING PEPTIDES84		
8.1	Background and state of the art	84

8.2	Methodology	87
8.2.1	Stock solutions	87
8.2.2	Mass spectrometric analysis protocol	87
8.3	Results and Discussion	88
8.4	Conclusions	92
CHAPTER 9 HYBRID PEPTIDE-PORPHYRIN SELF-ASSEMBLING MATERIALS		93
9.1	Background and state of the art	93
9.2	Methodology	95
9.2.1	Peptide-porphyrin hybrids studied in methanol.....	97
9.2.2	Peptide controls studied in methanol.....	98
9.2.3	Peptide-porphyrin hybrids studied in THF	99
9.2.4	Peptide controls studied in THF	100
9.3	Results and Discussion	101
CHAPTER 10 GENERAL CONCLUSIONS AND OUTLOOK		110
CHAPTER 11 REFERENCES		112

List of Figures

Figure 1 a) Bottom up and b) Top down construction of materials (Smith et al., 2011)	15
Figure 2 a) Tobacco Mosaic Virus coat protein and its self-assembly structure, and b) Flagellin protein, structural characteristics (Schlick et al., 2005), (Erhardt et al., 2010)	16
Figure 3 Abalone shell internal organic and inorganic structure (Espinosa et al., 2009)	17
Figure 4 a) <i>Tethya aurantia</i> marine demosponge (Brutchev and Morse, 2008) b) Optical micrograph of sponge spicules c) Electron micrograph of one type of axial channel (Weaver and Morse, 2003).....	18
Figure 5 EAK16 self-assembling peptide cross beta structure (Zhang et al., 1993).....	19
Figure 6 Self-Assembly Mechanism of the diphenylalanine peptide into various structures.	20
Figure 7 Self-assembling pathway of the lanreotide peptide (Valery et al., 2003).....	22
Figure 8 MAX 1 Beta hairpin motif self-assembly pathway	23
Figure 9 a) Templating mechanism of silica on fd filamentous virus b) Optical image of the silica coated virus (Grelet et al., 2011).....	24
Figure 10 Nanowire fabrication from the diphenylalanine peptide nanotubes	25
Figure 11 Silica dynamic templating model of the lanreotide nanotubes (Pouget et al., 2007)	26
Figure 12 a) Templating of gold nanoparticles by laminated beta-sheet fibrils a) Peptide (VK) ₄ -VPPT-(KV) ₄ , b) Hierarchical self assembly c) Templating with gold nanoparticles (Lamm et al., 2008).....	27
Figure 13 a) Adenovirus structure b) Triple beta helix motif of adenovirus fiber shaft (the three polypeptide chains are symbolized with green, red and blue) c) Triple beta-spiral motif d) Adenovirus fiber shaft sequence – The consensus repeat sequences for proline and glycine containing repeats are shown at the bottom of the sequence; ϕ symbolizes hydrophobic residues and X any amino acid (van Raaij et al., 1999).....	28
Figure 14 Left: Position of the original building block in the triple beta helix motif of the fiber shaft structure – Right: Transmission Electron Microscopy image of the NSGATIG peptide fibrils (Negative staining).....	29
Figure 15 Parallel and anti parallel self-assembly model of 3 stranded peptide sheets at 300K. Hydrogen bonds are shown in white dashed lines (Tamamis et al., 2009).....	30
Figure 16 Schematic representation of the design logic of the peptides.....	31
Figure 17 Transmission Electron Micrographs of peptide fibrils incubated with metallic nanoparticles solutions (Kasotakis et al., 2009).....	32

Figure 18 Cartoon representation of the de novo designed peptides, endowed with new functionalities. Red triangles and green cylinders represent amino acid substitutions in the original building block sequence that are exposed on the surface of the fibrils	34
Figure 19 JEOL JEM-2100 Transmission Electron Microscope (JEOL)	36
Figure 20 (Left) Tungsten Filament, (Right) Single Crystal LaB ₆ filament (wikipedia).....	37
Figure 21 Left: Negative staining protocol, Right: Electron microscopy grid.....	38
Figure 22 Stains for Transmission Electron Microscopy.....	38
Figure 23 a) Photoluminescence Spectroscopy experimental setup b) Photoluminescence process.....	40
Figure 24 MALDI-TOF mass spectrometry (Biochemistry, Stryer).....	41
Figure 25 Experimental setup for the formation of Dityrosine.....	42
Figure 26 Transmission electron image of <i>Cylindrotheca fusiformis</i> diatom.....	43
Figure 27 Amino acid sequence of the nat-Sil1A protein (Kroger et al., 1999)	44
Figure 28 Hydrolysis rate of γ -glycidoxypopyltrialkoxysilane.....	45
Figure 29 Proposed TEOS polycondensation pathway from silicatein-enzyme active site....	46
Figure 30 Peptide sequence of the original building block: the positions of amino acid substitutions are marked in red.....	49
Figure 31 Negative staining of the NSGAITIG peptide fibrils.....	50
Figure 32 Peptide fibrils after in vitro silification for 15h. No negative staining was used, so the contrast afforded is only due to the silica nanoparticles. The NSGAITIG peptide fibrils nucleate the formation of silica particles on their surface (Scale bar: 100nm)	50
Figure 33 TEOS hydrolysis and formation of particles in the absence of peptides	51
Figure 34 Preformed silica particles in the absence of peptides	52
Figure 35 NSGAITIG peptide fibrils incubated with preformed silica particles.....	52
Figure 36 NSGAITIG peptide fibrils with silica particles derived from sodium silicate (without negative staining).....	53
Figure 37 TEM micrographs of the NSGAITIG peptide fibrils after the solution has been washed 3 times with water. No negative stain was used, so the contrast afforded is only due to the silica nanoparticles	54
Figure 38 a) NSGAITIG fibrils after incubating for 15 days in TEOS solution (Scale bar: 100nm). The diameter has increased from 23nm to 65nm as the in vitro silification continues. The inset in (a) shows the uniform size of the silica-coated fibrils. (Scale bar: 100nm). b) Silica nanotubes after calcination of fibers (Scale bar: 100nm).....	55
Figure 39 a) Area of EDS analysis of NSGAITIG peptide fibrils after incubating for 15 days with TEOS solution (Scale bar: 100nm). b) EDS analysis spectrum.....	55

Figure 40 (Left) The N-A-G-A-I-T-I-G peptide fibrils (Negative staining with Phosphotungstic acid 1%), (Right) In vitro silification for 15h. No negative staining was used, so the contrast afforded is only due to the silica nanoparticles (Scale bar: 300nm)	56
Figure 41 (Left) The Ac-N-S-G-A-I-T-I-G peptide fibrils (Negative staining with Phosphotungstic acid 1%), (Right) In vitro silification for 15h. No negative staining was used, so the contrast afforded is only due to the silica nanoparticles (Scale bar: 100nm)	57
Figure 42 Negative staining with Phosphotungstic acid 1% of (Left) the NCGAITIG and (right) the NTGAITIG peptide fibrils	57
Figure 43 Peptide fibrils after In vitro silification for 15h. No negative staining was used, so the contrast afforded is only due to the silica nanoparticles. (Left) The NCGAITIG and (Right) the NTGAITIG	58
Figure 44 (Left) Negative staining of ASGAITIG peptide fibrils and (Right) In vitro silification for 15h	59
Figure 45 (Left) Negative staining of FSGAITIG peptide fibrils and (Right) In vitro silification for 15h	59
Figure 46 (Left) Negative staining of HSGAITIG peptide fibrils and (Right) In vitro silification for 15h	59
Figure 47 Proposed catalytic pathway of TEOS, from self-assembling peptides. (inspired by the mechanism proposed by (Cha et al., 1999)	61
Figure 48 Silica templating proposed mechanism (inspired by the mechanism proposed by (Adamson et al., 2007)	61
Figure 49 Semiconductor nanoparticles as a function of their emission wavelength (Modified from (Medintz et al., 2005))	63
Figure 50 a) Energy gap of Semiconductor nanoparticle according to its size	64
Figure 51 a) Emission of six different quantum dots b) Fluorescent properties of the quantum dots according to their size (Medintz et al., 2005).	65
Figure 52 Synthesis of CdSe (TOPO capped) quantum dots (Klimov, 2003)	65
Figure 53 CdSe/ZnS quantum dots functionalized with Mercaptoacetic acid	66
Figure 54 Photoluminescence (PL) spectra of the CdSe/ZnS nanocrystals (At room temperature) with average diameter a) 2.6nm and b) 3.96nm	73
Figure 55 Transmission electron microscopy images of a) Peptide fibril film at the water/chloroform interface b) Closer magnification of the film. Upper left: Fast Fourier Transform analysis (FFT) of the parallel-stacked fibrils. Upper right: Magnified image showing the 2.8nm distance between the fibrils.	74
Figure 56 Schematic representation of the self-assembled fibril films templated with quantum dots.	75

Figure 57 Optical images, after the 24h incubation of the peptide fibril films with the Qdots, under UV light. In both images CS and NS peptide fibril films were incubated with a) Green and b) Red quantum dots.....	76
Figure 58 Transmission electron microscopy images of the control NS peptide a) with green Qdots and b) with red Qdots. No particular oriented arrangement was observed since the peptide is not attaching covalently the Qdots.....	77
Figure 59 Transmission electron microscopy images of the thiol containing CS peptide with green Qdots a) fibril film with oriented templating of the Qdots b) Low magnification image of the film c) Schematic representation of the Qdot average local structural arrangement templated by the fibril film.....	78
Figure 60 a) Distance between the between the centers of the Qdots perpendicular to the axis of the fibril and b) Distance between the centers of the Qdots along the axis of the fibril, for the green Qdots.....	78
Figure 61 Transmission electron microscopy images of the thiol containing “CS” peptide with red Qdots a) fibril film with oriented templating of the Qdots b) Low magnification image of the film c) Schematic representation of the Qdot average local structural arrangement templated by the fibril film.....	79
Figure 62 a) Distance between the between the centers of the Qdots perpendicular to the axis of the fibril and b) Distance between the centers of the Qdots along the axis of the fibril, for the red Qdots.....	80
Figure 63 Förster Resonance Energy Transfer process (http://www.ncl.ac.uk/bioimaging/techniques/fret/)	81
Figure 64 Photoluminescence experiments on the solid-state samples with a) Green and b) Red quantum dots. (Solid lines: Quantum dots, Dashed lines: Qdots with peptides, Dashed dot: Qdots on peptide film)	82
Figure 65 Dityrosine and Disulfide bridges (Yoburn et al., 2003).	84
Figure 66 a) Part of the tendon from adult dragonfly (<i>Zyxomma</i> sp.) c) Fluorescence of resilin in the tendon wing under white light and ultraviolet light b) Fluorescence of a molded rod with recombinant resilin protein under white light and d) ultraviolet light. 85	85
Figure 67 Dityrosine formation scheme: (1) Tyrosine and radical formation by UV (2) radical recombination (3) dityrosine isomerization and formation.....	86
Figure 68 Self-assembling peptide ribbons (Scale bar: 140nm)	88
Figure 69 Fluorescence spectrum of dityrosine formation in the peptide solution.....	89
Figure 70 Cuvettes under the UV microscope of a) irradiated peptide solution and b) irradiated water solution.....	89
Figure 71 Fluorescent spectrum of dityrosine formation in the tyrosine residue solution.....	90
Figure 72 Mass Spectrum of non-irradiated and irradiated peptide Scale: 400-1000.....	91
Figure 73 Mass Spectrum of non-irradiated and irradiated peptide Scale: 1400-1700.....	91

Figure 74 a) Hemoglobin b) Iron containing heme group c) Structure of the simplest porphyrin (http://legacy.owensboro.kctcs.edu/gcaplan/anat2/notes/APIINotes6%20Blood%20RBC.htm)	94
Figure 75 The five hybrid coupled derivatives: monoaminoporphyrin-FF-Boc (Boc-FF-P) (A), monoaminoporphyrin-FF-Fmoc (Fmoc-FF-P) (B), monoaminoporphyrin-F-Fmoc (Fmoc-F-P) (C), monoaminoporphyrin-FF (FF-P) (D) and monoaminoporphyrin-F (F-P) (E).....	96
Figure 76 Scanning electron microscopy analysis of the peptide-porphyrin conjugates (7mM concentration), prepared in 20% HFIP and 80% methanol and subsequent dried on glass slides after one day of incubation.....	97
Figure 77 Scanning electron microscopy analysis of the control peptides and the porphyrin molecule (7mM concentration), prepared in 20% HFIP and 80% methanol and subsequent dried on glass slides after one day of incubation. a) Boc-FF, b) Fmoc-FF, c) FF, d) Fmoc-F, e) Porphyrin molecule.....	98
Figure 78 Scanning electron microscopy analysis of the peptide-porphyrin conjugates (7mM concentration), prepared in 20% HFIP and 80% THF and subsequent dried on glass slides after one day of incubation. a) Boc-FF-P, b) Fmoc-FF-P, c) FF-P, d) Fmoc-F-P, e) F-P	99
Figure 79 Scanning electron microscopy analysis of the control peptides and porphyrin molecule, (7mM concentration), prepared in 20% HFIP and 80% THF and subsequent dried on glass slides after one day of incubation a) Boc-FF, b) Fmoc-FF, c) FF, d) Fmoc-F, e) Porphyrin molecule.....	100
Figure 80 High-Resolution TEM (HRTEM) of sections of the spheres embedded in resin. 101	

CHAPTER 1 INTRODUCTION

1.1 Top Down – Bottom Up

The field of science that is bridging the gap between Chemistry, Physics, Mathematics and Biology is Materials Science. Materials Science is an interdisciplinary field, which studies the fundamental properties of materials for applications in science and engineering. Since scientists investigate the structure from atomic or molecular to macroscopic scale there have been many branches of technology developed at the end of the 20th century. Around 1980 K. Eric Drexler described how conventional macro or micro machines could build even smaller ones with final target to build up machines at the level of molecules. He used as an example the biochemical systems, where those machines, such as ribosomes or bacterial flagella, already exist at such scale (Drexler, 1981). Later on in his book “Engines of Creation: The Coming Era of Nanotechnology”, he described a new type of technology composed of molecules, whose dimensions are in nanoscale, and it was named “Nanotechnology” (Drexler, 1986). His ideas were supported theoretically long time ago, at 1959, by the renowned physicist Richard Feynman, with the famous lecture “*There’s Plenty of room at the Bottom. An Invitation to Enter a New Field of Physics*”. Feynman mentioned in his talk that: “What I want to talk about is the problem of manipulating and controlling things on a small scale”. He described theoretically the problems and the challenges to develop the field of nanotechnology and also the benefits of manipulating molecules in the nanoworld such as the creation of nano machines, data storage, electron microscopy and fast computers (Gazit, 2007).

For starting building up machines, motors or more complex 3D scaffolds we have to understand “what are the basic units composing matter?” Biology and Biotechnology has contributed a lot in understanding the interactions of living matter and how Nature fabricates macromolecular structures using nanoscale “building block” molecules. The two new emerging Nanotechnology branches are Bionanotechnology and Nanobiotechnology. Bionanotechnology uses all the knowledge behind molecular recognition and assembly of building blocks in order to fabricate nanostructured materials and Nanobiotechnology uses nanostructured tools and principles for applications to biology. For mimicking Nature and constructing materials for the nanoworld there are two main approaches: Top-down and Bottom-up (Gazit, 2007).

Top-down approach uses various methods of modern and old lithography. Since the word lithography is coming from the Greek word Λιθογραφία (Lithografia), which contains the word “Λίθος” meaning “Stone” and “Γραφή” meaning “Writing”, top-down techniques require a bulk material that is scaled down from macro to nano dimensions (Figure 1). The most common used lithographic technique is Photolithography. This technique briefly requires our substrate, a photosensitive material (negative or positive), a pattern mask and UV radiation. The type of the photoresist and the mask give us the final pattern on the substrate. The disadvantages of this technique are the high cost of the equipment, the limited access to clean room facilities, required for the high quality of materials, the poor resolution below ~20nm and the low biocompatibility of these structures in biomedical applications.

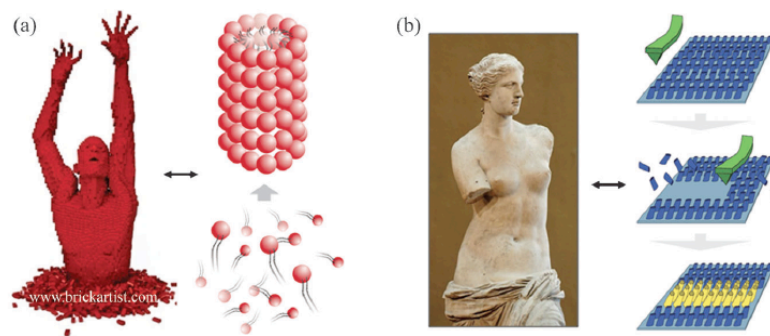


Figure 1 a) Bottom up and b) Top down construction of materials (Smith et al., 2011)

Bottom up process is developed mainly with self-assembly, the spontaneous association of biological “building blocks” into highly organized structures. Nature has developed the “Bottom-up” fabrication for millions of years using mainly as building blocks the 20 natural amino acids, nucleotides, lipid molecules and sugars. In molecular assembly the interactions are controlled by weak bonds such as a) hydrogen bonds, b) ionic bonds, c) van der Waals interactions, d) hydrophobic interactions and e) water mediated hydrogen bonds.

We have abundant examples of how nature uses the self-assembly process. Some examples are self-organization of viruses, phospholipid membranes, intracellular and extracellular fibrous assemblies, nucleic acids, biological motors, polysaccharides, amyloid fibrils and silks (Gazit, 2007).

Tobacco Mosaic Virus (TMV) is an RNA virus that its capsid looks like a hollow protein tube of 300x18nm in size and a 4nm-wide central channel (Figure 2a). The protein case is composed of ~2130 identical protein subunits that self-assemble into a helical motif

around the RNA (Schlick et al., 2005). The virus is stable in temperatures $\sim 60^{\circ}\text{C}$ and pH solutions ranging from 2-10. The wild-type TMV virion capsid offers a great templating surface through electrostatic interactions. The amino acids responsible for those interactions are arginine (Arg (R)), Lysine (Lys (K)), aspartic acid (Asp (D)) and glutamic acid (Glu (E)). Furthermore, novel types of interactions can be inserted through genetic engineering of the virion.

The flagellum exists in prokaryotic and eukaryotic cells and provides sensing and locomotion. The bacterial flagellum is composed from the protein flagellin. The size of the filament is 20nm in width and can reach $\sim 15\mu\text{m}$ in length (Figure 2b). The flagellin protein scaffold is composed of ~ 30.000 self-assembling subunits. Each subunit contains four domains D0, D1, D2 and D3. D2 and D3 domains are solvent exposed and can be used, through genetic engineering, for templating inorganic materials (Erhardt et al., 2010).

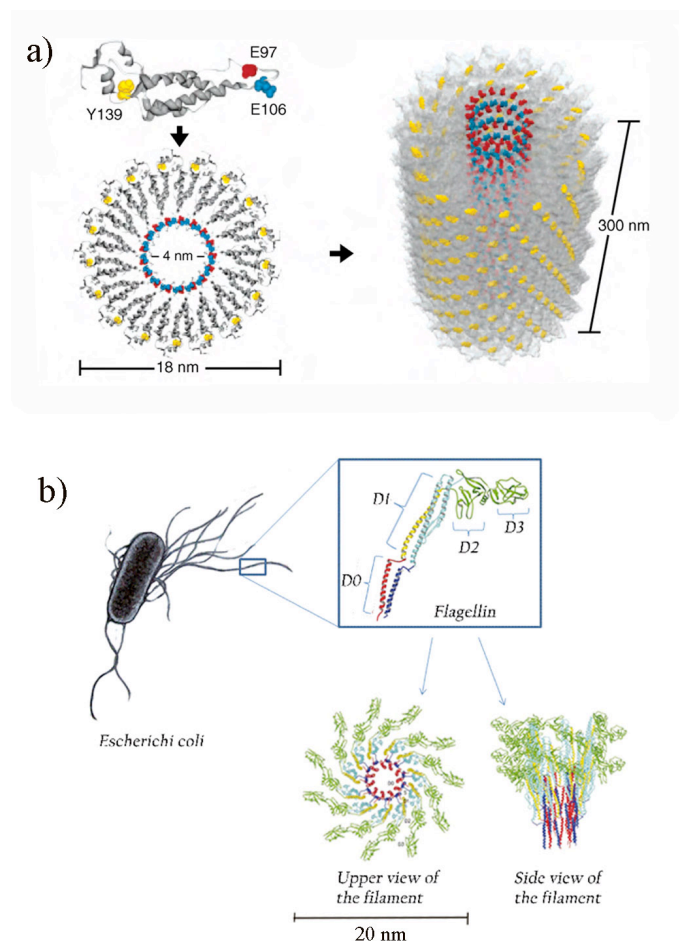


Figure 2 a) Tobacco Mosaic Virus coat protein and its self-assembly structure, and b) Flagellin protein, structural characteristics (Schlick et al., 2005), (Erhardt et al., 2010)

1.2 Biological composite materials

Nature provides numerous examples of materials, which combine the assembly of proteinaceous building blocks and inorganic materials. These materials adopt complex hierarchical structures ranging from nano- to macroscopic scale. Characteristic examples of these fascinating structures are Abalone shell and Marine sponges. The organic component, mainly proteins, is endowed with specific amino acids that promote chemical, hydrophobic and electrostatic interactions and acts as a template for the epitaxial organization of the mineral component; this organization results in strong and tough composite materials (Meyers et al., 2006).

Abalone shell or Nacre is a remarkable example of how nature can combine weak constituents for fabrication of high performance materials (Figure 3). Nacre contains the mineral phase, mainly aragonite (CaCO_3) at $\sim 95\%$ and protein biopolymers, intercalating between the building blocks at $\sim 5\%$. Nacre is 3000 times tougher than aragonite. The nacre structure is compared to “brick and mortar” which this gives the material its unique mechanical properties. The “bricks” are flat polygonal crystals of aragonite and the “mortar” is composed of polysaccharide and protein fibers. Inspired from its highly sophisticated structure that has evolved over millions of years we can design new synthetic composite materials (Espinosa et al., 2009).

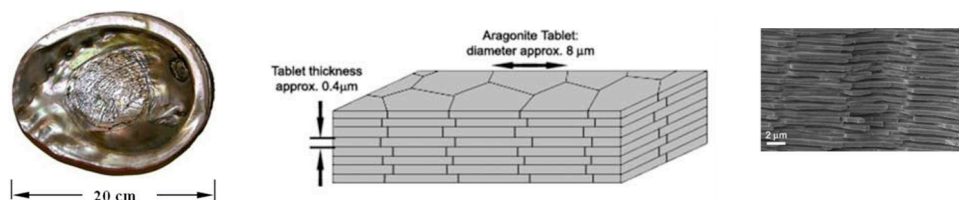


Figure 3 Abalone shell internal organic and inorganic structure (Espinosa et al., 2009)

Tethya aurantia, which belongs to the demosponges family, is an orange puffball sponge and its spicules (Figure 4a, b) have approximately $30\mu\text{m}$ in diameter and 2mm in length. They compose the 75% of the dry weight of the sponge. In situ identification and manipulation is easy and *Tethya aurantia* is a useful model of silicon biotechnology research. The axial channel (Figure 4c) of the spicule is composed of organic filament that consists of three closely related protein subunits silicatein α , β and γ (Shimizu et al., 1998). Natural and recombinant silicatein subunits have been found to catalyze the formation of biosilica from

various silica precursors such as Tetraethoxysilane (TEOS) (Cha et al., 1999). Silicatein has homology to the Serine-type proteases due to the presence of a “catalytic triad” and a strongly nucleophile Serine (Ser (S)) in the active site of the enzyme (Shimizu et al., 1998). Knowledge of the mechanisms of biomineralization can lead to nanofabrication of artificial building blocks that imitate similar biotemplating behavior.

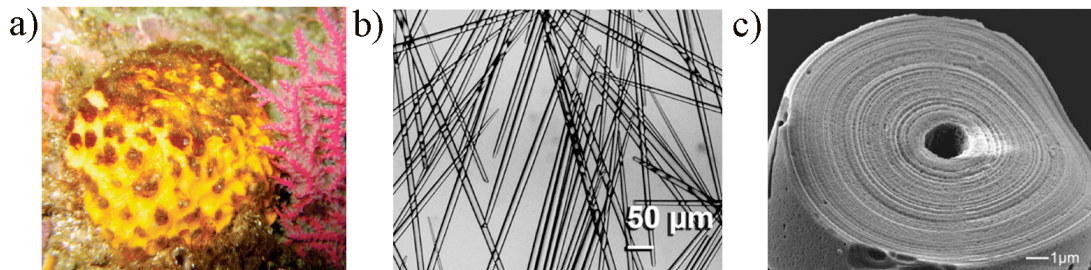


Figure 4 a) Tethya aurantia marine demosponge (Brutchey and Morse, 2008) b) Optical micrograph of sponge spicules c) Electron micrograph of one type of axial channel (Weaver and Morse, 2003)

CHAPTER 2 SELF-ASSEMBLY AND APPLICATIONS

2.1 Self-assembling peptides corresponding to natural sequences

The last two decades there are numerous discoveries of small proteins, or else peptides, that self-assemble into various structures such as belts, tapes, tubes, vesicles, fibrils or monolayers (Aggeli et al., 1997b) (Gazit, 2005; Toksoz and Guler, 2009; Zhang, 2003).

One of the pioneers for the discovery of self-assembling peptides was Shuguang Zhang (MIT) (Zhang et al., 1993). While working on genetics and structural biology of yeast, he serendipitously discovered that a fragment from the protein Zuotin, that binds left handed Z-DNA, can assembly into well-ordered beta-sheet structures.

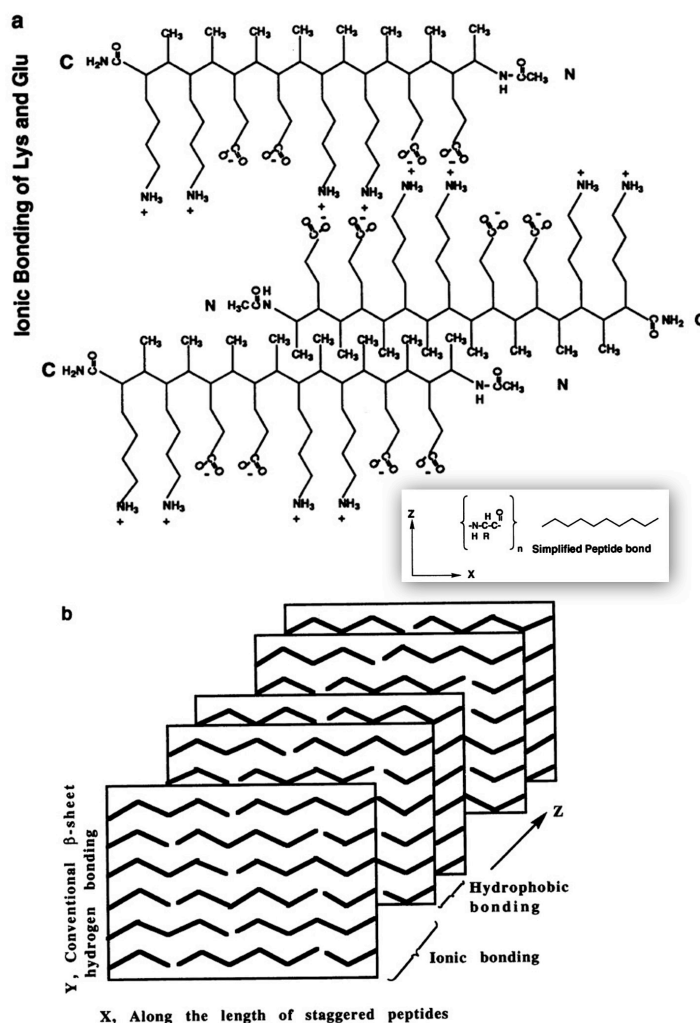


Figure 5 EAK16 self-assembling peptide cross beta structure (Zhang et al., 1993)

Named as peptide Lego®, the EAK16 peptide contains the repetitive motif of alternating hydrophilic and hydrophobic residues, where every other residue in the peptide is alanine (Ala (A)) (Ac-HN-Ala-Glu-Ala-Glu-Ala-Lys-Ala-Lys-Ala-Glu-Ala-Glu-Ala-Lys-Ala-Lys-CONH₂) (Figure 5). The peptide was shown to self assemble into cross-beta amyloid fibrils in aqueous solutions and when salt was added, the assembly was changed to a macroscopic membrane (Zhang et al., 1993). As shown in Figure 5 the alanine (Ala (A)) residues from one strand are interacting with the alanines of another strand via hydrophobic interactions. When the peptide is at neutral pH the lysine (Lys (K)) and glutamic acid (Glu (E)) residues are charged and interact via ionic bonds on the opposite side. Hydrophobic and ionic interactions alternate along the z-axis and the final “cross-beta” structure is formed, with beta-strands being perpendicular to the fibril axis. After this breakthrough, he followed a unique de novo design of a self-assembling peptide library (Zhang, 2002) using different types of self assembling peptides. These peptides can form various types of structures (Vesicles, tubes, fibrils, hydrogels) and the applications can range from tissue engineering to drug delivery and biological surface engineering (Zhao et al., 2010) (Yang et al., 2009).

Ehud Gazit (Tel-Aviv University) was investigating self-assembly mechanisms derived from the A β (1-42) peptide involved in Alzheimer’s disease. While studying smaller fragments of the A β (1-42) peptide, he discovered that a dipeptide composed of two phenylalanines (Phe-Phe (F-F)) can self assemble into rigid hollow nanotubes. This building block assembly is proposed to follow the π - π stacking interaction mechanism between the aromatic residues of the phenylalanines. This peptide depending on the environment can self-assemble into various structures, such as tubes, fibrils, and spheres as shown in Figure 6.

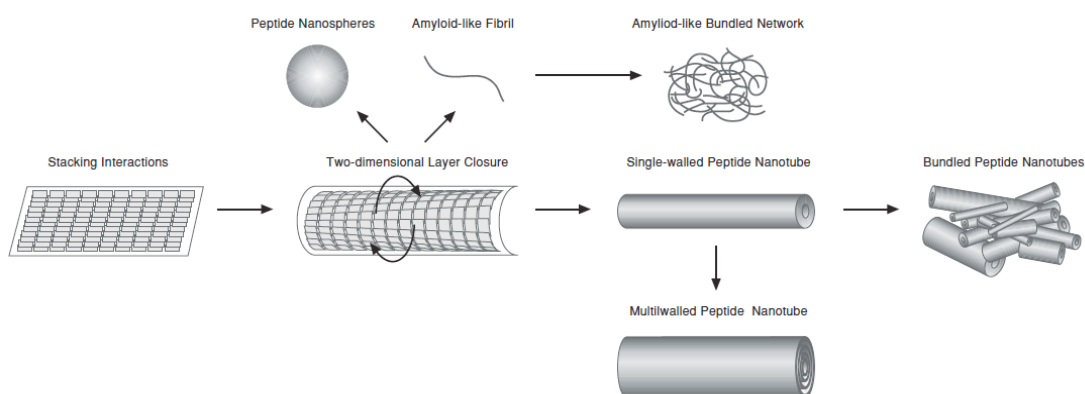


Figure 6 Self-Assembly Mechanism of the diphenylalanine peptide into various structures (Reches and Gazit, 2006)

Aggeli and colleagues were investigating a peptide originating from the transmembrane domain of IsK protein. The peptide has 24 amino acids (NH₂-Lys-Leu-Glu-Ala-Leu-Tyr-Val-Leu-GlyPhe-Phe-Gly-Phe-Phe-Thr-Leu-Gly-Ile-Met-Leu-Ser-Tyr-Ile-Arg-COOH, termed K24) and forms hydrogels. These hydrogels consist of peptide fibril tapes in beta-sheet conformation and this is mainly attributed to the amphiphilic character of the peptide. One end, polar amino acids exist (Lys (K), Glu (E)) and provide coulomb interactions and amphiphilicity to the molecule while aromatic residues (Tyr (Y), Phe (F)) provide intramolecular π - π interactions (Aggeli et al., 1997a). The design of a shorter new peptide, which is endowed with polar and hydrophobic residues (CH₃CO-Gln-Gln-Arg-Phe-Gln-Trp-Gln-Phe-Glu-Gln-Gln-NH₂, termed DN1), confirmed the prediction of beta-stranded structure and this peptide formed gels similar to K24 (Aggeli et al., 1997b). This design technique contributed to the de novo design of short peptides with self-assembling abilities and fascinating macromolecular structures.

2.2 Self-assembling peptides corresponding to non-natural sequences

Following the previous examples of self-assembling peptides originating from natural sequences, scientific groups moved on a new field, the “de novo” designed self-assembling peptides. In this field all the possible interactions and conformations are taken into account in order to construct a short peptide with a predicted structure of our need. A common used building block conformation in that of beta-hairpin. The beta-hairpin is a protein motif of 2 beta-strands, anti-parallel to each other, joined with a turn of two to five amino acids.

A remarkable de novo designed self-assembling peptide is coming from the pharmaceutical industry. The lanreotide cyclic peptide, which is used as a synthetic analogue of somatostatin, a hormone inhibitor for treatment of acromegaly, has been studied extensively from Artzner, Paternostre and colleagues. This peptide (NH₂-(D)Naph-Cys-Tyr-(D)Trp-Lys-Val-Cys-Thr-CONH₂) follows the folding motif of beta-hairpin and the beta strands are stabilized by a disulphide bridge. Figure 7 shows extensively the levels of the peptide assembly and packing for the final formation of hexagonally packed nanotubes. Figure 7a shows the disulphide bridge and the hydrogen bonds between the residues. According to the molecular models there is clear separation of the aromatic (red color), aliphatic (blue color) and hydrophilic residues (green color). The combination of dimers (Figure 7b) makes filaments with hydrophilic inner and outer surface, stabilized with

hydrogen bonds and hydrophobic interactions. 26 filaments are packed together to form the nanotube (Figure 7c) and finally the nanotubes are arranged hexagonally to form a liquid crystalline columnar phase structure (Figure 7d) (Valery et al., 2003).

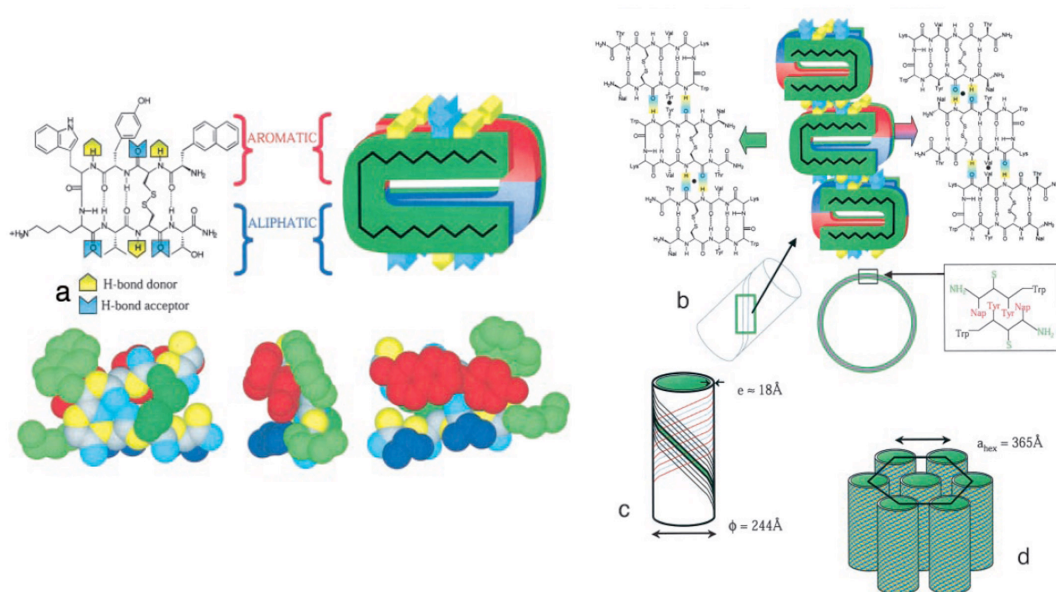


Figure 7 Self-assembling pathway of the lanreotide peptide (Valery et al., 2003)

Schneider and colleagues adopted also the beta-hairpin motif to construct self-assembling peptides. The synthetic peptide termed MAX 1 ($\text{H}_2\text{N-Val-Lys-Val-Lys-Val-Lys-Val-Lys-Val-}^{\text{D}}\text{Pro-Pro-Thr-Lys-Val-Lys-Val-Lys-Val-Lys-Val-CONH}_2$). The design strategy behind is divided into two parts: The composition of alternating polar (Lys (K)) and non polar (Val (V)) amino acids helps in the adoption of beta-sheet conformation and the tetrapeptide turn (Val-^DPro-Pro-Thr) helps in the formation of the beta turn. The D- and L-proline are used because they do not induce steric interference between each other (Bean et al., 1992). These two important parameters contribute to the formation of the final beta-hairpin structure (Figure 8). The alteration of polar and non-polar residues allows the peptide to self-assemble only in controlled pH environment. As shown in Figure 8, at basic pH environment the lysine residues are not charged, hydrogen bonds are formed in the hairpin structure and the peptide adopts a beta-sheet conformation. Valine residues interact via hydrophobic forces with the adjacent peptides. When the pH is reduced to acidic the lysine residues are charged and are being repulsed, so the peptide loses its beta-structure. These alterations in the structure have been monitored by Circular Dichroism and Rheology studies. The peptide forms responsive hydrogels useful for drug delivery and biomedical applications (Schneider et al., 2002).

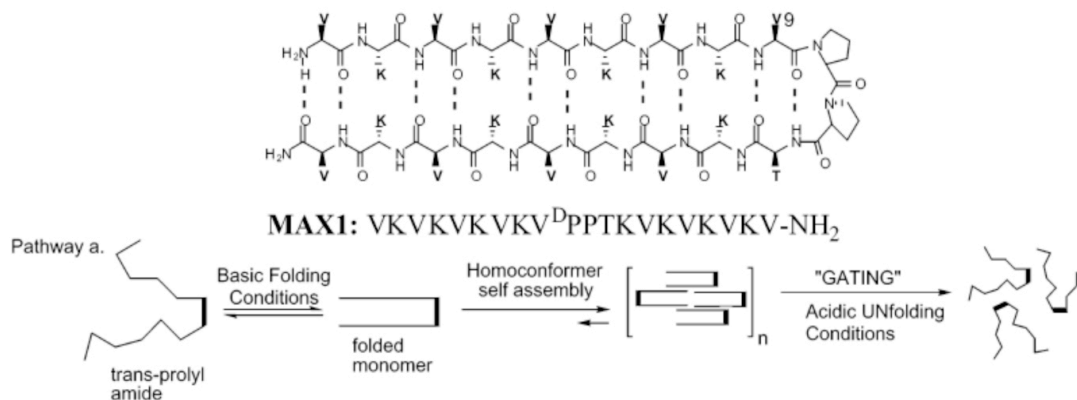


Figure 8 MAX 1 Beta hairpin motif self-assembly pathway
(Schneider et al., 2002)

2.3 Biological composite materials from self-assembled proteins/peptides and inorganic compounds

2.3.1 Natural self-assembling proteins

“Bottom up” approaches provide many advantages such as rational design and synthesis of new peptide building blocks and controlled assembly below the limits of the conventional lithographic techniques. The new challenge is how to template those highly ordered nanostructures with inorganic materials (Dickerson et al., 2008) (Chen and Rosi, 2010). Following the literature of templating natural self-assembling proteins we distinguish the examples of filamentous viruses (TMV, *fd*) and bacterial flagella protein, flagellin.

The tubular capsid surface of Tobacco Mosaic Virus (TMV) is rich in glutamic acid (Glu (E)), aspartic acid (Asp (D)), lysine (Lys (K)) and arginine (Arg, (R)) residues. The combination of these charges gives an overall negative charge above the isoelectric point (pI 3.0-3.5) and a positive below. The isoelectric point of silicic acid is around pI=2.1 (Minones et al., 1984) so the templating can be performed between those values via electrostatic forces (Shenton et al., 1999) (Royston et al., 2006). Similar method is followed for the deposition of silica on the filamentous DNA *fd* virus. The pI of the virus is 4.2 so when the reaction pI is around 3 electrostatic interactions can occur between the positively charged virus and the negative silica precursors (Figure 9) (Grelet et al., 2011).

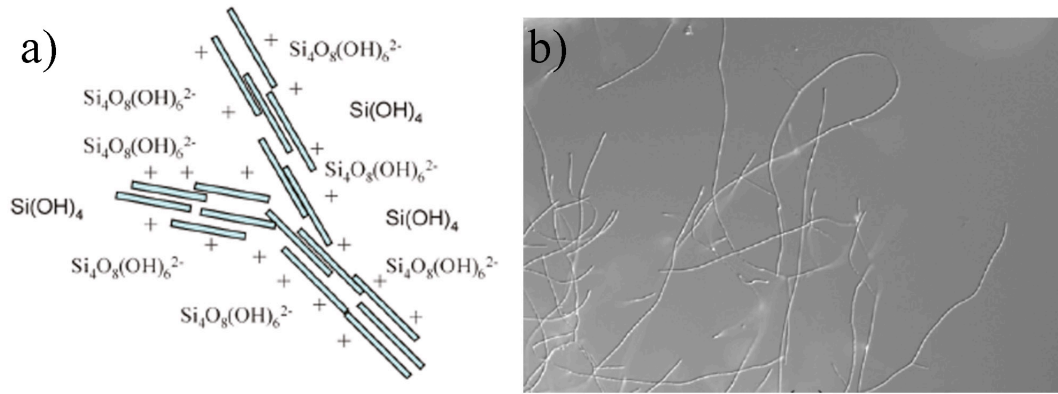


Figure 9 a) Templating mechanism of silica on fd filamentous virus b) Optical image of the silica coated virus (Grelet et al., 2011)

Shenton et al reported the templating of the Tobacco Mosaic Virus (TMV) with lead sulfide (PbS) and cadmium sulfide (CdS) crystallites through the numerous glutamic acid (Glu (E)) and aspartic acid (Asp (D)) residues exposed on the surface of the TMV virion (Shenton et al., 1999).

Harris reported the insertion of thiol groups (through cysteine (Cys (C))), using genetic engineering, on the TMV surface. These modifications seemed not to play a significant role in the assembly and stability of the virus. These genetically modified scaffolds were used for the deposition of gold (Au), silver (Ag) and palladium (Pd) nanoparticles and creation of metallic biocomposite nanowires (Lee et al., 2005).

From various bacterial flagella the mostly investigated is *E.coli* flagellin protein, FliTrx. As mentioned previously, the protein that composes the self-assembled structure contains two domains (D2 and D3), which are solvent exposed, and through genetic engineering modifications different functional residues can be displayed on the surface of the flagellum. A loop peptide, which is composed of four times the peptide “Gly-His-His-His-His-His (GHHHHHH)”, has been investigated for the templating of gold (Au), Cu (copper), Co (Cobalt), Pd (Palladium) and Cd (Cadmium) nanoparticles (Kumara et al., 2007b). The same year Kumara reported the templating of ZnS/Mn and cadmium telluride (CdTe) quantum dots on the surface of bacterial flagella nanotubes carrying the same poly-histidine loop (Kumara et al., 2007a). Another loop which exposes one time the peptide “Arg-Lys-Arg-Lys-Arg-Lys-Arg (RKRKRKR)” is used as a template for gold (Au) nanoparticles and the final peptide with three times repeat of the sequence “His-Asp-Glu-

Asp-Glu-Asp-Glu (HDEDEDE) binds successfully cobalt (Co) and silver (Ag) nanoparticles (Kumara et al., 2007b).

2.3.2 Self-assembling peptides

Templating of self-assembling peptides is a very challenging and interesting method for the fabrication of biological composite materials because it gives us the possibility to endow simple building blocks both with functional and structural characteristics. Some paradigms of assembly and templating are given below, focusing on the previously discussed self-assembling peptides.

Following the complete study of the self-assembling mechanism, Ehud Gazit's group decided to focus on applications by creating a peptide library of minor substitutions and changes to the original building block in order to endow the structure with different functionalities. The original building block itself can be used as mold for casting metallic silver and creating silver nanowires with dimensions of ~20nm (Figure 10) (Reches and Gazit, 2003). Gazit moved one step further to the fabrication of coaxial metal/insulator/metal nanowires. After introducing a thiol linker peptide to the original diphenylalanine peptide nanotubes, the tubes were templated inside with silver nanoparticles as described above and outside with gold nanoparticles that were attached to the thiol groups. (Carney et al., 2006). This remarkable application opens new routes for the fabrication of coaxial metallic nanowires for future integration into microelectronic devices.

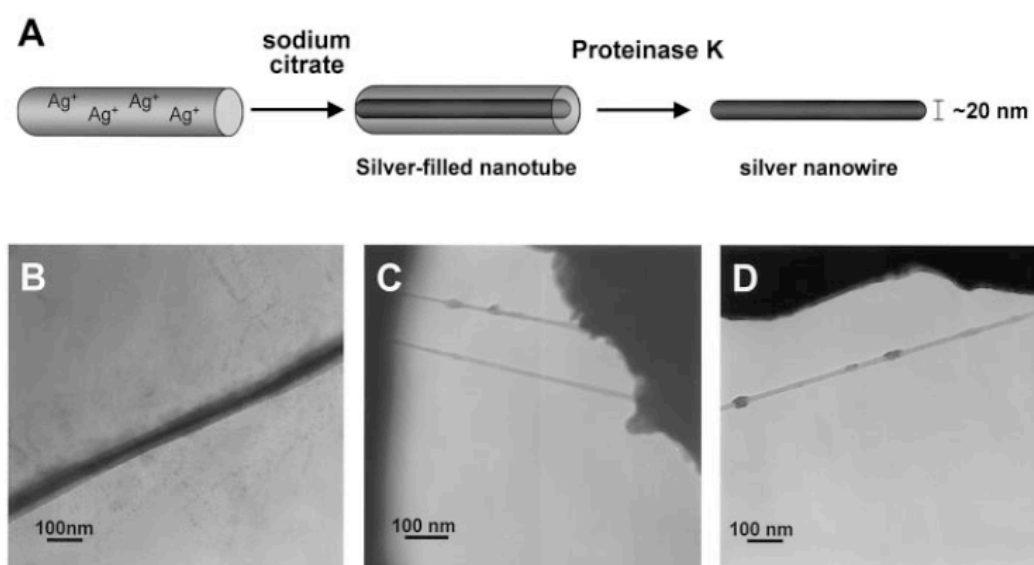


Figure 10 Nanowire fabrication from the diphenylalanine peptide nanotubes (Reches and Gazit, 2003)

Artzner and colleagues focused on the templating of the lanreotide nanotubes with silica. Upon incubation with silica precursors double-walled silica nanotubes were observed. The mechanism that is proposed is a “dynamic template model” in which the surface of the lanreotide nanotube is positively charged and attracts the negatively charged hydrolysed silica precursors through electrostatic interactions; at the same time, the negatively charged precursors attract free lanreotide molecules for the neutralization of the system (Figure 11) (Pouget et al., 2007). This mechanism can be used for the explanation of templating in other biological systems and can be exploited further for the synthesis of composite biomaterials.

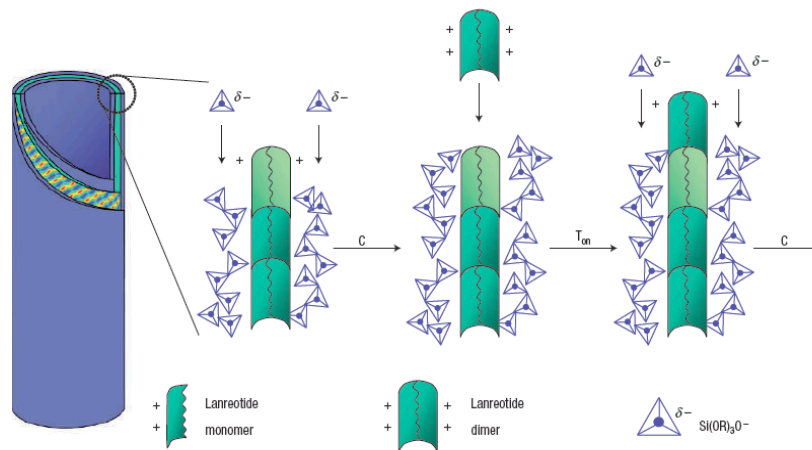


Figure 11 Silica dynamic templating model of the lanreotide nanotubes (Pouget et al., 2007)

Schneider and colleagues investigated the precise arrangement of nanoparticles between the self-assembling structures of the MAX1 peptide variant. In contrast with the original Max1 peptide sequence the newly designed peptide has the two prolines, located in the beta turn, both in L-conformation. The ^LPro-^LPro instead of ^DPro-^LPro changes completely the assembly pathway. The peptide has now the tendency to adopt an extended conformation and assembles into laminated beta-sheet fibrils instead of beta-hairpins. After the structural characterization the ribbon-like structures were templated with gold nanoparticles through a bifunctional linker. The mercaptopropionate (MPA) attaches to the gold particles through a gold-sulfur bond (Au-S) and to the peptide with its negatively charged carboxyl group in aqueous solution (Figure 12) (Lamm et al., 2008).

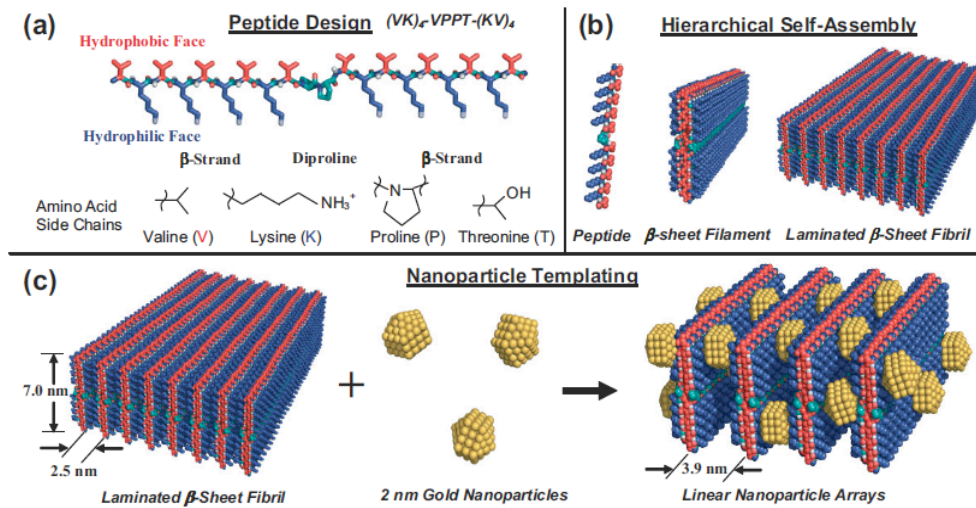


Figure 12 a) Templating of gold nanoparticles by laminated beta-sheet fibrils a) Peptide $(VK)_4VPPT-(KV)_4$, b) Hierarchical self assembly c) Templating with gold nanoparticles (Lamm et al., 2008)

CHAPTER 3 ADENOVIRUS FIBER AS A SELF-ASSEMBLY SYSTEM

The work presented in this thesis is oriented towards the design and study of self-assembled octa-peptides for the synthesis of composite biomaterials. For better understanding the mechanisms of protein folding several studies have been carried out in models such as smaller de novo designed peptides derived from natural self-assembled proteins. The adenovirus fiber protein served as a source of inspiration for the study. The adenovirus capsid is icosahedral and at each of the 12 vertices, trimeric fibers point out, used for attachment with cells (Figure 13a, b). The crystal structure of the fiber shaft and head domain was solved at 2.4 Å resolution (van Raaij et al., 1999). Each fiber monomer contains 582 amino acids. In the shaft we can clearly see that there is a repeating sequence motif with hydrophobic amino acids (orange and green residues at Figure 13d) alternating with hydrophilic ones and glycine (Gly (G)) or proline (Pro (P)) at conserved positions (purple residues at Figure 13d). The basic repeat fold contains a beta-strand almost parallel to the axis of the fiber followed by a beta turn and another beta strand which runs at an angle of 45° relative to the fiber axis.

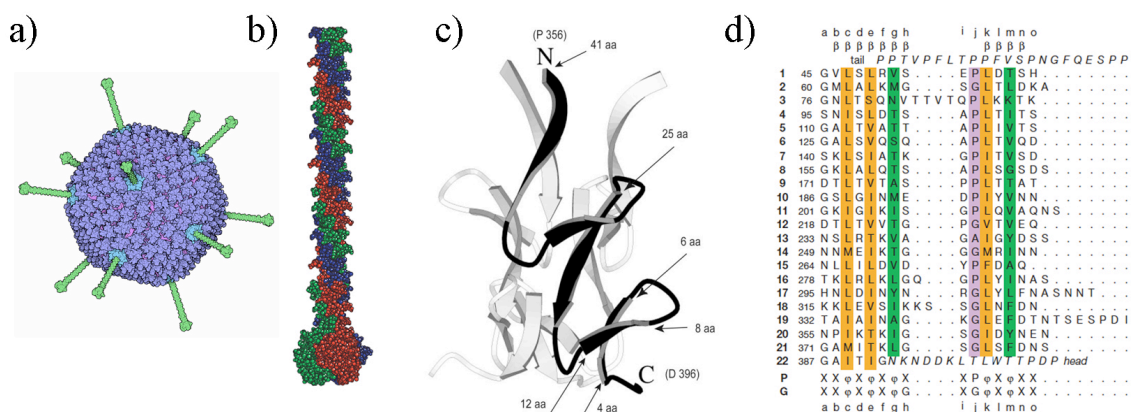


Figure 13 a) Adenovirus structure b) Triple beta helix motif of adenovirus fiber shaft (the three polypeptide chains are symbolized with green, red and blue) c) Triple beta-spiral motif d) Adenovirus fiber shaft sequence – The consensus repeat sequences for proline and glycine containing repeats are shown at the bottom of the sequence; φ symbolizes hydrophobic residues and X any amino acid (van Raaij et al., 1999)

The repeats are joined together by a solvent accessible loop. The inter-repeat displacement is 13Å with a clockwise rotation (50°) between the repeats. The core of the structure is stabilized by the contribution of hydrophobic interactions between the hydrophobic amino acids (van Raaij et al., 1999).

The folding motif of the shaft was extensively studied with peptides lacking the head part of the shaft. Various lengths of peptides from 41aa, 25aa, 12aa, 8aa and 6aa were synthesized and shown to self assemble into stable fibrillar morphologies (Luckey et al., 2000), (Papanikolopoulou et al., 2005). The fibrils showed green birefringence upon staining with Congo red and had the amyloid –like morphology when studied with electron microscopy. The fibrils were also characterized by X-ray fiber diffraction and showed a characteristic amyloid like X-ray diffraction pattern (Papanikolopoulou et al., 2005). This pattern is called cross-beta; it shows a strong meridional reflection at 4.8Å that corresponds to the hydrogen bonding distance between beta-strands and an equatorial reflection at 10-11Å that corresponds to the stacking distance between beta-sheets (Serpell and Smith, 2000).

We have chosen the octapeptide N-S-G-A-I-T-I-G (residues 385-392, Asparagine-Serine-Glycine-Alanine-Isoleucine-Threonine-Isoleucine-Glycine) as the original building block for this study. This peptide corresponds to a region in the adenovirus protein sequence, which involves a loop and a β-strand (Figure 14 left). The peptide self-assembles into amyloid -type fibrils with dimensions of 10nm in width and some microns in length (Figure 14 right). The peptide was characterized with Transmission Electron Microscopy (TEM), Atomic Force Microscopy (AFM) and X-ray fiber diffraction.

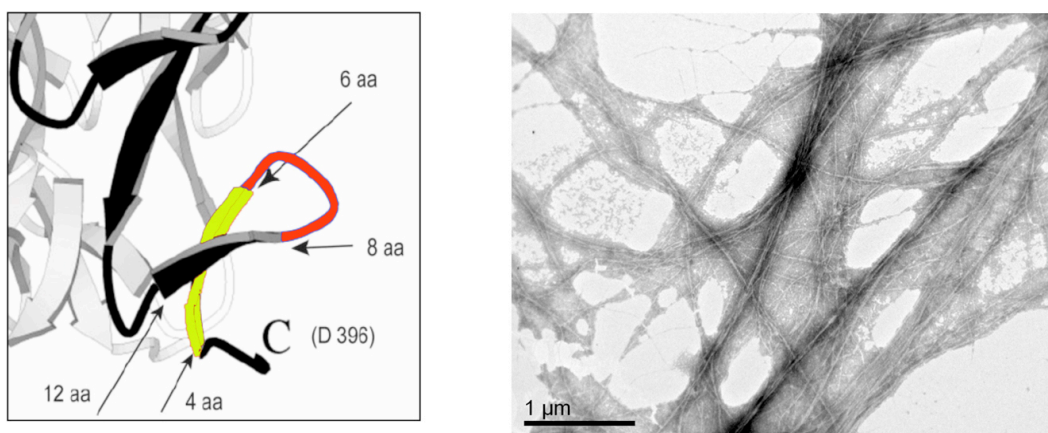


Figure 14 Left: Position of the original building block in the triple beta helix motif of the fiber shaft structure – Right: Transmission Electron Microscopy image of the NSGATIG peptide fibrils (Negative staining)

Very important tool for the design of new self-assembling peptides and their enrichment with functional groups is the crystal structure of the peptide in its final assembled conformation. According to the crystal structure of the native protein the N-S-G residues are located at the loop and the A-I-T-I-G residues at the beta-strand. Since it is difficult to crystalize the amyloid fibrils the only technique for the analysis of structure is X-ray fiber diffraction. This technique gives us the distances between the peptides along the axis of the fibril but not the exact position of the exposed or hidden residues. This is the reason that Molecular Dynamics Simulations (MDS) were performed in order to understand how the peptides are arranged along the fibril. The MDS conditions were carried out in aqueous solutions containing multiple copies of the peptide; they were run at different temperatures (replica-exchange method) and using the solvent as a continuous medium (implicit solvent). The simulations showed that the part of the peptide responsible for the cross beta amyloid core was formed by the A-I-T-I (Ala-Ile-Thr-Ile) hydrophobic moiety (Figure 15). This part adopts a beta-strand conformation and the N-S part (Asn1-Ser2), which remains out of the fibril core, forms a type-II turn. The peptides were shown to prefer a parallel arrangement along the axis of the fibril (Tamamis et al., 2009).

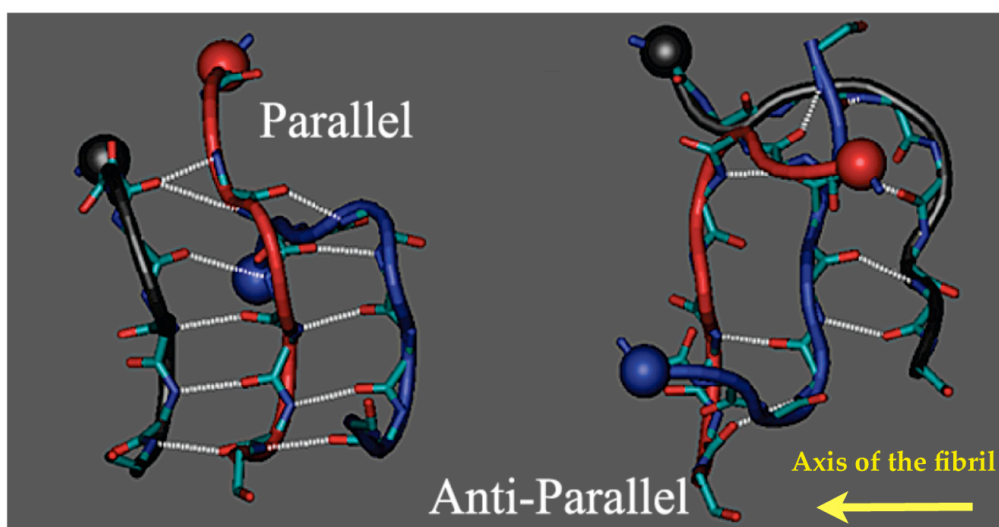


Figure 15 Parallel and anti parallel self-assembly model of 3 stranded peptide sheets at 300K. Hydrogen bonds are shown in white dashed lines (Tamamis et al., 2009).

In the Master thesis “Design and study of composite biomaterials based on self-assembling peptides from natural fibrous proteins” (2008), we investigated the design and structural characterization of new self-assembling peptides, which form amyloid type fibrils and were used as templates for metal binding and nanowire fabrication.

In order to endow the new designed peptides with metal binding affinity we decided to incorporate cysteine (Cys (C)) in the sequence of the original building blocks at positions 1 (Asn (N)) and/or 2 (Ser (S)), since cysteine is the most common metal binding amino acid. A peptide library was created for studying first the capability of the new rationally designed peptides to form self-assembling peptides, and second, the interactions with inorganic matter.

We started by replacing the serine (Ser (S)) residue from the original building block sequence NSGAITIG to a cysteine residue since this is the minimal one to try. The new peptide sequence was NCGAITIG. In case that there would be accessibility problems for the thiol group of cysteines the two first amino acids of the new peptide were swapped, to give the peptide CNGAITIG. Finally we substituted the asparagine for a cysteine at the original NSGAITIG scaffold and the resulting peptide was CSGAITIG (Figure 16). All peptides self assemble into amyloid type fibrils and were thoroughly characterized with Transmission Electron Microscopy (TEM), Atomic Force Microscopy (AFM) and X-ray fiber diffraction.

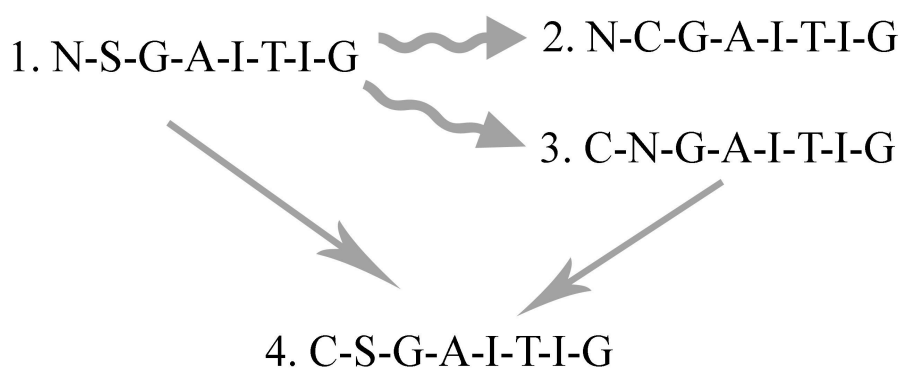


Figure 16 Schematic representation of the design logic of the peptides

The metal binding ability of the peptides was tested using three different metal colloidal nanoparticles: silver, gold and platinum. As shown in Figure 17 the NSGAITIG peptide showed affinity only for gold and platinum and very low binding to silver; the NCGAITIG peptide as well as the CNGAITIG peptide showed affinity to all metals and this proved that the cysteine residues must be accessible at the outside of the amyloid fibril core in order to serve as nucleation sites for the metals. To our surprise, the NSGAITIG peptide even though it lacks the cysteine residue, binds gold and platinum colloidal particles very well. This result was quite puzzling; however recent studies suggest that peptides with hydroxyl-containing amino acids show high affinity for metals. In literature there are various peptides, which contain Serine (Ser (S)) or Threonine (Thr, (T)) in their sequence and show

affinity to gold and silver nanoparticles (Chiang et al., 2007). These findings are supported theoretically by the work of Corni and colleagues. They studied theoretically the role of Serine (Ser (S)) and Tyrosine (Tyr (Y)) amino acids in the reduction of chloroaurate (III) (AuCl_4^-) ions. The hydroxyl group attaches to the gold ion, substituting one Cl^- , and the new complexes are more thermodynamically favorable in the ionized form of $\text{AuCl}_3-\text{Ser-O}^-$ and $\text{AuCl}_3-\text{Tyr-O}^-$. The two complexes show further probability for gold reduction, with higher rates for the $\text{AuCl}_3-\text{Tyr-O}^-$ complex (Toroz and Corni, 2011).

Therefore, in order to test the hypothesis that the serine (Ser (S)) residue might be responsible for the metal binding we designed the NAGAITIG peptide with a minimal substitution of the serine (Ser (S)) to alanine (Ala (A)). The experimental results indeed confirmed that the NAGAITIG peptide self-assembles into amyloid fibrils that do not bind gold (Kasotakis et al., 2009).

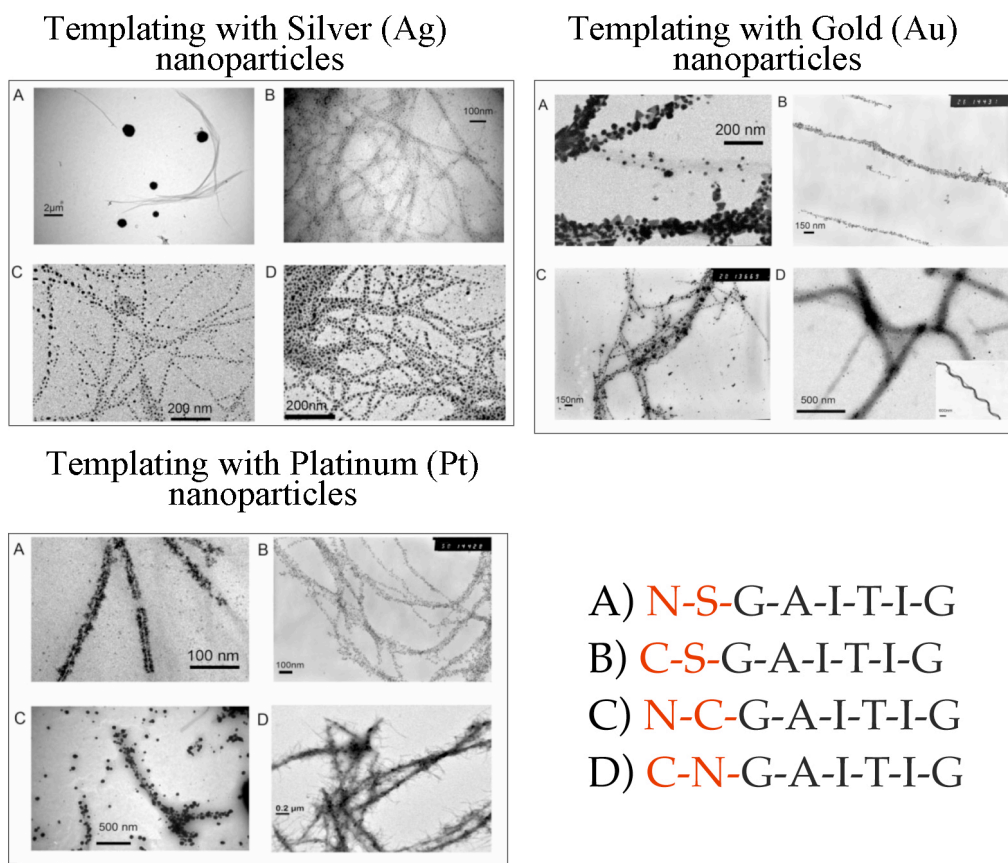


Figure 17 Transmission Electron Micrographs of peptide fibrils incubated with metallic nanoparticles solutions (Kasotakis et al., 2009)

The hypothesis of the contribution of serine (Ser (S)) to binding to metals is corroborated by the fact that in the CSGAITIG peptide continuous metal coverage of the amyloid fibril is observed. This can be attributed to the simultaneous presence of two adjacent metal nucleating sites provided by both the cysteine and serine (Ser (S)) residues.

CHAPTER 4 RATIONALE OF THESIS PROJECT

The aim of this PhD project is to investigate and develop a minimal self-assembling peptide system that will be able to change functionality with minor amino acid substitutions while keeping its self-assembling ability intact. The original system that will be used and modified is the adenovirus derived self-assembling octapeptide NSGAIIG.

According to the model presented in Figure 18, this self-assembly system will have an amino acid sequence “core” responsible for the scaffold formation (blue color) and each time the design for the desired functionality will be done at the exposed residues of the scaffold (red, green color). A functionality that has already been incorporated is the introduction of thiol containing residues for the metallic nanoparticles attachment and the direct positioning of the amyloid fibrils. These functions could also be combined for creating higher macromolecular architectures.

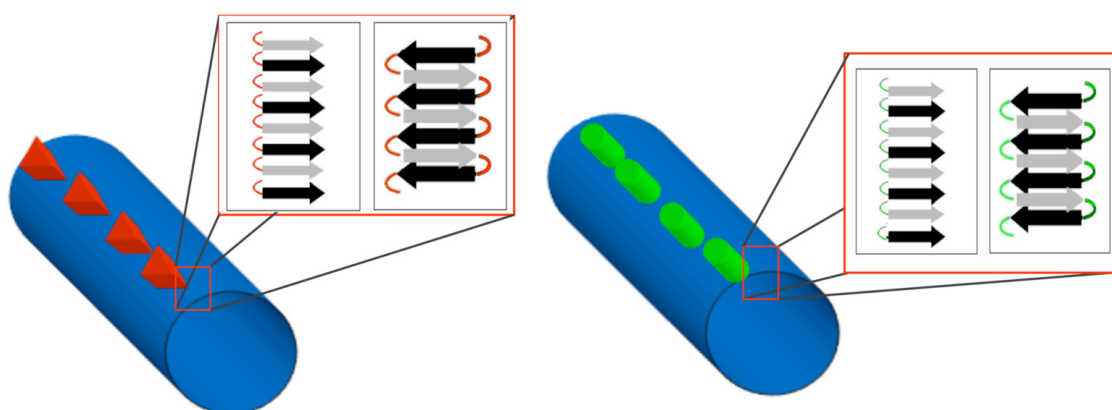


Figure 18 Cartoon representation of the de novo designed peptides, endowed with new functionalities. Red triangles and green cylinders represent amino acid substitutions in the original building block sequence that are exposed on the surface of the fibrils

The thesis is structured into three main chapters that are dealing with amino acid substitutions on the original building block sequence, their self-assembling ability study and the examination of the targeted functionality.

The first part (CHAPTER 6) of this work focuses on the ability of the original building block (NSGAIIG) and derivatives to template silica. The objective was to investigate the eventual role of the serine (Ser (S)) residue in the templating, as well as the fabrication of silica nanotubes through templating and subsequent removal of the biological

materials. Transmission Electron Microscopy (TEM) and Energy-dispersive X-ray spectroscopy (EDS) were the techniques used for our investigation.

The second part (CHAPTER 7) reports on formation of two-dimensional peptide films in the water/chloroform interface and their subsequent templating with preformed TOPO- capped CdSe/ZnS Quantum dots. The peptides used are the previously studied CSGAITIG that contains a thiol for specific attachment to the quantum dots, and the original building block NSGAIIG as a negative control. Transmission Electron Microscopy (TEM), and Photoluminescence (PL) reveal the fabrication of highly ordered arrays of quantum dots on the two dimensional films and the changes in the photoluminescent properties of the quantum dots depending on their size.

The third part (CHAPTER 8) reports on the formation of cross-linked amyloid fibril networks using a UV LASER source. The peptide used is a new derivative of the original building block that contains a tyrosine (Tyr (Y)) residue. The peptide is able to self-assemble into amyloid type ribbons and form cross-links through the dityrosine bond formation using the UV radiation as an energy source for the beginning of the reaction. The samples were analyzed using Mass Spectrometry (MS), Matrix-Assisted Laser Desorption Ionization (MALDI) and optical microscopy. Such a cross-linking material can be used in biomedical applications.

Finally, in the fourth part (CHAPTER 9) another commercially available self-assembling system is used for the fabrication of hybrid materials with photoelectronic properties. The self-assembling system in the diphenylalanine peptide mentioned in the introduction, and its derivatives, which was covalently conjugated with porphyrin molecules. The self-assembly of this system was tested in various concentrations and solvents. To our surprise the diphenylalanine-porphyrin hybrids do not self-assemble into nanotubes and form nanospheres of various sizes depending on the solvent. The samples were analyzed using Scanning Electron Microscopy (SEM) and Photoluminescence (PL). These materials can be proposed for the fabrication of new type of solar cells.

CHAPTER 5 TECHNIQUES

5.1 Transmission Electron Microscopy (TEM)

Transmission Electron Microscopy (TEM) is a powerful technique for imaging materials at the resolution of atoms. The first electron microscope was built by Knoll & Ruska at 1931 and it became commercially available at 1939. Since then there is an exponential evolution on the power and the resolution that microscopes can reach. Nowadays electron microscopy is used for polymers, inorganic materials and biological proteins or tissues. The most important part of this experimental technique is the sample preparation. Each class of materials requires different techniques in order to make the material thin and transparent but also electron dense for imaging in TEM. Biological materials since they are transparent, they require additional contrast, which is provided by specific stains described below. Looking closer to the microscope setup, it consists of an electron source, the electromagnetic lenses, the specimen area and the viewing screen (Figure 19). The electromagnetic lenses in combination with apertures are used to guide the electron beam in order to be coherent and give us the best resolution that we can have.

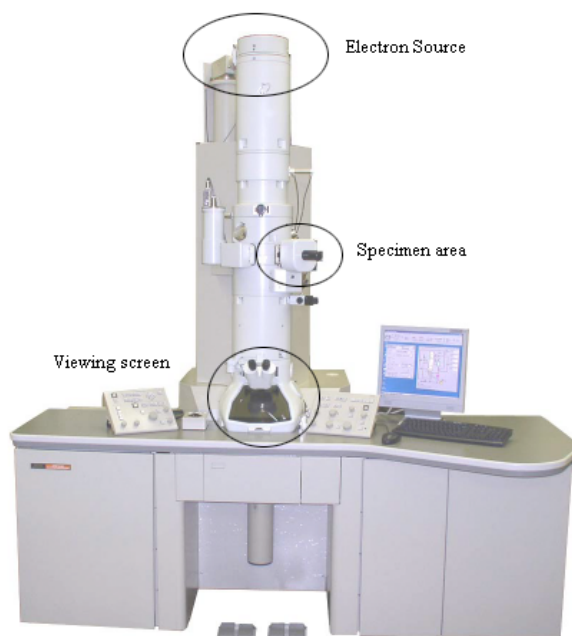


Figure 19 JEOL JEM-2100 Transmission Electron Microscope (JEOL)

Also the electron source plays a very important role for the quality of image that we obtain. The electrons are generated through thermionic emission from a filament, usually tungsten or a single crystal such as Lanthanum Hexaboride LaB_6 (Figure 20). The image that is generated from LaB_6 crystal is almost 10 times brighter than the image we get from tungsten and the life of the filament is 4 times more ($\sim 400\text{-}600\text{hr}$).

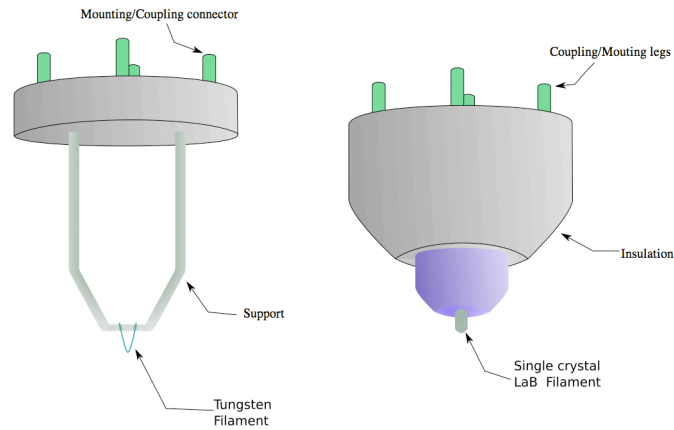


Figure 20 (Left) Tungsten Filament, (Right) Single Crystal LaB_6 filament (wikipedia)

The electrons are accelerated using high voltage, usually 80kV . After the beam passes through the sample is collected again with electromagnetic lenses and it is guided to a fluorescent screen. Modern technologies have introduced high quality cameras for real time observation on computers and high quality pictures.

Biological samples comparing to the inorganic ones are easier to perform and require less time and effort. Our sample is usually on a grid, which is made from copper or nickel and is covered with a very thin film of formvar or carbon membrane, which keeps the sample in place (Figure 21 right). The grid has 300 areas of observation of approximately $60 \times 60 \mu\text{m}$ area. In order to observe biological samples specific staining techniques are required to improve the contrast of the samples, since biological samples are transparent. This method is called negative staining; a heavy metal solution such as Uranyl acetate is embedded on the grid with the sample, in order to be deposited around the molecule or structure and provide contrast for better visualization (Figure 21 left).

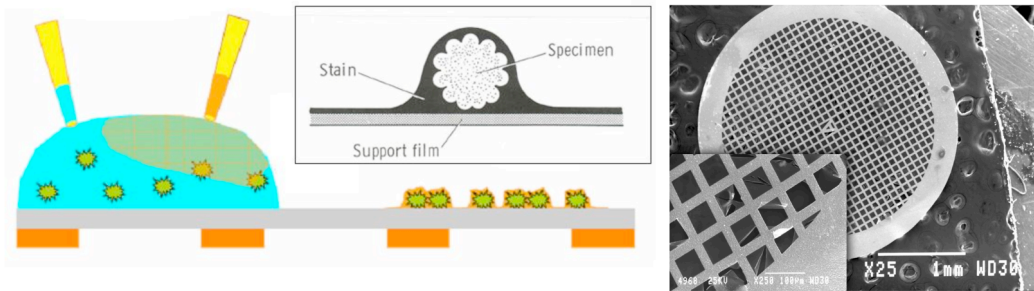


Figure 21 Left: Negative staining protocol, Right: Electron microscopy grid

The negative staining protocol usually depends on the pH of the sample. The Figure 22 below summarizes the stains used according to the pH we have.

Stain	Normal pH range for use
Sodium phosphotungstate (PTA)	5-8
Uranyl acetate	4-6
Sodium silicotungstate	5-8
Ammonium molybdate	5-7
Methylamine tungstate	6-7

Figure 22 Stains for Transmission Electron Microscopy

5.2 Energy-Dispersive X-ray Spectroscopy (EDS)

In this technique X-rays are not used for structure determination but for elemental analysis. When the sample contains information of various types of particles the elemental identity cannot be proved with imaging techniques. EDS analysis can be used to certify the existence of certain elements. The principle is based on the unique atomic structure of each element and the specific interaction between each one and the beam of X-rays. EDS is applied when TEM analysis is performed and focusing on the sample we can get information in detail. The X-ray beam is focused on the desired area and is causing excitation of some electrons that are located in the inner energy shells of the atoms. Then an electron from outer shells is filling the gap and the difference in energy is released as X-ray. All these X-rays are characteristic of each transition and of each atomic structure that they are emitted from. The

setup is composed from the source of the X-ray beam, the X-ray detector, the pulse processor and the analyzer. The pulse processor is measuring the outcoming signal and transfers it to the analyzer which most of the times is connected to a computer for real time measurement.

5.3 Photoluminescence Spectroscopy (PL)

Photoluminescence spectroscopy is a useful method for studying the electronic structure of materials. The technique is causing no damage to the sample and the materials can be retrieved back easily from their dry or liquid state. Semiconductor materials are mostly investigated for the determination of their energy band gap; however impurity levels and defect detection can be studied as well as recombination mechanisms and material quality.

According to Figure 23b the energy difference between the valence band and the conduction band is called energy band gap (E_g). The basis of this method can be described as follows: Photons of energy greater than the band gap energy are directed to the sample, they are absorbed and raise an electron from the valence band up to the conduction band across the forbidden energy gap. This process is called photo-excitation. The electron loses part of the energy under nonradiative relaxation upon arriving to the conduction band and finally falls back to the valence band, converting the energy into a luminescent photon, which is emitted from the material. Thus the energy of the emitted photon is a direct measure of the band gap energy, E_g . The process of photon excitation followed by photon emission is called photoluminescence.

Figure 23a shows the experimental setup where light, generated in various wavelengths, is focused on the sample and the radiation is absorbed. The photo excitation of the electronic structure and the relaxation process is followed by the emission of photons of specific energy and wavelength. Through collection lenses the information is analyzed by a detector. We usually record the Intensity of the photons (counts) versus the wavelength (λ , nm).

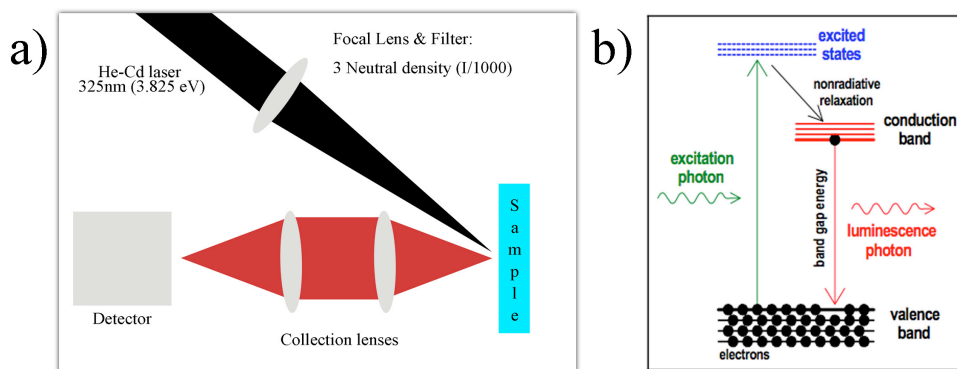


Figure 23 a) Photoluminescence Spectroscopy experimental setup
 b) Photoluminescence process

5.4 Mass Spectrometry (MS) - Matrix-Assisted Laser Desorption – Ionization (MALDI)

The MALDI technique is an analytical technique of Mass spectrometry. Biomolecules and large organic molecules can be analyzed with this technique. It is based on the following protocol. The sample (e.g. protein) is deposited in a specific matrix solution, which is composed of crystallized molecules and solvents that allow the sample to dissolve. Since the solvents evaporate the sample is co-crystallized with the matrix. This step is very important for the quality of the Mass spectrum. The sample is applied on a metallic plate and is ionized by applying a laser beam. After the generation of ions, an electric field is applied in order to accelerate the ions. They travel through the “flight tube” and depending on their mass they travel to the detector in different times (Figure 24). The Time of Flight (TOF) is the measure of mass of the sample.

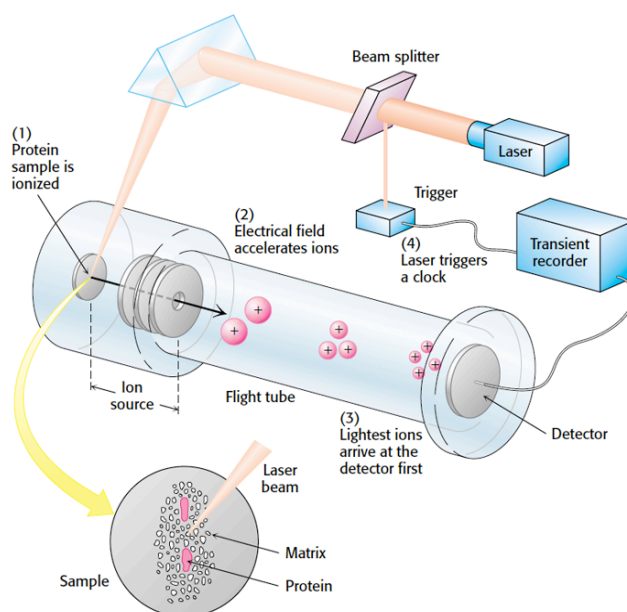


Figure 24 MALDI-TOF mass spectrometry (Biochemistry, Stryer)

5.5 Dityrosine formation through Laser-Induced Fluorescence (LIF)

Laser-induced fluorescence (LIF) is a spectroscopic method for the analysis of the structures of molecules, detection of certain chemical reactions and real time visualization of reactions. This method uses two pulses, a strong pump and a weak probe. The pump pulse excites our sample and triggers the process under investigation. A second delayed pulse, the probe, monitors the reaction products formed.

One way to form covalent crosslinking between two tyrosines (Dityrosine) is using Ultraviolet laser radiation (Giulivi et al., 2003). In our experiment the “pumping” is realized with a nanosecond excimer laser KrF UV excimer Laser (25ns) operating at 248nm. The beam is guided through mirrors to a quartz cuvette, where the sample is deposited. Irradiation is performed at ambient atmosphere. The output fluence of the “pump” beam was $F_{pump} \sim 64 \text{ mJ cm}^{-2}$. The probe fluence was $F_{probe} \sim 5 \text{ mJ cm}^{-2}$. Both laser beams are focused perpendicularly onto the sample. The induced emission is collected by an optical fiber oriented nearly perpendicularly to the sample, at $\sim 2 \text{ cm}$ away from its surface. It is spectrally analyzed in a spectrograph and the spectrum is recorded on an ICCD camera interfaced to a computer. Cut-off filters ($>290\text{nm}$) are used for blocking any probe beam scattered light (Figure 25) (Bounos et al., 2006).

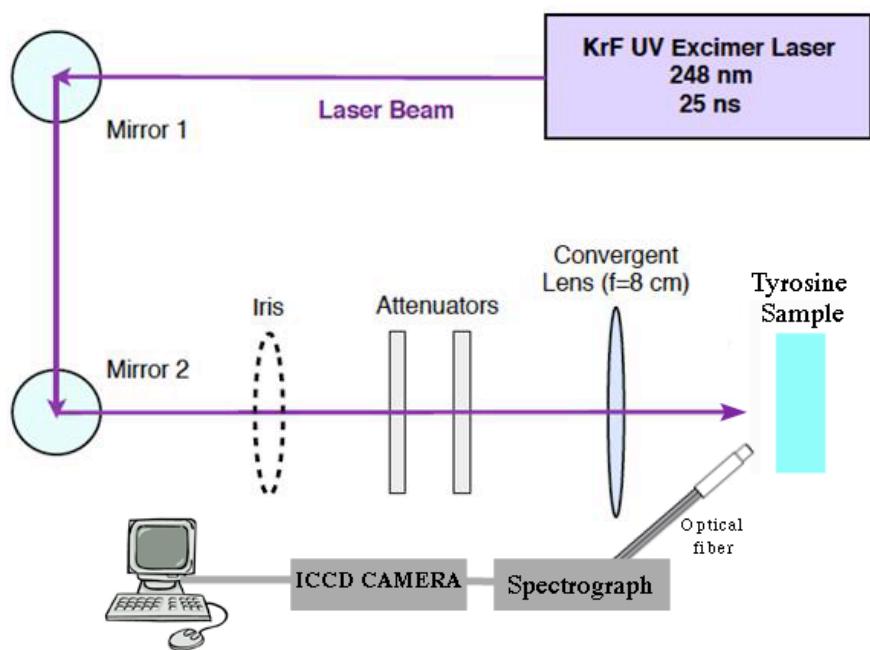


Figure 25 Experimental setup for the formation of Dityrosine

5.6 Experimental contributions - collaborations

Fast Fourier Transform analysis and modeling of Qdot 2D arrangement templated on peptide films was performed by PhD student Athanasia Kostopoulou, in Dr. Alexandros Lappas laboratory, at IESL-FORTH in Heraklion, Crete. Dr. Miguel Spuch synthesized the quantum dots during his post-doc in Dr. Alexandros Lappas laboratory. Atomic absorption spectroscopy measurements were performed by Dr. M. Mitraka at the University of Thessaloniki, Department of Chemical Engineering.

Photoluminescence spectroscopy was performed in the Microelectronics Research Group of IESL-FORTH based at the Department of Physics, under the scientific and technical assistance of Professor Nikos Pelekanos, Dr. Rahul Jayaprakash and Dr. Maria Androulidaki.

LIF experiments were performed at IESL-FORTH in Heraklion, Crete, under the scientific and technical assistance of Dr. Alexandros Selimis and MSc. Maria Sygletou. Mass Spectrometry was performed by Dr. Jana Alonso in the Proteomics Unit-Fundación IDICHUS, Hospital Clínico Universitario de Santiago de Compostela,

Molecular dynamics simulations were performed by Dr. Phanourios Tamamis and Prof. Georgios Archontis from the Department of Physics at the University of Cyprus.

CHAPTER 6 SILICA NANOPARTICLE

TEMPLATING BY THE SELF-ASSEMBLED

PEPTIDE FIBRILS

6.1 Background and state of the art

Biogenic oxides and especially silica is one of the most investigated minerals in nature. Earth's crust is composed of almost 30% from Silicon and it is rarely found as a single element. It is usually in its stable form of silicon dioxide SiO_2 or metal silicates. Industrial chemical synthesis of silica-based materials requires extreme conditions (temperature, pH, pressure) (Foo et al., 2004) and does not possess close analogies to the biosilification synthesis in Nature. There has been an extensive literature on the isolation and study of the proteins and peptides that are involved in biosilica formation. The proteins function under ambient temperatures, pressures and at neutral pH. However there are reports that biosilification can also occur at pH ~ 5.4 (Kroger et al., 2000). The organisms that contain those proteins are the frustules of diatoms and the spicules of marine sponges.

6.1.1 Family of Silaffin proteins

Diatoms are types of phytoplankton and belong to the group of algae. They are unicellular organisms and each cell is surrounded by a cell wall called frustule. This cell wall is composed of amorphous silica (SiO_2). The frustule provides access and protection from the environment. Diatoms have been studied extensively because the process of controlled silica formation and deposition was enigmatic. *Cylindrotheca fusiformis* has been a good model of study (Figure 26).

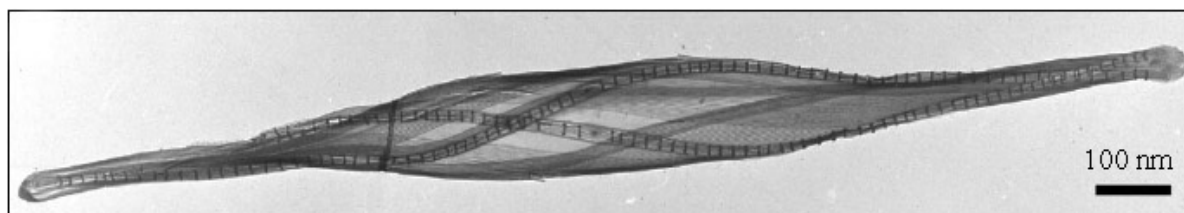


Figure 26 Transmission electron image of *Cylindrotheca fusiformis* diatom
(Kroger et al., 1999)

Three families of proteins were identified in the *C. fusiformis* cell wall: frustulins, pleuralins and silaffins (Foo et al., 2004). The silaffins are mainly three proteins: natSil-1A, natSil-1B and natSil-2. The gene, *sill*, which encodes the polypeptide that contains the previously mentioned proteins has been analyzed and it was found to contain seven repeated sequences, termed R1-R7 (shown in Figure 27).

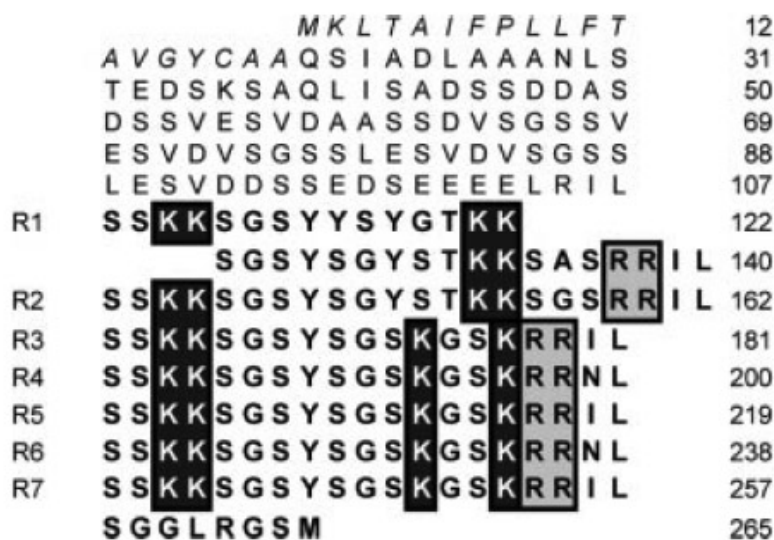


Figure 27 Amino acid sequence of the nat-Sil1A protein (Kroger et al., 1999)

The R3-R7 region corresponds to the silaffin precursor natSil-1A. Kroger and Sumper, following the difficult but successful extraction of silaffins from the organic matrix, proved that they contain many post-translationally modified lysine and serine (Ser (S)) residues (Kroger et al., 1999) (Kroger et al., 2002). They showed that the post-translationally modified protein has silica precipitation activity (condensating of an orthosilicic acid precursor) even around pH 4 whereas a synthetic part of the protein (the R5 peptide corresponding to the amino acids shown in Figure 27) without any modified residues showed silica-precipitating activity only above pH=7 (Kroger et al., 1999). Stone and colleagues further showed that the synthetic peptide based on the R5 region of the Sil1 protein catalyzes silica formation from Tetramethoxysilane (TMOS) and creates remarkable morphologies of silica particles at the nanoscale (Naik et al., 2003). Knecht and Wright studied a series of peptides based on the R5 peptide (H₂N-SSKKSGSYSGSKGSKRRIL-CO₂H) and suggested that the C-terminus RRIL motif serves as an organizing element that enables the formation of a supramolecular assembly of peptides creating locally a high concentration of amine - containing residues that promote *in vitro* silica precipitation (Knecht and Wright, 2003). The

same group reported the formation of TiO₂ particles from the non-natural precursor Titanium (IV) bis(ammonium lactato)-dihydroxide (TBALDH) and the role of R5 peptide variants in particle formation (Sewell and Wright, 2006).

6.1.2 Family of Silicatein proteins

Apart from the silaffin templating mechanism, which is mediated by the electrostatic interactions between the polycationic amino acids and the negatively charged precursors, there is another catalytic mechanism originating from proteins found in the spicules of marine sponges. Their axial filament consists of a family of proteins, named silicateins. The silicatein structure is homologous to the human cysteine protease, Cathepsin-L (Shimizu et al., 1998). In the silicatein structure there is a site that contains a catalytic triad composed of the amino acids “Serine-Histidine-Aspartic acid” which exists also in serine proteases. Morse and colleagues demonstrated that silicatein filaments catalyze silica formation. After the isolation of the protein filaments from the spicules they dissolved the protein together with unhydrolyzed silica precursor (Tetraethoxysilane Si(OC₂H₅)₄, (TEOS)) around neutral pH. The pH of the environment plays a critical role in the rate of TEOS and other silica alkoxide hydrolysis. It has been shown (Figure 28) that the rate of hydrolysis is faster on acidic and basic environments whereas near neutral pH the rate is very slow (Brinker, 1988).

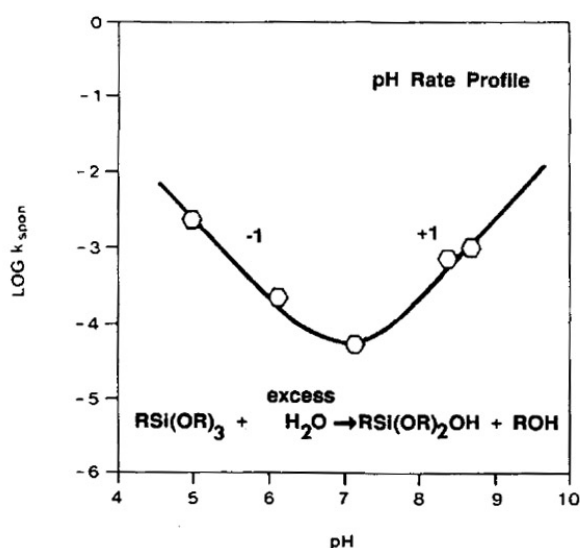


Figure 28 Hydrolysis rate of γ -glycidoxypropyltrialkoxysilane in aqueous solution as a function of the pH (Brinker, 1988)

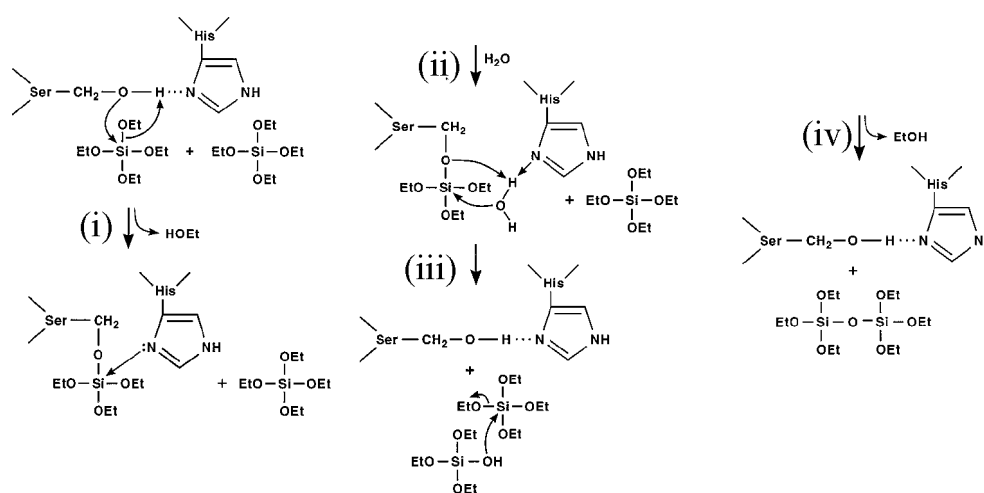


Figure 29 Proposed TEOS polycondensation pathway from silicatein-enzyme active site
(Cha et al., 1999)

The polycondensation pathway is described in Figure 29. The nucleophilicity of the serine oxygen is increased because of the hydrogen bond between the hydroxyl of the serine and the histidine's nitrogen. The oxygen attacks on the silicon and displaces an ethanol molecule. A water molecule assists in the hydrolysis of the Ser-Si(OC₂H₅)₃ bond. The hydroxyl of the HO-Si(OC₂H₅)₃ intermediate, starts a new nucleophilic attack to another TEOS molecule, resulting in the condensation of the first disiloxane product. The polycondensation continues to happen and the silicatein filaments after some hours become completely coated with silica particles.

Morse and colleagues inspired by this templating mechanism synthesized small bifunctional molecules that mimic the silicatein enzymatic active site and promote the silica condensation (Roth et al., 2005). Among these molecules the cysteamine and ethanolamine molecules are candidates for high catalytic activity towards tetraethoxysilane (TEOS) at neutral pH.

Later on, the same group decided to synthesize a novel system of diblock copolymers that mimic the serine (Ser (S)) and histidine residues located in the silicatein active site. The two polymers were hydroxylated poly(1,2 Butadiene) to mimic the role of serine (Ser (S)) and poly(2-vinylpyridine) to mimic the role of histidine (Adamson et al., 2007). The polymers showed high rates of catalysis, using TEOS silica precursor, and it was the first time that such a bioinspired synthetic system was reported.

6.1.3 De novo designed self-assembling peptides that template biosilica

Self-assembling peptides have also been used as model for templating biosilica. Aggeli and colleagues have chosen the 11 amino acid peptide DN1, (CH₃CO-Gln-Gln-Arg-Phe-Gln-Trp-Gln-Phe-Glu-Gln-Gln-NH₂), which self-assembles into amyloid type tapes. The peptide contains an arginine residue (Arg, (R)) that provides positive charge to the peptide and attracts the negatively charged silica precursors. Following the complete coating of the fibrils with silica, the sample was treated with calcination that removes the biological material and leaves the silica nanotube intact (Meegan et al., 2004). This technique opens a new field for post-modification and handling of the silica nanotubes (Yang et al., 2011b).

Pochan and Schneider reported the use of the previously reported MAX1 (H₂N-Val-Lys-Val-Lys-Val-Lys-Val-Lys-Val-^DPro-Pro-Thr-Lys-Val-Lys-Val-Lys-Val-Lys-Val-CONH₂) and its derivative MAX 8 (H₂N-Val-Lys-Val-Lys-Val-Lys-Val-Lys-Val-^DPro-Pro-Thr-Lys-Val-Glu-Val-Lys-Val-Lys-Val-CONH₂) to study the interaction of the peptide hydrogels with silica. Polycondensation of the silica precursor follows on the surface of the fibrils due to the high number of lysines (Lys (K)) and a silica layer is formed around the fibrils. Through rheological studies, the peptide-silica gels acquire stiffer hydrogel structure upon increasing the concentration of silica precursor. This control of the elasticity has promising applications for multifunctional biomaterials (Altunbas et al., 2010).

The lanreotide peptide was described previously in chapter 2.3.2, in which positively charged surface of the nanotubes attracts the negatively charged silica precursors and at the same time the precursors help in the elongation of the nano scaffold. Following silica templating on the surface of the nanotubes, calcination of the sample was performed for the removal of the biological template and bundles of millimetre-sized nanotubes were fabricated (Pouget et al., 2007).

6.2 Methodology

6.2.1 In vitro silification protocol

Lyophilized peptide powders with purity >95% (were purchased from Eurogentec, Belgium) were dissolved and studied in aqueous Tris-HCl buffer (25 mM, pH 8) at 6mg/ml concentration.

For the in vitro silification protocol the peptides were diluted at 1.5mg/ml final concentration in Tris-HCl buffer (0.56ml, 25 mM, pH 8) and Tetraethoxysilane (TEOS) (1ml, 4.5mmol), purchased from Sigma, was added to the solution. A biphasic solution was formed and the reaction was performed with gentle shaking for 15 hours.

For testing the interaction of peptide fibrils with Sodium silicate ($\text{NaSiO}_3 \cdot 5\text{H}_2\text{O}$), 50 microliters of stock solution of peptide 3mg/ml was mixed with 50 microliters of Sodium silicate (100mM, Tris-HCl buffer, 25 mM, pH 8) and was left 3 days for incubation.

For imaging peptide fibrils all the samples were placed on a 300 mesh formvar coated copper grid, purchased from BAL-TEC, and after 2 min the excess of the fluid was removed with a filter paper. Then 8 microliters of Phosphotungstic acid 1% was added on top and after 2 min the excess of the fluid was removed with a filter paper.

For imaging the silica containing samples all the samples (8 microliters) were placed on a 300 mesh carbon coated nickel grid, purchased from BAL-TEC, and after 2 min the excess of the fluid was removed with a filter paper and directly observed without any additional staining.

The identity of Silicon element was confirmed by energy dispersive X-ray spectroscopy (EDS).

For calcination the samples were incubated in an oven 3 h at 600° C at room atmosphere.

6.3 Results and Discussion

While investigating the mechanism of the binding of gold and platinum nanoparticles to the original building block NSGAITIG (Figure 17) it became interesting to see if serine (Ser (S)), in position 2, (Figure 30) could behave as an active nucleophilic residue. For this reason the in vitro silification templating was tested following the in vitro silification protocol of Morse and colleagues (Cha et al., 1999). According to this protocol silica tetraethoxysilane (TEOS) is used as a precursor and the pH of the solution should be around 7, in order to avoid the fast hydrolysis of TEOS at basic environments (Figure 28). According to https://www.genscript.com/ssl-bin/site2/peptide_calculation.cgi the isoelectric point of all the peptides studied was calculated around 7 to 7,5. It should be noted that the peptides have the C-terminal group amidated. The pK of the N-terminal amino group in single aminoacids is around 9. However, in peptides and proteins the pK of the N-terminal amino group ranges from 7 to 8. (Pace et al., 2009) (Thurkill et al., 2006) (Tanford, 1962).

For this reason we have chosen to work at pH 8, above the isoelectric point of the peptides in order to have the amino-terminal group uncharged. Under these conditions, there should be no templating contribution due to positively charged N-termini.

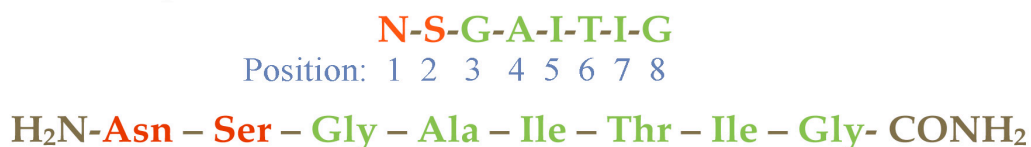


Figure 30 Peptide sequence of the original building block: the positions of amino acid substitutions are marked in red

The self-assembly of the NSGAITIG peptide was studied first in the prerequisite solvent. Figure 31 shows the negative staining TEM images before the in vitro silification process in order to confirm that the peptides are able to self-assemble into amyloid type fibrils in Tris pH 8 buffers. The dimensions of the fibrils are around 10nm in width and several microns in length. These dimensions are typical for this peptide and generally for amyloid type peptides with cross beta-sheet structure (Papanikolopoulou et al., 2005) (Kasotakis et al., 2009) (Sedman et al., 2011).

Following the formation of the amyloid type fibrils the in vitro silification protocol was tested. At the same time a control solution without peptides in it was tested as well. As shown in Figure 32 the formation of silica particles is observed after 15h. The peptide is fully

coated with spherical silica particles of 9nm regularly positioned on the surface. A possible explanation might be that the silica precursors attach to the nucleophilic serine (Ser (S)) residues and start the nucleation of silica. This hypothesis will be tested extensively through the chapter.

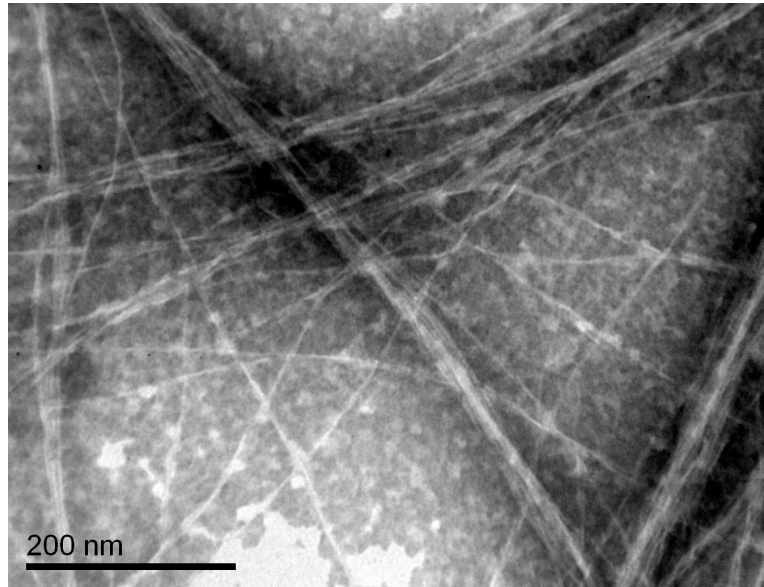


Figure 31 Negative staining of the NSGAITIG peptide fibrils

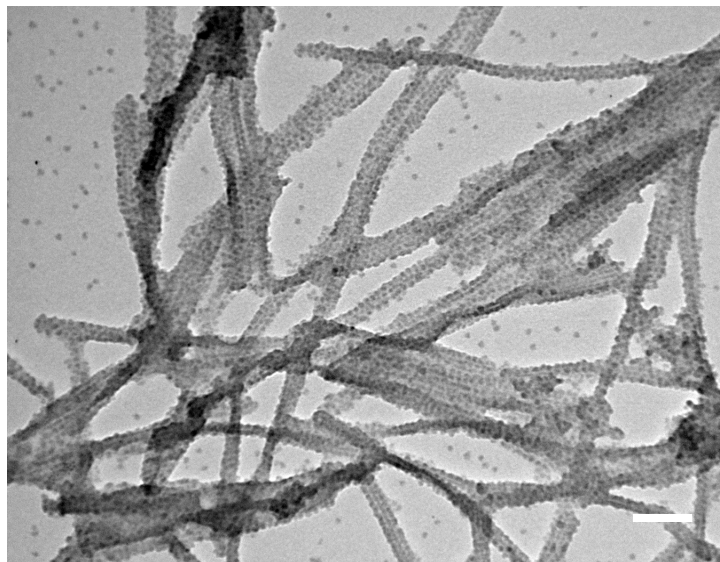
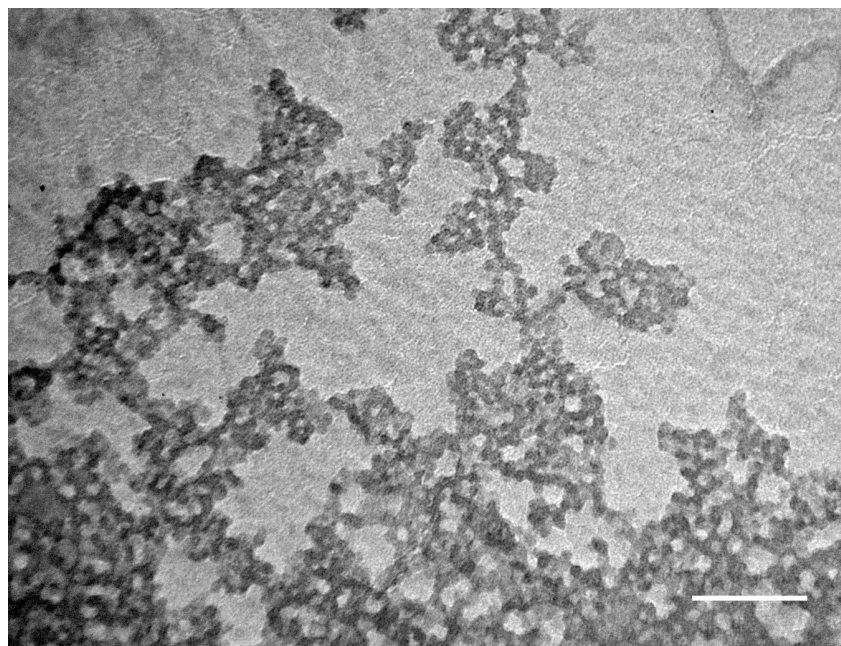


Figure 32 Peptide fibrils after in vitro silification for 15h. No negative staining was used, so the contrast afforded is only due to the silica nanoparticles. The NSGAITIG peptide fibrils nucleate the formation of silica particles on their surface (Scale bar: 100nm)

In the control solution without peptides, formation of spherical silica particles is observed as well (Figure 33). This happens normally because the hydrolysis of TEOS occurs inevitably at solutions with acidic or basic pH, and much more slowly around neutrality (Brinker, 1988).

A very important question that has emerged is whether the fibrils bind to silica precursors and start nucleation of silica or silica particles form first and then bind to them.



*Figure 33 TEOS hydrolysis and formation of particles in the absence of peptides
(Scale bar: 100nm)*

Testing the post nucleation of silica particles on the surface of the peptide fibrils, the control solution with the silica particles was incubated for several days. After extensive washing, in order to eliminate free silica precursors, silica particles (50 microliters) (Figure 34) were mixed with a fresh stock solution of NSGAITIG peptide fibrils (50 microliters, 3mg/ml). Figure 35 shows that the fibrils cannot template preformed silica particles, which are mainly in the form of SiO₂. This result suggests that the TEOS hydrolysis should be initiated on the fibrils, followed by polycondensation and formation of the silica particles on the surface of the fibrils.

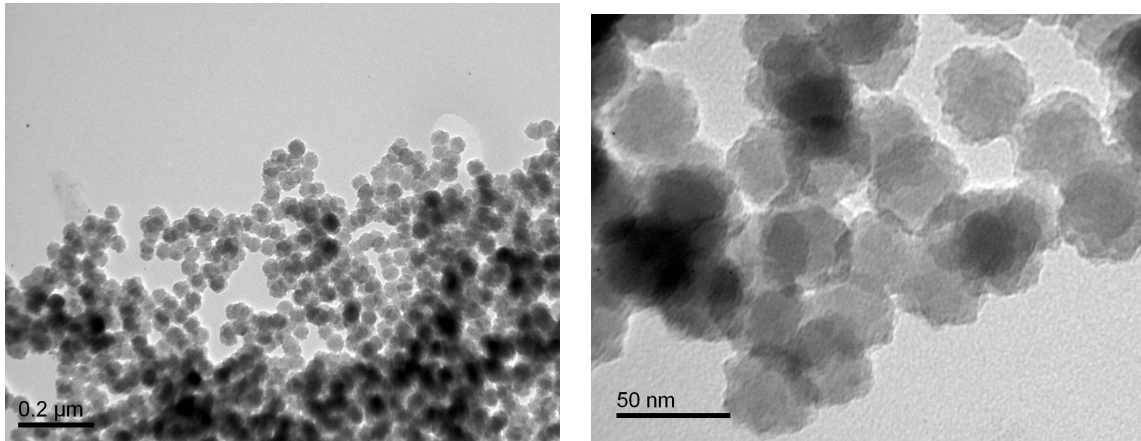
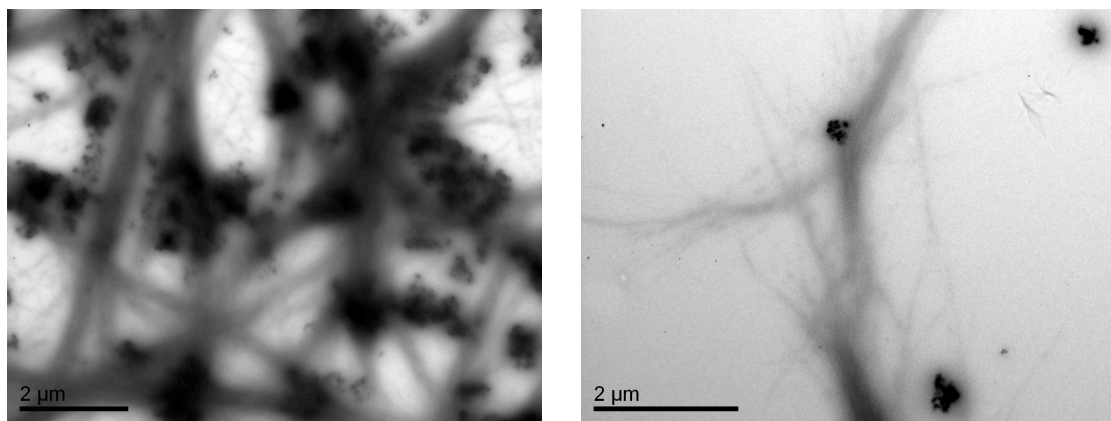
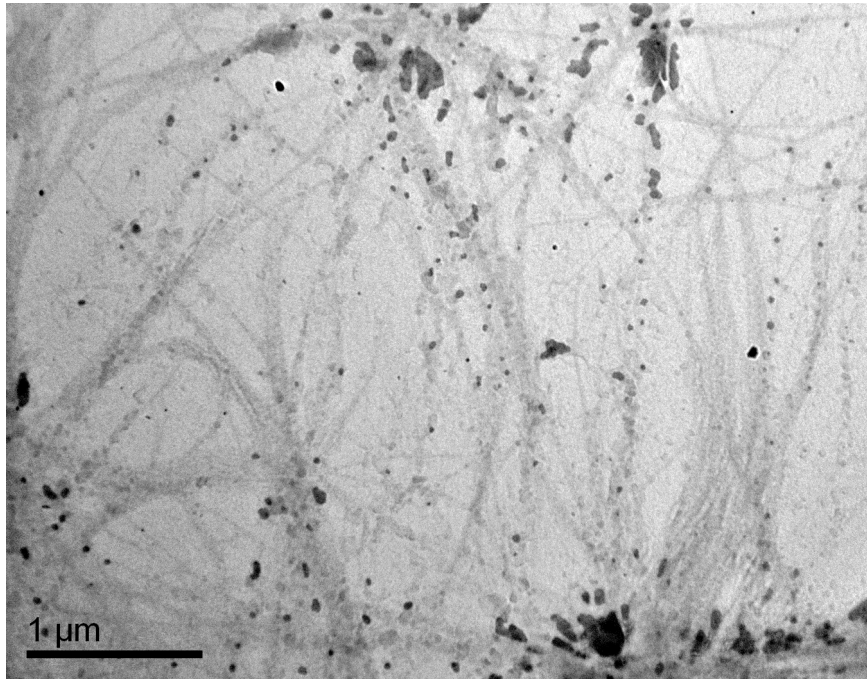


Figure 34 Preformed silica particles in the absence of peptides



*Figure 35 NSGAIIG peptide fibrils incubated with preformed silica particles
(without negative staining)*

Another interesting control was to test the nucleation of silica from another precursor, sodium silicate. 50 microliters of 100mM stock solution in Tris buffer pH 8 were mixed with 50 microliters of preformed NS peptide fibril solution in the same buffer. The condensation reaction proceeds according to the following steps: **i)** $(\text{HO})_3\text{Si-OH} + \text{OH}^- \rightarrow (\text{HO})_3\text{SiO}^- + \text{H}_2\text{O}$ **ii)** $(\text{HO})_3\text{SiO}^- + (\text{HO})_3\text{Si-OH} \rightarrow (\text{HO})_3\text{Si-O-Si-(OH)}_3 + \text{OH}^-$. As shown in (Figure 36), there is formation of silica particles (corresponding to the high electron density aggregates in the figure), but these are segregated from the peptide fibrils and are not attached to them. This experiment suggests that the templating of silica is not mediated by electrostatic interactions between the negatively charged silica precursors and the amyloid fibrils.



*Figure 36 NSGAITIG peptide fibrils with silica particles derived from sodium silicate
(without negative staining)*

We subsequently checked the stability of the particles on the surface of the fibrils. A washing protocol was followed; spinning the silica coated samples (10.000 rpm for 5min), removing the supernatant and re-suspension in water (with additional sonication). This protocol was repeated 3 times. After the washing procedure was performed, the background particles were eliminated and the NS peptide silica particles remained attached on its surface (Figure 37).

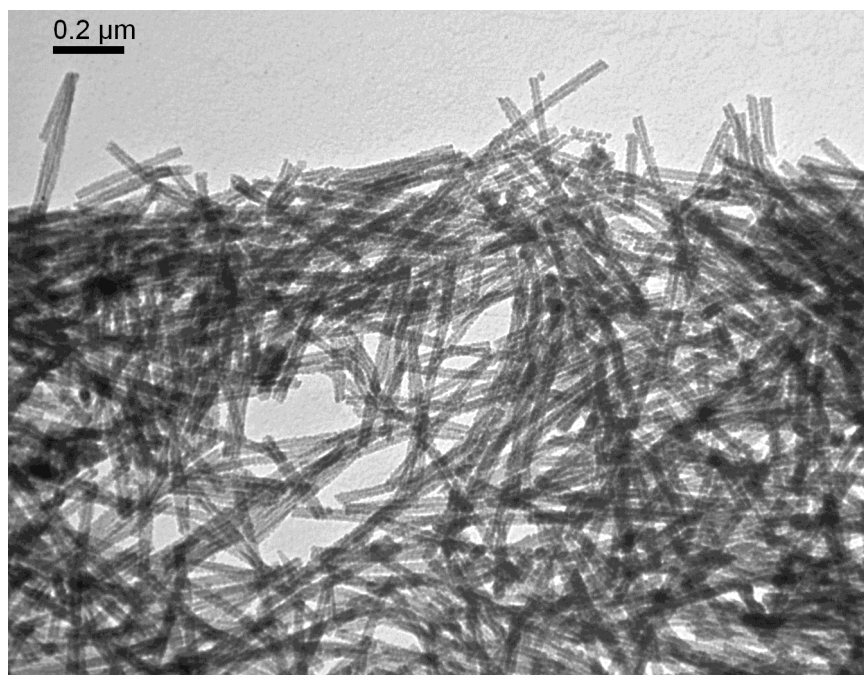


Figure 37 TEM micrographs of the NSGAIITIG peptide fibrils after the solution has been washed 3 times with water. No negative stain was used, so the contrast afforded is only due to the silica nanoparticles

Presumably, the *in vitro* silification process can continue until the entire silica precursor is consumed. The silica precursor was incubated with the peptides for longer times and the reaction was continued for 15 days. Figure 38a shows that the diameter of the peptide-silica fibers has increased from 23 \pm 2.5nm to 65 \pm 3.3nm. After imaging the sample that was incubated for 15 days we performed calcination at 600 C, to remove the biological template and keep the silica nanotube. Figure 38b shows the hollow silica tubes that are not destroyed by the high temperature and they keep a uniform inner diameter.

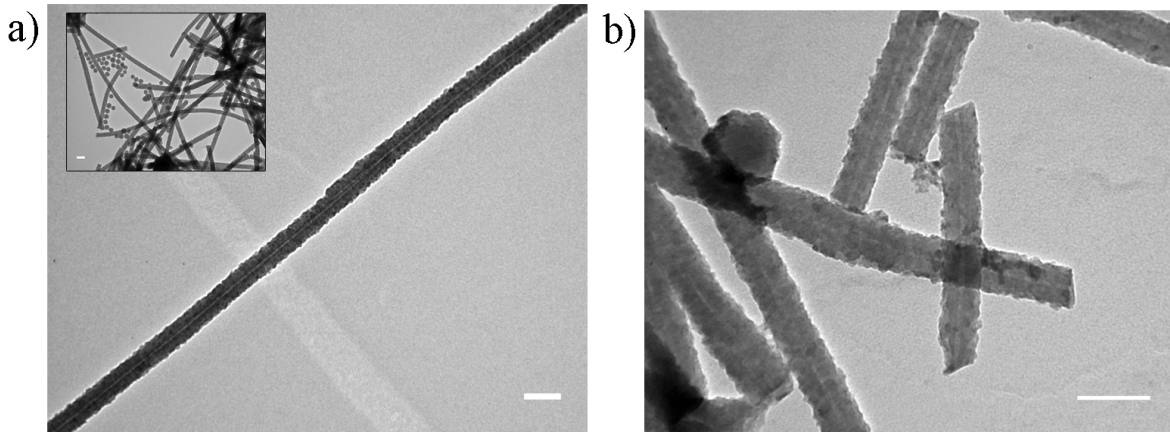


Figure 38 a) NSG AITIG fibrils after incubating for 15 days in TEOS solution (Scale bar: 100nm). The diameter has increased from 23nm to 65nm as the *in vitro* silification continues. The inset in (a) shows the uniform size of the silica-coated fibrils. (Scale bar: 100nm). b) Silica nanotubes after calcination of fibers (Scale bar: 100nm)

Finally EDS analysis was performed in order to test the composition of the inorganic phase on the surface of the fibril. Figure 39a shows the image where the EDS was taken and Figure 39b shows the intensive peaks of silicon (Si) and oxygen (O) elements that compose the inorganic phase. Nickel (Ni) and Carbon (C) peaks are coming from the carbon-nickel grid used for imaging our sample.

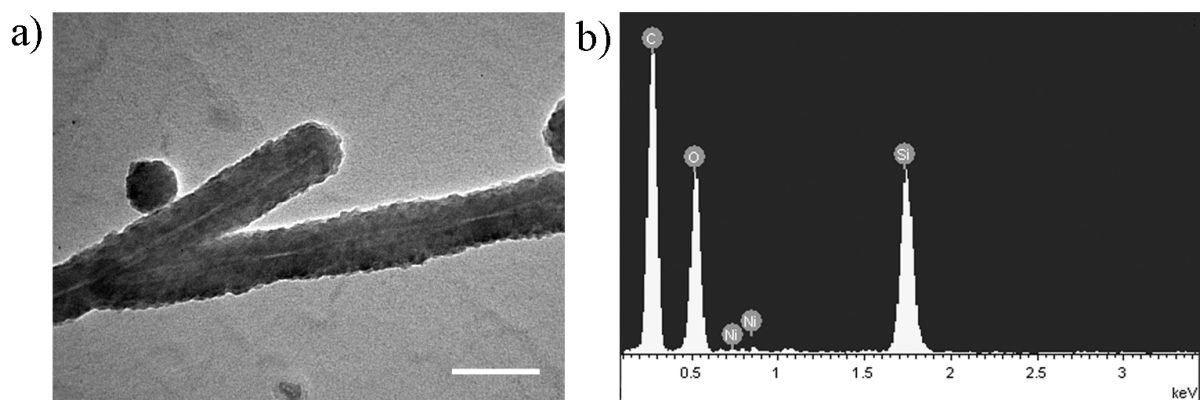


Figure 39 a) Area of EDS analysis of NSG AITIG peptide fibrils after incubating for 15 days with TEOS solution (Scale bar: 100nm). b) EDS analysis spectrum

In order to test an eventual role of the serine (Ser (S)) residue in the templating process we designed the $\text{NH}_2\text{-NAGAITIG-CONH}_2$ peptide in which serine (Ser (S)) is substituted with an alanine (Ala (A)). Figure 40 shows that the modification does not alter the final amyloid type structure for the peptide; however, this peptide does not nucleate silica particles on its surface.

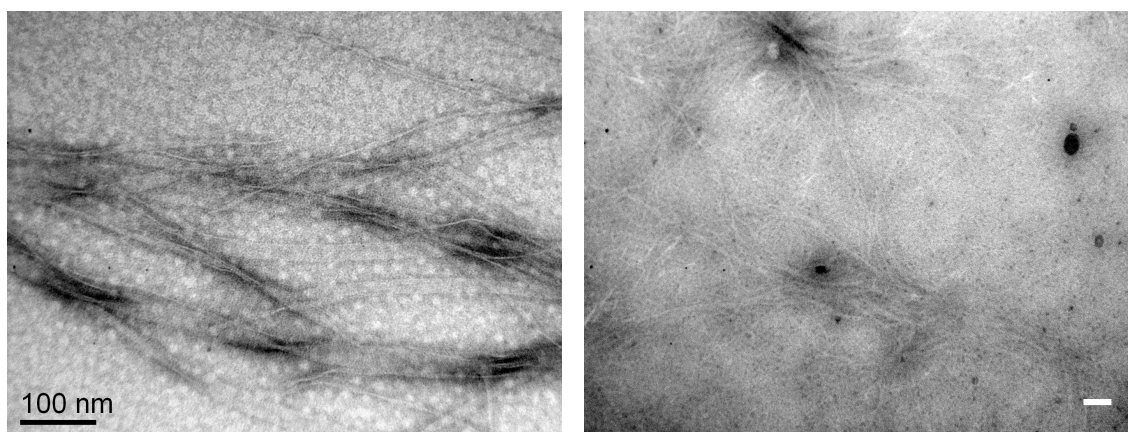


Figure 40 (Left) The N-A-G-A-I-T-I-G peptide fibrils (Negative staining with Phosphotungstic acid 1%), (Right) In vitro silification for 15h. No negative staining was used, so the contrast afforded is only due to the silica nanoparticles (Scale bar: 300nm)

We subsequently studied the N-terminal acetylated original building block, Ac-NSGAITIG-CONH₂. As shown in Figure 41, the Ac-NSGAITIG-CONH₂ self-assembles into fibrils that do not attach silica particles. Therefore, silica templating necessitates 1) the hydroxyl group of a serine (Ser (S)), and 2) a free amino terminal group. In the event of a nucleophilic character of the serine (Ser (S)), the free amino terminal group might be a possible candidate for abstracting the serine (Ser (S)) proton and making it nucleophilic.

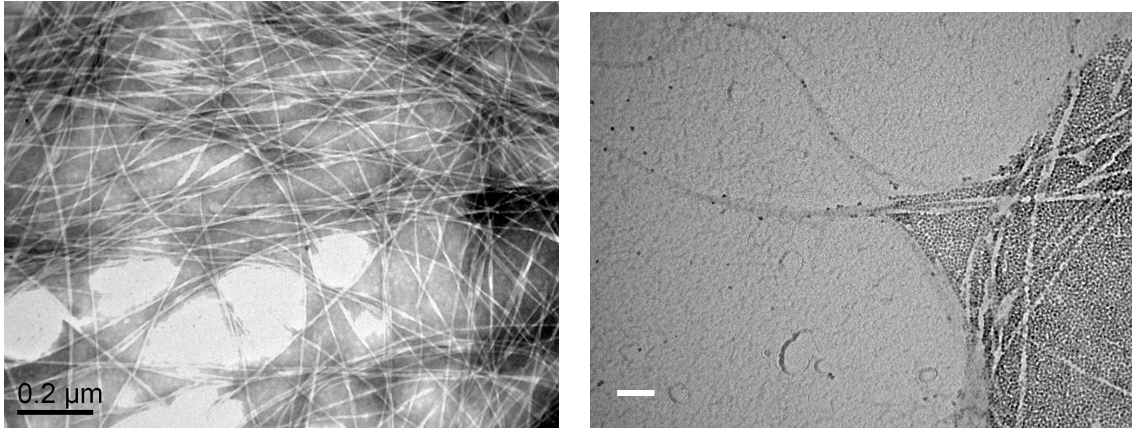


Figure 41 (Left) The Ac-N-S-G-A-I-T-I-G peptide fibrils (Negative staining with Phosphotungstic acid 1%), (Right) In vitro silification for 15h. No negative staining was used, so the contrast afforded is only due to the silica nanoparticles (Scale bar: 100nm)

We further tested the role of another hydroxyl-containing amino acid, threonine (Thr (T)) in the second position of the peptide sequence as well as the role of Cysteine (Cys (C)) in this position. Both cysteine and threonine can play the role of a nucleophilic residue in unconventional catalytic triad proteases (Oinonen and Rouvinen, 2000). The two peptides NCGAITIG and NTGAITIG were tested first for their self-assembly. The peptides, according to Figure 42, form amyloid type fibrils.

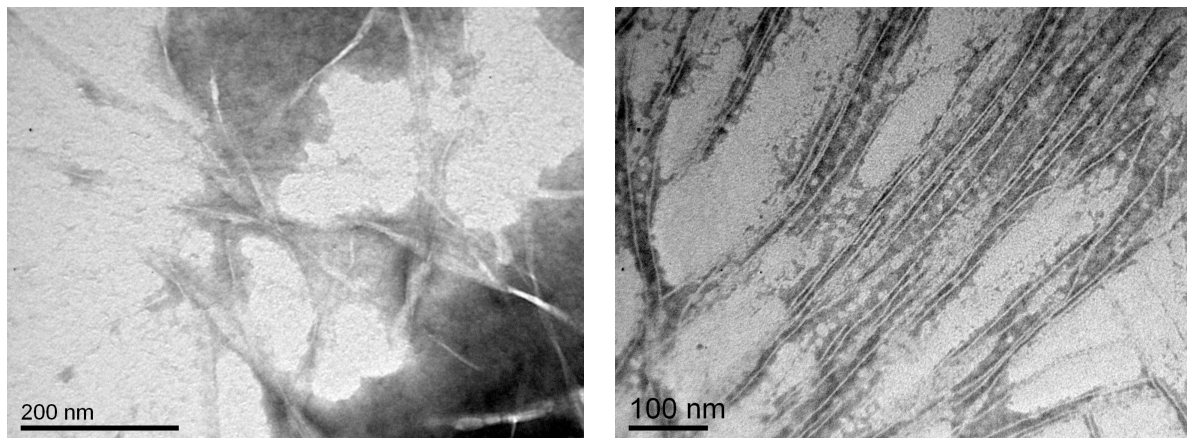


Figure 42 Negative staining with Phosphotungstic acid 1% of (Left) the NCGAITIG and (right) the NTGAITIG peptide fibrils

Then the *in vitro* silification protocol was tested and the peptides attach silica nanoparticles (Figure 43).

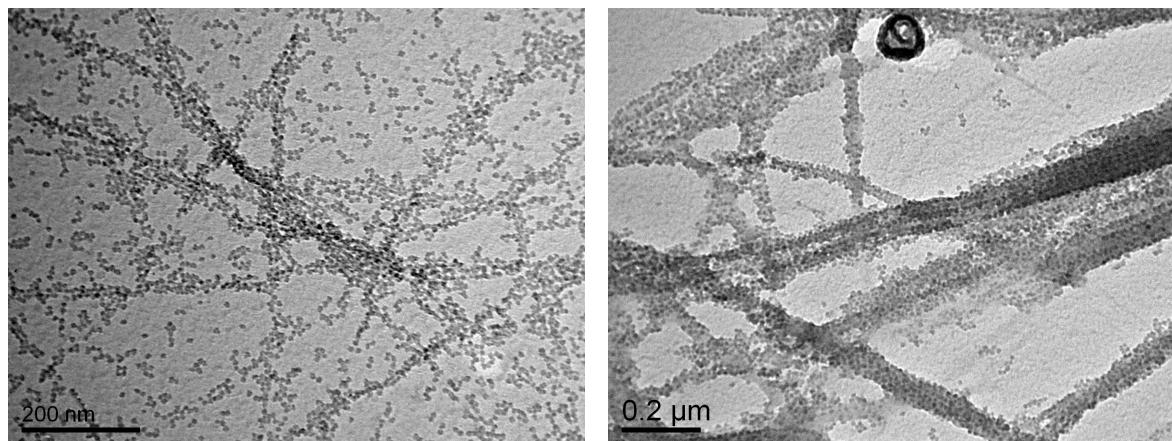


Figure 43 Peptide fibrils after In vitro silification for 15h. No negative staining was used, so the contrast afforded is only due to the silica nanoparticles. (Left) The NCGAITIG and (Right) the NTGAITIG

Finally the substitutions in the first residue position of the octapeptide were tested as well. First we designed the NH₂-ASGAITIG-CONH₂ peptide where Asparagine (N) is substituted with an alanine, the simplest and non-reactive amino acid. Secondly NH₂-FSGAITIG-CONH₂ was studied in order to evaluate the eventual interference of a bulky amino acid and finally, NH₂-HSGAITIG-CONH₂ to mimic the catalytic center of classical Serine proteases (Fairhead et al., 2008).

In Figure 44– 46 (left) the self-assembly of the peptides is shown. All peptides self-assemble into amyloid fibrils. In Figure 44– 45 (right) the silica nanoparticle attachment it is illustrated. All peptides show silica templating activity: we can therefore conclude that the residue in the first position does not play a critical role in the templating mechanism. Additionally the HSGAITIG peptide shows complete coating; one possible explanation is that the (His (H)) residue might provide extra attraction for making the serine highly nucleophilic.

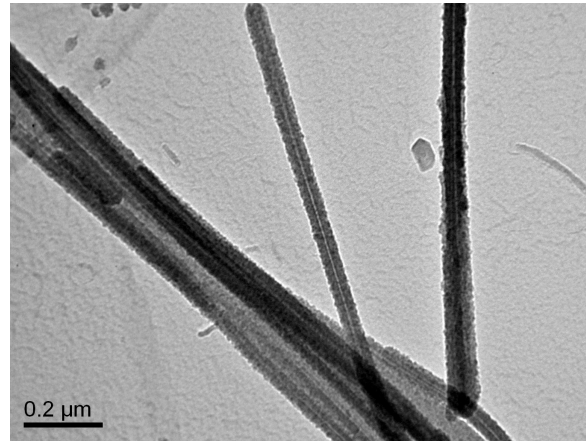
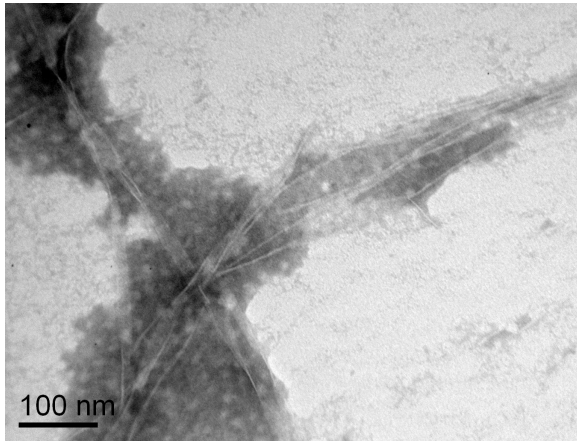


Figure 44 (Left) Negative staining of ASGAITIG peptide fibrils and (Right) In vitro silification for 15h

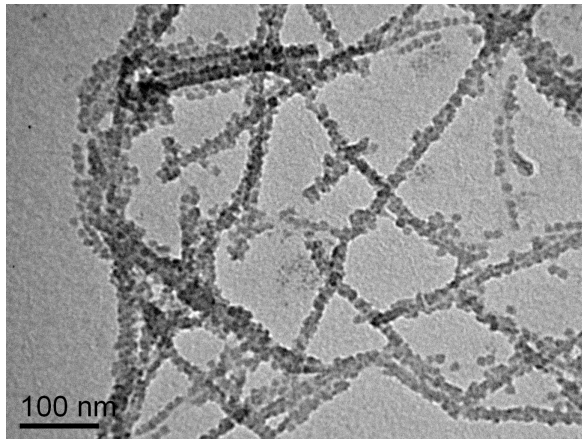
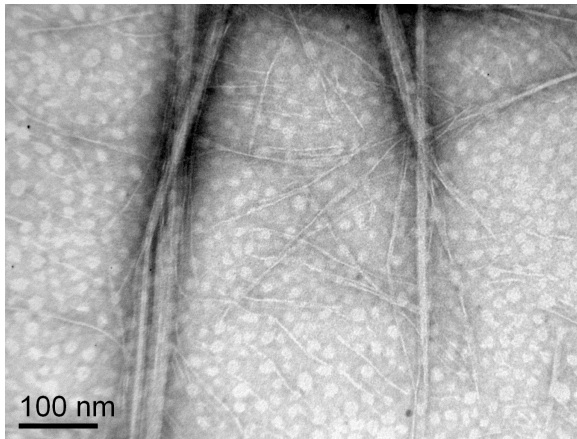


Figure 45 (Left) Negative staining of FSGAITIG peptide fibrils and (Right) In vitro silification for 15h

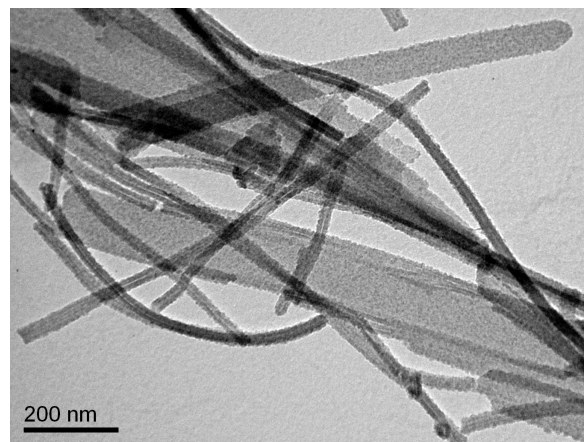
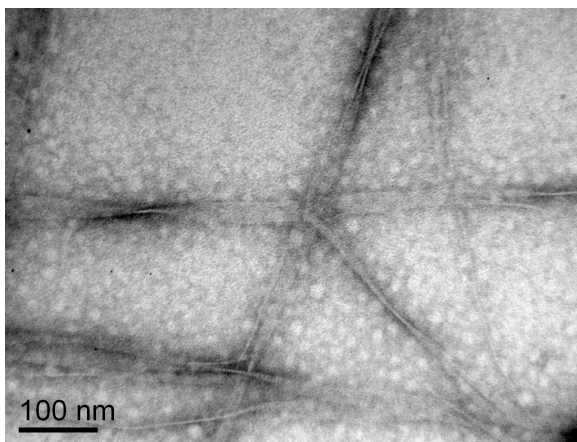


Figure 46 (Left) Negative staining of HSGAITIG peptide fibrils and (Right) In vitro silification for 15h

6.4 Conclusions

In this chapter, amyloid peptide fibrils have been used as scaffolds for the templating of silica precursors, demonstrating another biomimetic system for silica templating (Coradin and Lopez, 2003).

As we discussed in CHAPTER 3 molecular dynamics simulations provide an approximate position of the residues relative to the fibril axis. Looking at the model structure of the NSGAITIG (Tamamis et al., 2009), the position of the N-terminal α -amino group of the peptide is located very close to the Serine (Ser (S)) residue. This is reminiscent of the active site arrangement of certain enzymes, termed N-terminal hydrolases, where the presence of an amino terminal group close to Serine/Threonine/Cysteine activates the residue and makes it highly nucleophilic for the hydrolysis of peptide bond (Oinonen and Rouvinen, 2000) (Brannigan et al., 1995) (Chilov et al., 2007).

Summarizing all the previous data a possible templating mechanism can be suggested for the role of the NSGAITIG peptide and its derivatives in the biosilica formation. The mechanism works as follows: A hydrogen bond is formed between the α -amino group of the first residue of the peptide and the Serine hydroxyl group. The Serine oxygen increases its nucleophilicity and attacks the silicon atom of TEOS. An ethanol molecule is eliminated and a tetrahedral intermediate is formed. Addition of a water molecule completes the hydrolysis of TEOS. The disiloxane product is formed after the attack of the $(\text{CH}_3)_3\text{Si-OH}$ to the second TEOS molecule (Figure 47). The condensation further continues at the surface of the fibrils to give silica nanoparticles.

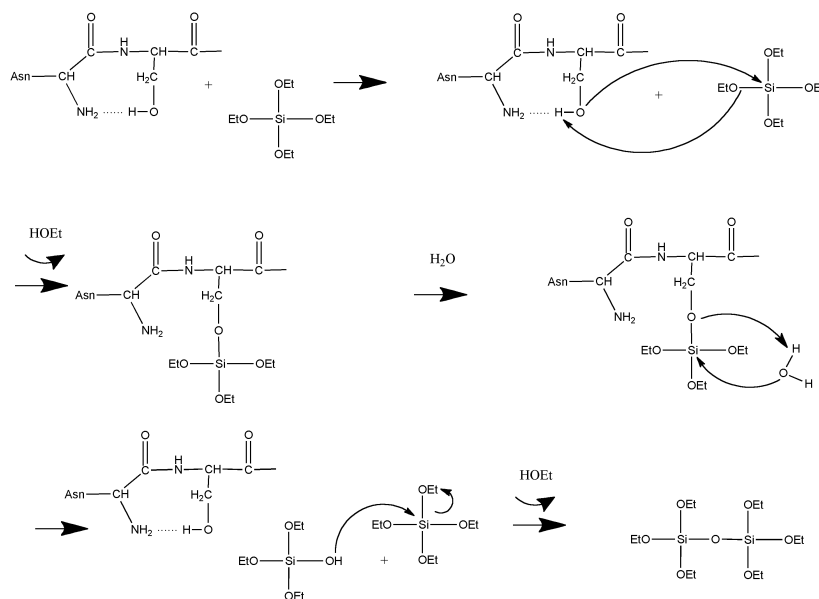


Figure 47 Proposed catalytic pathway of TEOS, from self-assembling peptides. (Inspired by the mechanism proposed by (Cha et al., 1999))

A schematic representation of the mechanism of silica templating on the fibril surface is shown in Figure 48. Initially the TEOS silica precursors are hydrolyzed at the vicinity of the fibrils by the serine residues. Partially hydrolyzed molecules would first aggregate into oligomers and then crosslink at the immediate vicinity of the fibril, forming seeds that further promote the deposition of a solid silica sheath.

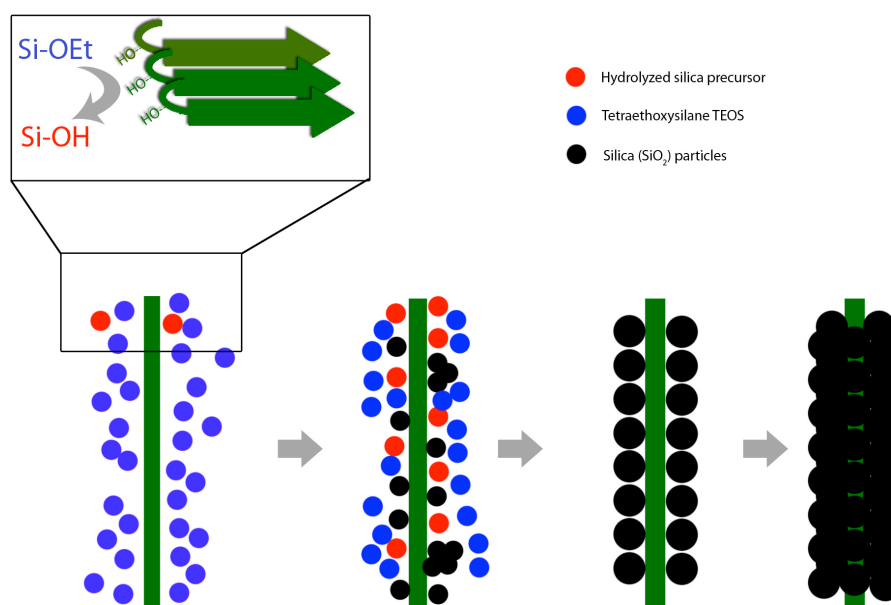


Figure 48 Silica templating proposed mechanism (inspired by the mechanism proposed by (Adamson et al., 2007))

Another important outcome of this work is the biotemplated fabrication of silica nanotubes. Silica nanotubes have been synthesized using inorganic and organic templates (Yang et al., 2011b). One key parameter, after the selection and the successful templating of silica to the desired scaffolds, is the mold scaffold to be easily removed without damaging the silica nanostructure. Carbon nanotubes can be used as mold scaffolds. The chemistry involved for silica deposition is considered toxic and requires high temperatures (Kim et al., 2008). On the contrary peptide based mold scaffolds require ambient temperatures and aqueous based solvents.

To our knowledge, this is the first time that a self-assembling peptide fibril mimics the templating mechanism of silicateins and is able to template silica nanotubes. Previous attempts are based on cationic interactions with negatively charged silica precursors and calcination of hybrid structure for obtaining the inorganic silica nanotube (Acar et al., 2011) (Yuwono and Hartgerink, 2007) (Meegan et al., 2004; Pouget et al., 2007) (Wang et al., 2011).

Apart from silica, it is reasonable to hypothesize that these self-assembling peptides could template other non-biogenic oxides through the same templating mechanism. Silicatein filaments were found to template titanium dioxide (TiO_2) at neutral pH, as well as barium titanate (BaTiO_3) starting from barium fluorotitanate (BaTiF_6) (Sumerel et al., 2003), (Brutchev et al., 2006). Silicatein filaments are also capable of hydrolysis and condensation of a precursor of gallium oxide (Kisailus et al., 2005). Finally, Dickerson reported the successful germanium oxide (GeO_2 , germania) precipitation from peptides that are endowed with hydroxyl and imidazole containing amino acids (Dickerson et al., 2004).

CHAPTER 7 2D SELF-ASSEMBLY OF PEPTIDE FIBRIL FILMS TEMPLATED WITH QUANTUM DOTS

7.1 Background and state of the art

Materials science has shown great attention to the synthesis and templating of various types of nanoparticles. The physical and chemical properties make them potential candidates for applications in medicine (Chan et al., 2002; Juzenas et al., 2008; Klostranec and Chan, 2006), photovoltaics (Sengul and Theis, 2011), electronics (Beaulac et al., 2008) and catalysis (Ratanatawanate et al., 2009). In Medicine and mainly in Biology, there is always the need of labeling cells or single proteins in order to study interactions or attachment *in vivo* or *in vitro*. So far the use of conventional genetically encoded fluorophores (e.g. GFP) or organic dyes (e.g. Rhodamine) has been proved useful but the problems of broad emission/absorption profiles and limited effectiveness of imaging in longer times has placed some limitation in use.

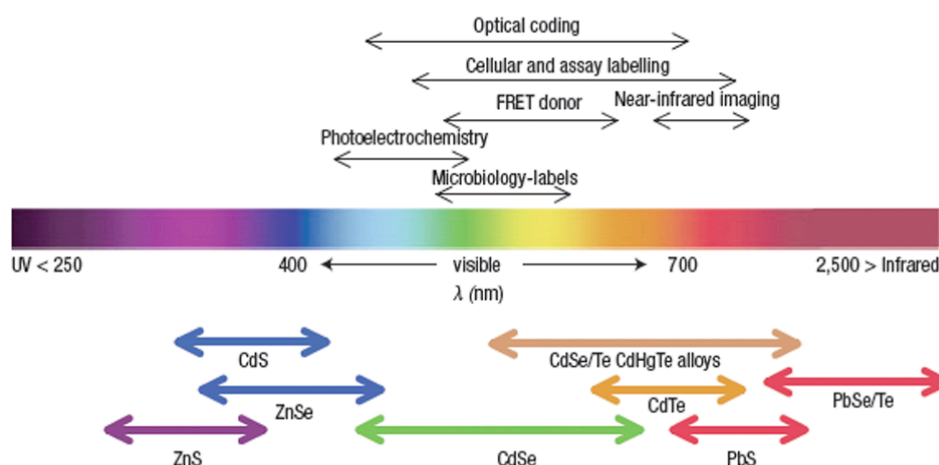


Figure 49 Semiconductor nanoparticles as a function of their emission wavelength (Modified from (Medintz et al., 2005))

Quantum dot fluorophores have entered the molecular labeling, bringing a large amount of advantages (Medintz et al., 2005). As shown in Figure 49 they cover broader emissions from far Ultraviolet (UV) to far Infrared (IR) radiation, compared to the areas of interest. Some of their unique properties are the high quantum yield, narrow symmetric photoluminescence (PL), high resistance to photo-bleaching and resistance to photo- and chemical degradation.

Quantum dots are zero-dimensional semiconductor crystals with their properties to differ from the same bulk semiconductor material. The bulk material has a fixed band gap depending on the nature of the semiconductor (Figure 50a). Scaling down the semiconductor material and reaching to dimensions that are smaller than the separation of an electron and hole in the material, known as exciton Bohr radius, quantum confinement effects happen. The equation between the energy band gap and the radius of the nanocrystal is given by the formula shown in Figure 50b.

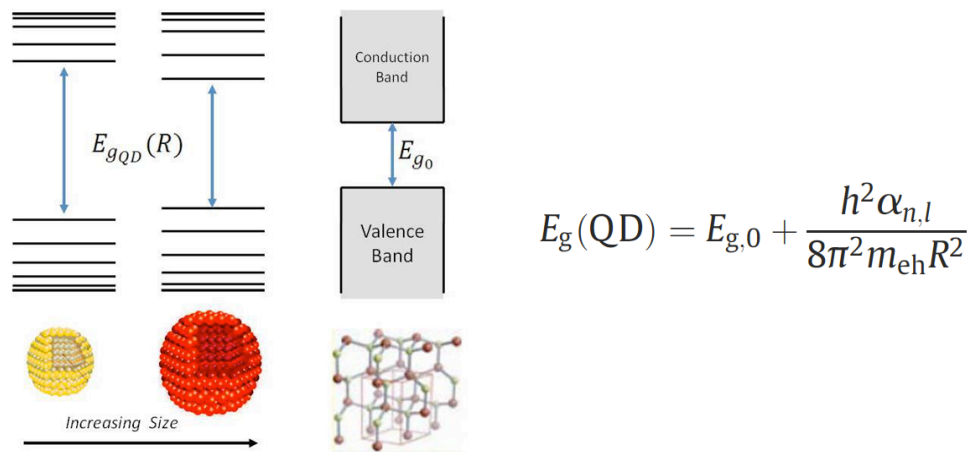


Figure 50 a) Energy gap of Semiconductor nanoparticle according to its size

b) Energy gap equation (Klimov, 2003)

The parameters of the equation are $E_{g,0}$: Energy bandgap of bulk semiconductor, α : atomic orbitals, m_{eh} : effective mass of electron-hole pair, R : radius of nanocrystal. It describes that when the semiconductor material is getting smaller in size the energy bandgap is increasing. This explains the different color of the quantum dots when they are irradiated with high energies (UV radiation). When the quantum dots absorb light they emit photons in a specific wavelength. The bigger the gap the smaller the emission wavelength and the light

emitted goes toward blue. Figure 51a shows the emission wavelength of quantum dots according to their size (Figure 51b).

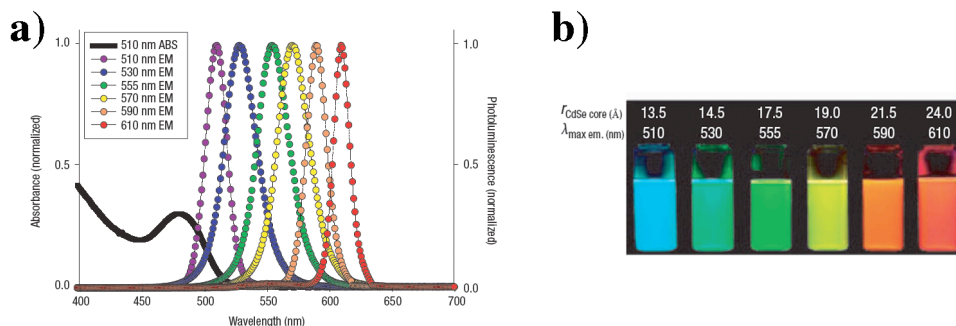


Figure 51 a) Emission of six different quantum dots b) Fluorescent properties of the quantum dots according to their size (Medintz et al., 2005).

7.1.1 Synthesis of quantum dot nanoparticles

Most of the quantum dots are synthesized using a three-component system composed of precursors, organic surfactants, and solvents (Dabbousi et al., 1997). This method is considered toxic due to the precursors (Cadmium (Cd), Lead (Pb)), the solvents and the high temperatures used. Figure 52 shows a typical example of CdSe quantum dot nanoparticle synthesis, where the nucleation and growth is happening after a quick injection of metal and chalcogenide precursors into the hot, strongly coordinating solvent (360° C). This solvent is a mixture of hydrophobic surfactants, trioctylphosphine (TOP) and trioctylphosphine oxide (TOPO), in order to keep the quantum dots in a high monodisperse level. The different size of the quantum dots is achieved by stopping the reaction, which happens when we remove the heat source (Klimov, 2003).

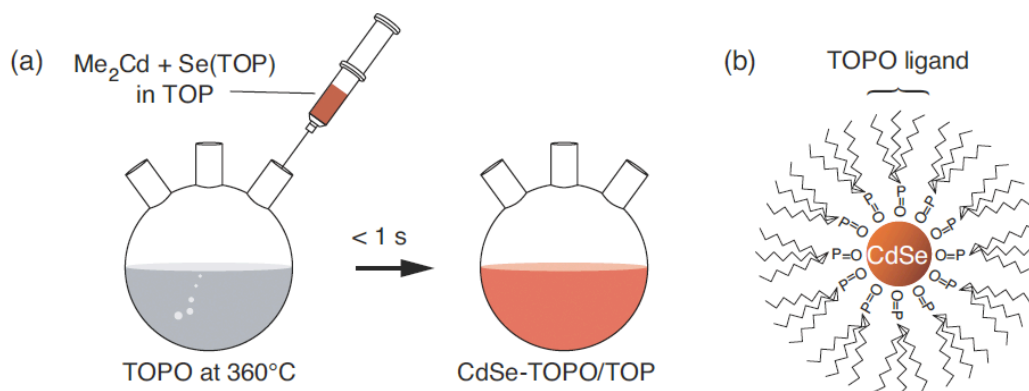


Figure 52 Synthesis of CdSe (TOPO capped) quantum dots (Klimov, 2003)

However there are some drawbacks that material scientists are trying to overcome in order to make quantum dots ideal nanoparticles for the applications mentioned above. The synthesis of Qdots requires toxic components and high temperature and there are some attempts to use better environmental friendly techniques (Yu and Peng, 2002). Quantum dots can be toxic for cells if they start to aggregate inside the cell. Finally the “coating” of the quantum dots and the transfer into aqueous solutions is compulsory for further functionalization and deposition. Since there is a diversity of quantum dots the capping of the surface can be performed with various types of techniques such as: Monothiolated caps, silane shell, hydrophobic interactions, copolymer interactions and direct attachment of protein or peptide to the quantum dot surface (Medintz et al., 2005). In Figure 53 below we can see the common method to functionalize the quantum dots with mercaptoacetic acid for subsequently transferring them to aqueous buffer.

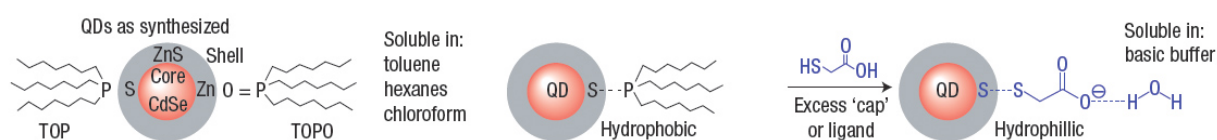


Figure 53 CdSe/ZnS quantum dots functionalized with Mercaptoacetic acid (Medintz et al., 2005)

7.1.2 Core-shell Quantum dots

After the synthesis of the quantum dots one critical step is the modification and protection of their surface. A great percentage of atoms (~80%) reside on the surface of the dot and this fact is affecting in a great extent the optical and structural properties of the particles (Reiss et al., 2009). The organic ligands we mentioned before (TOP, TOPO) they passivate to some extent the surface, but the protection is not sufficient. In order to passivate better the surface of the particles there is the need to grow epitaxially another semiconductor (shell) that surrounds the core particle. There are different types or core/shell particles and each type has to do with the differences in the band gap of the semiconductors used. CdSe/ZnS core shell particles belong to the Type I systems were the shell material has a higher band gap than the core. More specifically the energy band gap (E_g) of ZnS is 3.61eV and for CdSe 1.74eV. The properties of Type-I core-shell system are a) increasing

fluorescence quantum yield by passivating the surface of the core and b) isolating the core from the environment and reducing degradation.

7.1.3 Templating of quantum dots on natural proteins

During the last decade extensive research was carried out on the controlled and specific organization of semiconductor nanoparticles (Dong et al., 2010) (Dong et al., 2010) (Ithurria et al., 2011). The optical, electrical, mechanical and magnetic properties of the ordered nanoparticles most of the times differ substantially from those in solution and this opens a new field for the investigation of the inter-particle interactions. In a recent review Kumacheva and colleagues (Nie et al., 2010) addressed the importance of self-assembly as a simple and low cost method for the controlled assembly of nanocrystals and categorized the processes into four domains:

- a) Self-assembly in solution
- b) Self-assembly using templating methods
- c) Self-assembly at interfaces
- d) Assisted self-assembly

Kotov and colleagues reported the self-assembly of CdTe nanoparticles in two-dimensional free-floating sheets in bulk solution. The particles were stabilized with 2-(dimethylamino) ethanethiol, and the combination of electrostatic and hydrophobic interactions contributed to the stability of the structures (Tang et al., 2006). Combining the principles of non-covalent interactions and assembly at the air-water interface, various scientific groups are trying to advance the single crystal superlattices to ones with binary components (Dong et al., 2010). Some remarkable examples have been reported from Talapin and colleagues, where they investigated a long range of binary crystal superlattices and they found that the forces contributing for the assembly (Coulomb, van der Waals, charge-dipole, dipole-dipole) play crucial role in the crystallization of the binary components (Shevchenko et al., 2006). The properties of single crystals comparing to the situation that they are in close proximity differ.

Templating semiconductor nanoparticles on the surface of biological self-assembling molecules such as proteins and peptides has been shown to break the limitations that “top-down” techniques have for the fabrication of electronic devices. Bottom-up proteinaceous scaffolds can provide high selectivity, direction of crystal morphology and reproducibility at

the molecular level. There are many examples in literature about templating of self-assembling proteins with quantum dot nanoparticles.

The most common method to anchor nanoparticles on the surface of a biological scaffold is to introduce residues that are positively charged (Lysine (Lys (K)), Arginine (Arg (R)), Histidine (His (H))), negatively charged (Aspartic acid (Asp (D)), Glutamic acid (Glu (E))), incorporate thiols (Cysteine) or hydroxyl groups (Serine (Ser (S)), Threonine (Thr (T))).

Characteristic examples are the bacterial flagella nanotubes. Kumara reported the templating of ZnS/Mn and cadmium telluride (CdTe) quantum dots on the surface of bacterial flagella nanotubes. The protein that composes the self-assembled structure contains two domains (D2 and D3), which are solvent exposed, and through genetic engineering a loop of histidines was inserted for the successful binding of the nanoparticles (Kumara et al., 2007a).

Shenton reported the templating of the Tobacco Mosaic Virus (TMV) with lead sulfide (PbS) and cadmium sulfide (CdS) crystallites by the numerous glutamic acid (Glu (E)) and aspartic acid (Asp (D)) residues exposed on the surface of the TMV virion (Shenton et al., 1999).

Sone fabricated semiconductor nanowires using nanofibrils of self-assembled peptide amphiphiles and CdS crystallites. The successful templating was achieved through the aspartic acid (Asp (D)) residues exposed on the surface of the fibrils (Sone and Stupp, 2004).

7.1.4 1D, 2D & 3D Assembly of quantum dots

Yang reported the one-dimensional (1D) assembly of CdTe quantum dots on the surface of polymer nanofibers in the liquid-liquid interphase. The two solvents were water and chloroform. The quantum dots were dispersed in water after their surface modification with carboxyl groups and the polymer nanofibers, composed of poly(N-vinylcarbazole-co-glycidylmethacrylate) (PVK-co-PGMA), were dissolved in the chloroform phase. The templating reaction was performed between epoxy groups of the polymers and the carboxyl groups of the quantum dots (Yang et al., 2011a) (Reis et al., 2009). The high uniformity of the quantum dots on the surface of the nanofibers is very important for optoelectronic and sensor devices.

The two-dimensional assembly (2D) of TOPO capped CdSe/ZnS quantum dots have studied extensively by Gattas-Asfura using the Langmuir-Blodgett deposition method.

Langmuir films were utilized to determine the molar absorptivity of CdSe QDs and to study the capacity for manipulating the 2D organization of the QDs. Various parameters such as surface modification, particle size, surface pressure, influence the self-assembly of the QDs at the air-water interface (Gattas-Asfura et al., 2005), (Ji et al., 2005).

Henry reported the templating of three-dimensional (3D) self-assembled scaffold, composed of helical actin protein filaments and lipid bilayers, with peptide capped CdSe/ZnS quantum dots. The cysteines of the heptapeptide (Cys-Cys-Cys-Ser-Ser-Ser-Asp) bind through disulfide bonds to the ZnS shell and the aspartic acid (Asp (D)) coats the quantum dots with negatively charges; these along with the anionic actin filaments, attach to the surface of the cationic lipidic membranes. This new method puts forward the construction of novel 3D arrays of nanoparticles with modified properties (Henry et al., 2011).

7.2 Methodology

7.2.1 Peptide two dimensional (2D) film formation

The peptides (free N-termini, amidated C-termini) were purchased from Eurogentec (Belgium) and had a degree of purity higher than 95%. Lyophilized peptide powders were dissolved in chloroform at 2mg/ml concentration. Then 80 microliters were added to a 4ml vial and 1ml of chloroform was added extra. Finally 1ml of double distilled water was added and left to incubation for 24 hours.

7.2.2 Synthesis of TOPO-Capped CdSe/ZnS quantum dots

Chemicals: Cadmium oxide (CdO), oleic acid (OA), selenium (Se), trioctylphosphine (TOP), octadecene (ODE), TBP (tri-butyl phosphine), Zn(Et)₂ diethylzinc, hexamethyldisilathiane ((TMS)₂S), trioctylphosphine oxide (TOPO).

A mixture of 20mL of ODE, 6.3mL of OA and 0.064g of CdO was added in a 50mL 3-neck flask. The reaction was stirred and heated to 120°C under vacuum over 30min to eliminate the water. Stock solution of Se/TOP/ODE was prepared as follows: 0.148g of Se was dissolved in 9.482g of TOP in a 20mL vial under stirring conditions (this solution can be stored in the fridge of the glovebox for a long time). 195 microliters of Se/TOP mixture and 300 microliters of ODE were potted in a vial, using a syringe. The reaction temperature was raised to 300°C (225°C for slower reaction) under Ar. When the solution reached the desired temperature the Se/TOP/ODE solution was added fast. The color of the reaction has to change to dark-red in minutes. The reaction time will define the size of the particles, i.e., the wavelength of the emission desired. The cleaning process of the particles is carried out by placing a mixture of QD solution/2-propanol in a ratio of 2:10, in a centrifuge tube and centrifugation during 40min at 6000rpm. The solids are redispersed in toluene or chloroform.

7.2.3 ZnS coating of the CdSe quantum dots

ZnS stock solution was prepared as follows: 4.1g of TBP with 0.63g of Zn(Et)₂ in heptane and 160mg of (TMS)₂S. In a 50mL 3-neck-flask 10g of TOPO was heated to 120°C for 30min under vacuum while stirring. Then it was left to cool to 60°C under Ar. 1g of TBP was added by syringe and also 2mL of the previously formed CdSe Qdots in chloroform. The vacuum was switched on to eliminate the chloroform. The reaction was heated it up till 100°C slowly. The ZnS stock solution was added dropwise. Equal amount of ZnS stock solution was added for each qdot sample. Following the addition of this stock solution an increase in the intensity of the fluorescence is observed. 5 ml of anhydrous butanol was added at 60°C to prevent solidification. The particles were cleaned placing 2mL of QDs with 10mL of methanol in a centrifuge tube. This mix is centrifuged during 40min at 6000rpm. The solids were stored at room temperature in TOPO/butanol 2:1.

7.2.4 Templating of 2D self-assembled fibril films with Qdots

Lyophilized peptide powders were dissolved in chloroform at 2mg/ml concentration. Then 80 microliters were added to a 4ml vial and 1ml of chloroform was added extra. 80 microliters of quantum dots stock solution (CdSe/ZnS) was added. Atomic absorption spectroscopy (AAS) was performed to the quantum dot samples for the determination of the concentration (0.22 mg/ml for the green and 0.53 mg/ml for the red sample). Finally 1ml of double distilled water was added and let for incubation for 1 day. After 24h a “membrane” was formed at the water-chloroform interface.

7.2.5 Transmission electron Microscopy (TEM) analysis

TEM experiments were performed at the Department of Biology of the University of Crete using a JEOL JEM-2100, High Resolution, microscope, operating at 80 kV. For imaging the amyloid fibril films, 8 microliters from the interface were placed on a 300 mesh formvar-coated grid and after 2 minutes the excess of the fluid was removed with a filter paper. Finally the samples were negatively stained with 8 microliters uranyl acetate 1% for 2 min. For imaging amyloid fibril films templated with quantum dots, 8 microliters from the interface were placed on a 300 mesh carbon coated nickel grid, purchased from BAL-TEC,

and after 2 min the excess of the fluid was removed with a filter paper and directly observed without any additional staining.

7.2.6 Optical characterization

UV-Vis absorption spectra of the diluted solutions of the dots in chloroform placed in quartz cuvette were obtained on a Perkin Elmer LAMBDA 950, UV– NIR spectrophotometer equipped with an integrated sphere. At the same time the fluorescence was measured on a Fluoromax[®] -P Phosphorimeter. For the sample excitation a, 150-W xenon continuous output ozone free, lamp was used. The spectra were measured at 300 K with a grating for emission 1200 grooves/mm in front face collection mode and an emission detector R928P for high sensitivity in photon -counting mode.

Solid-state samples were prepared after drying a small volume of the corresponding colloidal solution on a piece ($10 \times 10 \text{ mm}^2$) of a single-crystalline silicon <100> wafer. Photoluminescence (PL) experiments were performed with a He-Cd CW laser operating at a wavelength of 325nm, with 35 mW power. The PL spectra were measured at 300 K and resolved by using a UV grating, with 600 grooves/mm and a sensitive, calibrated liquid nitrogen-cooled CCD camera.

7.3 Results and Discussion

The purpose of this study was to template the self-assembling peptide fibril films with quantum dots nanoparticles using thiol chemistry. The thiol chemistry is derived from the cysteine containing peptides; it is known that in the presence of thiols the TOPO molecules are displaced from the surface of the quantum dots and are replaced by thiols. Two different sizes of TOPO capped CdSe/ZnS quantum dots (Qdots) were used. The resulting structures were characterized using Transmission Electron Microscopy (TEM) and Photoluminescence analysis (PL).

Figure 54 shows the UV-Vis absorption and emission spectrums of TOPO capped CdSe/ZnS Qdots with two different particle sizes. The approximate mean diameter of the Qdots was calculated using the empirical fit developed by Yu et al (Yu et al., 2003) and confirmed using high resolution TEM. From the absorbance maximum the sizes of the quantum dots were calculated as follows: 2.6nm ($\lambda_A=526\text{nm}$) and 3.95nm ($\lambda_A=584\text{ nm}$) respectively. The red shift in the absorption is attributed to the bigger size of the nanoparticle. The emission wavelength of the particles determines the color of the particle under UV light. The one with emission at 548nm has a green color and the other at 610nm has a red color under UV light.

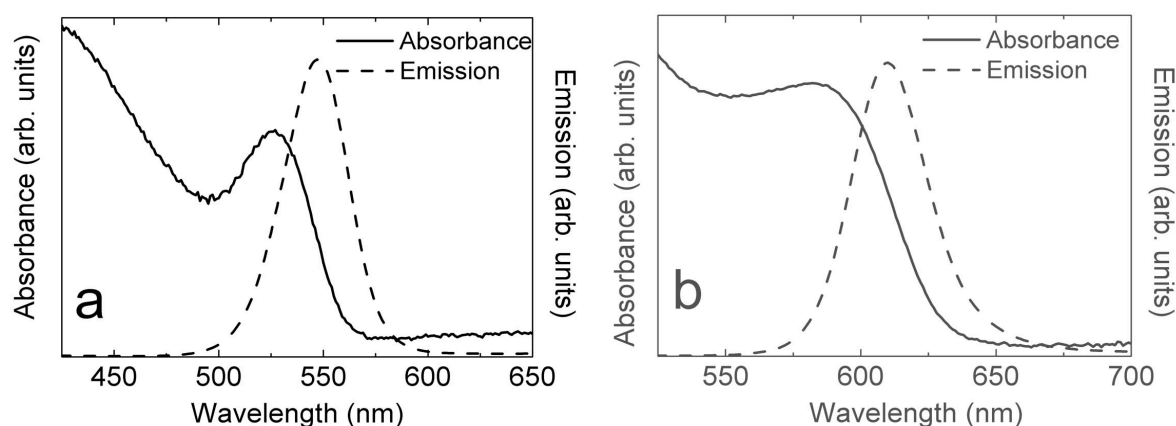


Figure 54 Photoluminescence (PL) spectra of the CdSe/ZnS nanocrystals (At room temperature) with average diameter a) 2.6nm and b) 3.96nm

The peptide used was the cysteine-containing $\text{NH}_2\text{-CSGAIITIG-CONH}_2$ that was previously demonstrated to bind silver, gold and platinum nanoparticles (Kasotakis et al., 2009).

Before the interaction with the quantum dots the peptides were studied for their self-assembling ability at the water/chloroform interface. The two-dimensional assembly at the air-water interface of a twelve amino acid peptide (LSFDNSGAITIG-NH₂, termed LSFD) has been previously studied by using the Langmuir-Blodgett film deposition method. The peptide is proposed to form flat beta-sheets at the air-water interface with the peptide adopting a fully extended conformation. The estimated experimental area per molecule for the beta sheets approaches the theoretical one which is calculated using the repeat distances of ~ 4.7 Å between *beta*-strands and ~ 3.5 Å per residue (Lepere et al., 2007). Moreover, our collaborating group at the University of Nottingham studied the assembly of the original building block NSGAITIG and its derivatives on mica and Highly Ordered Pyrolytic Graphite (HOPG) surfaces and confirmed the “film” like assembly of the peptides in the solid/liquid interface (Sedman et al., 2011).

Figure 55a shows a TEM image from the CS self-assembling peptide fibril film. The size of the film can reach up to 2×10 μm. Closer image of the peptide fibril film shows a high regular structure. Fast Fourier Transform Analysis (FFT) (Figure 55b upper left) reveals a regular spacing of 28 Å between the fibrils. This fact suggests that the octapeptide is in the fully extended conformation within the fibril lying at the water/chloroform interface (Lepere et al., 2007).

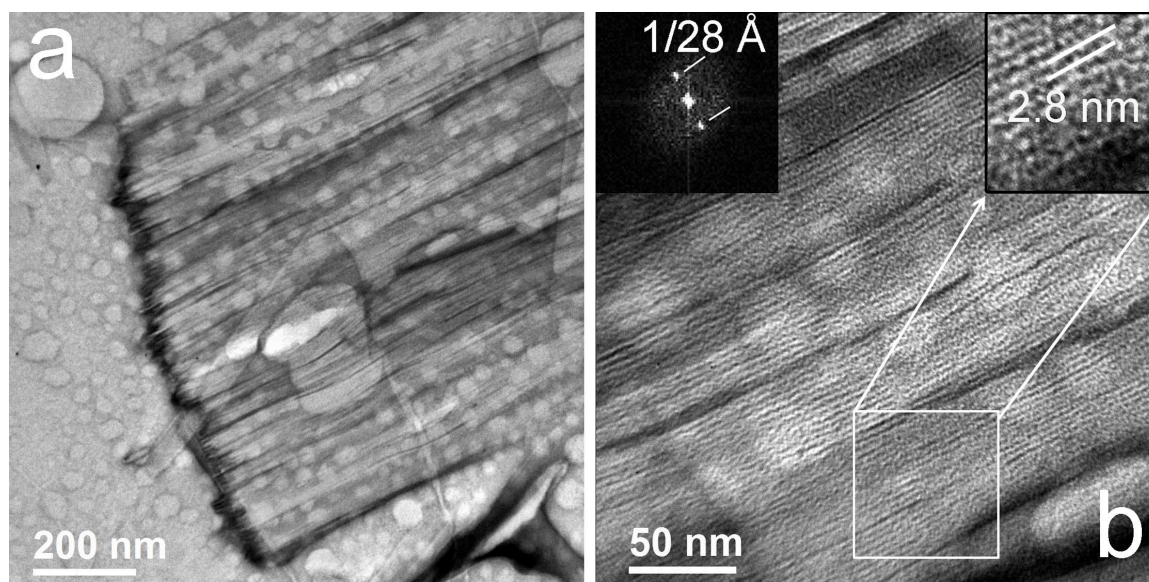


Figure 55 Transmission electron microscopy images of a) Peptide fibril film at the water/chloroform interface b) Closer magnification of the film. Upper left: Fast Fourier Transform analysis (FFT) of the parallel-stacked fibrils. Upper right: Magnified image showing the 2.8nm distance between the fibrils.

Following the complete characterization of the self-assembling peptide fibril film, formed by both CS and NS peptides we proceeded to the templating of the surface of the film, exposed in the chloroform phase, with the previously formed TOPO capped CdSe/ZnS Qdots. Figure 56 shows the schematic preparation of the amyloid type fibril films templated with quantum dots. For each peptide the same procedure was followed. The peptide was dissolved first in chloroform. Under these conditions, the peptide does not stay in the monomeric form and self-assembles into fibrils, as checked by electron microscopy. In separate vials the two different Qdots were dissolved in chloroform as well. The samples were mixed for 30 min under gentle shake. The cysteine containing peptide (CS) will participate in the ligand-exchange reaction whereas the control peptide (NS) will not show any binding ability to the Qdots surface. Water was subsequently added on top the solution and was left to relax for 24h. Figure 57 shows optical images of the vials under UV light lamp, after 24h. In the vials containing the CS peptide almost all the Qdots are seen visually to have been transferred to the water/chloroform interface (Figure 57 a, b left). This is due to the successful attachment of the largest percentage of the Qdots to the peptide fibril film. There is a part of Qdots that still remain in the chloroform phase. In the case of the control peptide NS, the Qdots largely remain in the chloroform with only the peptide fibril film being formed at the interface (Figure 57 a, b right).

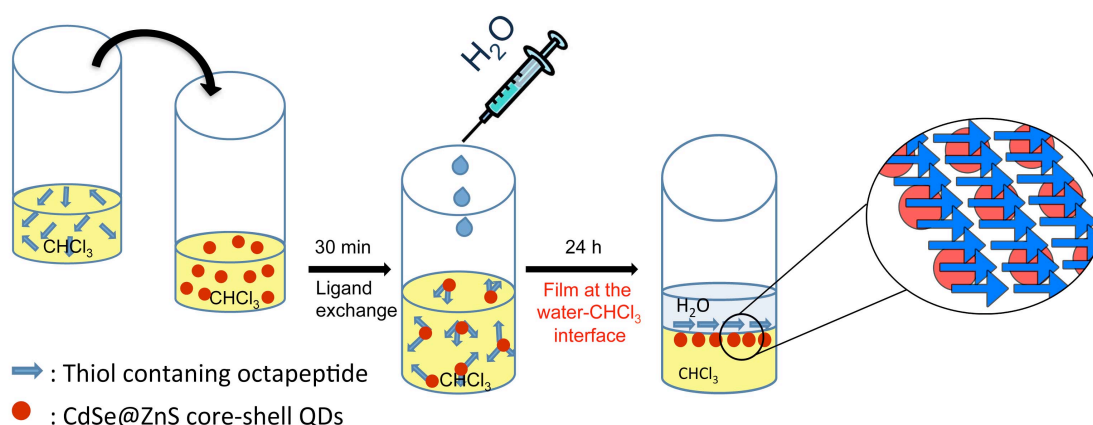


Figure 56 Schematic representation of the self-assembled fibril films templated with quantum dots.

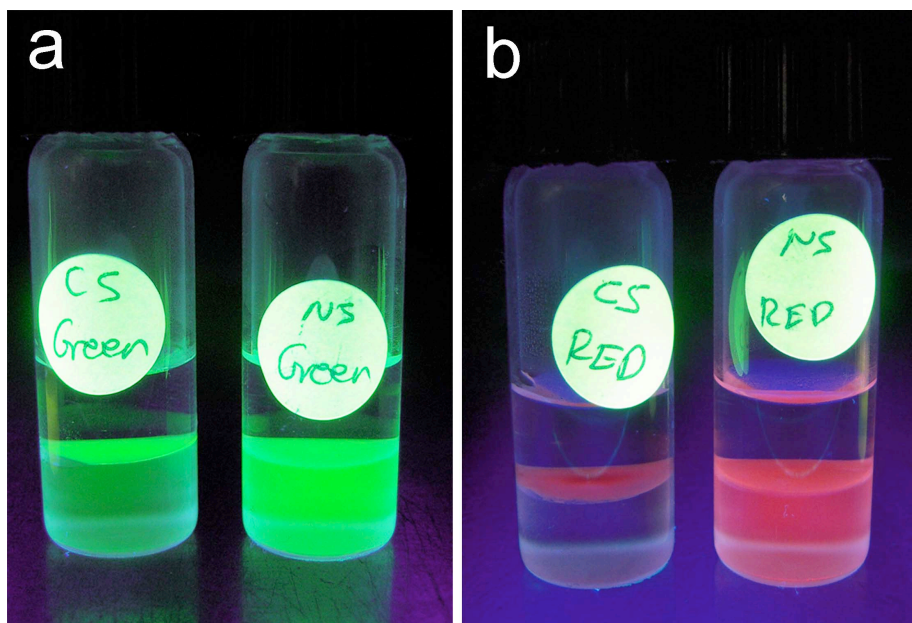


Figure 57 Optical images, after the 24h incubation of the peptide fibril films with the Qdots, under UV light. In both images CS and NS peptide fibril films were incubated with a) Green and b) Red quantum dots

All the samples were characterized using transmission electron microscopy. Figure 58 a, b shows the control peptide NS, to exhibit no oriented templating of the green and red Qdots on the surface of the amyloid fibril film respectively. This result was expected since there is no ligand-exchange effect between the NS peptide and the TOPO capped quantum dots. Some Qdots remain in the surface of the film since the sample for TEM analysis is lifted from the interface and takes along some part of the unbound Qdots from the chloroform phase.

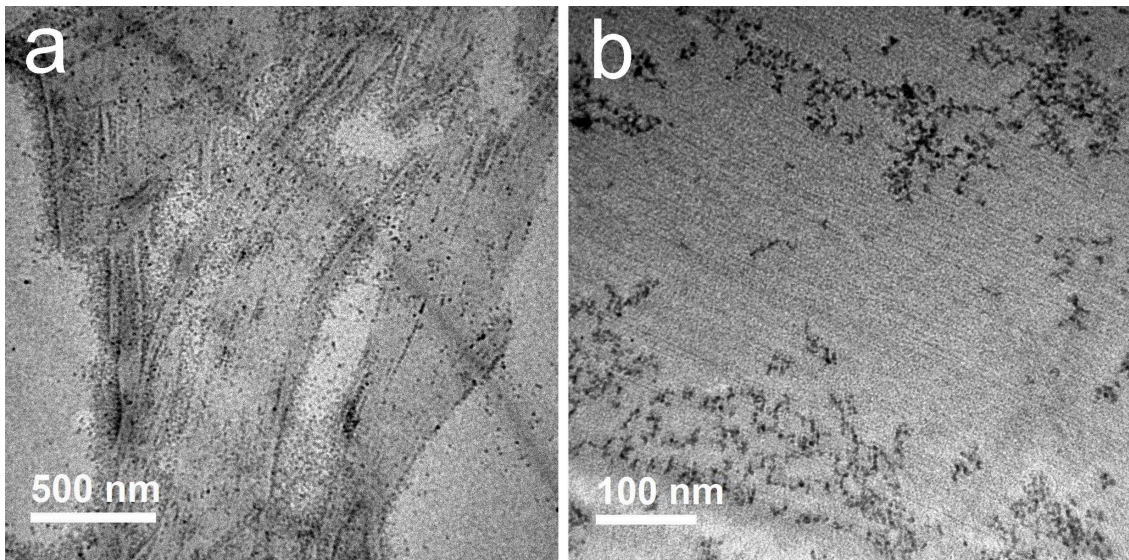


Figure 58 Transmission electron microscopy images of the control NS peptide a) with green Qdots and b) with red Qdots. No particular oriented arrangement was observed since the peptide is not attaching covalently the Qdots.

The TEM analysis of the cysteine containing peptide, CS, with the two different sizes of Qdots was followed. Figure 59 a shows regular arrangement of the 2.6nm sized, Qdots on the surface of the self-assembled peptide fibril film. There is a remarkable alignment of the Qdots on the surface of the film. Figure 59b shows a low magnification image for representation the size of the film. Figure 61a shows regular arrangement of the 4nm sized Qdots on the surface of the self-assembled peptide fibril film, showing similar ordering on the surface of the film. Figure 61b shows a low magnification image for representation the size of the film.

Figure 59c and Figure 61c shows a schematic arrangement of the Qdots on the surface of the film. The scheme is up to scale with the width of the fibril to be 2.8nm (Figure 55b), the size of the dots 2.6nm for the green and 4nm for the red Qdots respectively, and the TOPO layer thickness to be approximately 1nm (Ji et al., 2005). The shell thickness of the green Qdots is similar in both samples.

In Figure 59c the measured distances between the Qdots are $a=6.5 \pm 0.6\text{nm}$ between the centers of the Qdots perpendicular to the axis of the fibril and $b=5.9 \pm 0.6\text{nm}$ between the centers of the Qdots along the axis of the fibril. Those measurements derive from the Gaussian fitting of approximately 50 measurements of each distance (a , b) shown in Figure 60. According to these measurements there is space for only one more dot (dashed circle) to fit between the four.

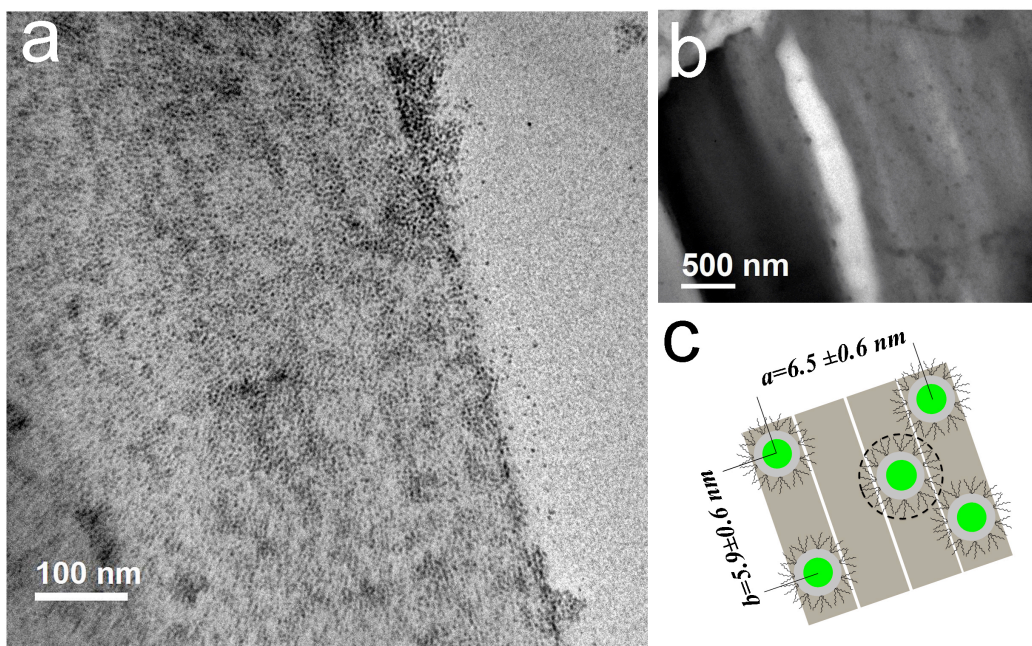


Figure 59 Transmission electron microscopy images of the thiol containing CS peptide with green Qdots a) fibril film with oriented templating of the Qdots b) Low magnification image of the film c) Schematic representation of the Qdot average local structural arrangement templated by the fibril film.

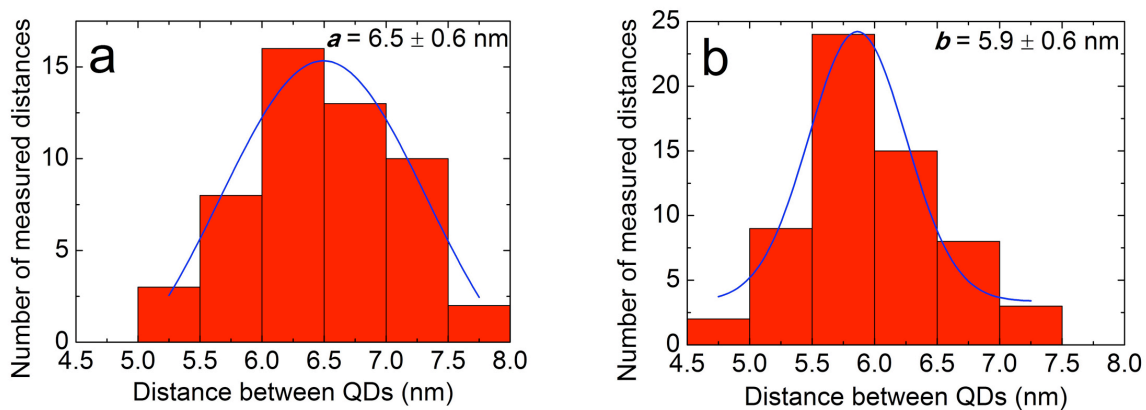


Figure 60 a) Distance between the between the centers of the Qdots perpendicular to the axis of the fibril and b) Distance between the centers of the Qdots along the axis of the fibril, for the green Qdots

In Figure 61c the measured distances between the Qdots are $a=14.4 \pm 1.7\text{nm}$ between the centers of the Qdots perpendicular to the axis of the fibril and $b=13.1 \pm 1.3\text{nm}$ between the centers of the Qdots along the axis of the fibril. Those measurements derive from the Gaussian fitting of approximately 50 measurements of each distance (a , b) shown in Figure 62. According to these measurements there is space for another dot (dashed circle) to fit between the four.

Although there are several binding sites on the surface of the fibrils it may not be possible to be occupied all at the same time, due to steric hindrance amongst the Qdots (Bui et al., 2010). This could be a reasonable explanation for the non- canonical and parallel ordering of the quantum dots between the fibrils.

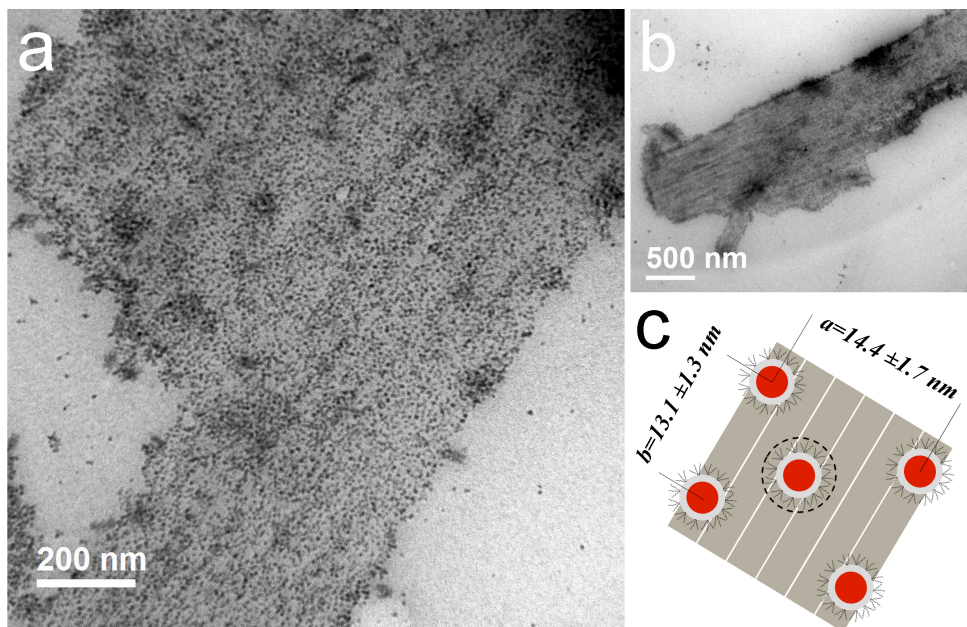


Figure 61 Transmission electron microscopy images of the thiol containing “CS” peptide with red Qdots a) fibril film with oriented templating of the Qdots b) Low magnification image of the film c) Schematic representation of the Qdot average local structural arrangement templated by the fibril film.

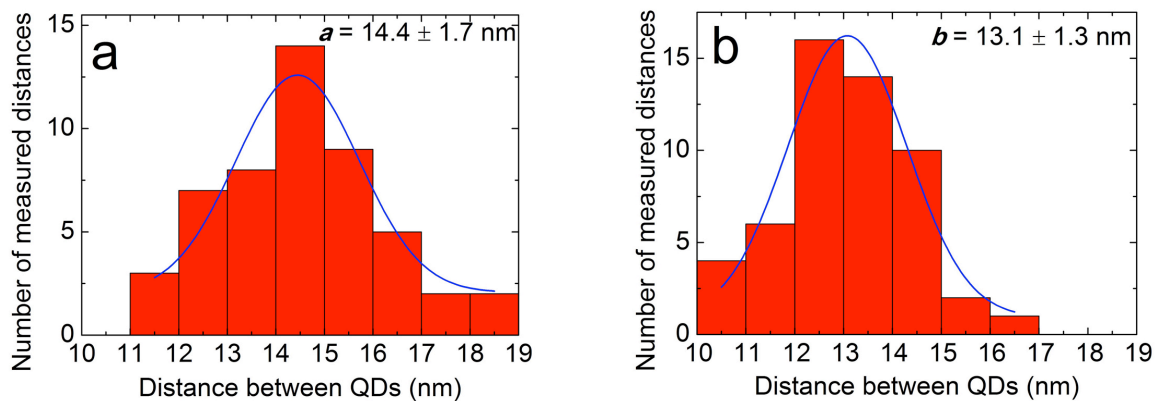


Figure 62 a) Distance between the between the centers of the Qdots perpendicular to the axis of the fibril and b) Distance between the centers of the Qdots along the axis of the fibril, for the red Qdots

Finally the peptide fibril films templated with Qdots have been characterized with Photoluminescence analysis. Three different types of samples were prepared for each Qdot size, 2.6nm ($\lambda_A=526\text{nm}$) for the green and 3.95nm ($\lambda_A=584\text{nm}$) for the red. The first was solely the preformed Qdots (Solid lines, Figure 64). The second was the Qdots conjugated with the CS peptide before the addition of the aqueous phase (Dashed lines, Figure 64). The third sample was the film templated with the Qdots after the 24h incubation (Dashed dot lines, Figure 64).

Both green and red dots show the same emission peak before and after conjugation with the peptide. When the dots are ordered on the surface of the self-assembled fibril film the emission peaks exhibit a red shift. In Figure 64a, the green quantum dots show a 12nm red-shift whereas in Figure 64b the red quantum dots show an 8nm red-shift. This red shift has been previously reported in the literature and is attributed to long-range resonance transfer or else Förster resonance energy transfer (FRET) (Kagan et al., 1996) (Piston and Rizzo, 2008).

According to FRET theory when two luminescent molecules (dyes, quantum nanocrystals) are within a certain distance (maximum 10nm) and are being excited by radiation, then energy transfer occurs upon relaxation from the molecule with the higher energy band gap (E_g) to the one with lower energy band gap (E_g). The molecule with the higher E_g is termed as donor and the other as acceptor (Figure 63).

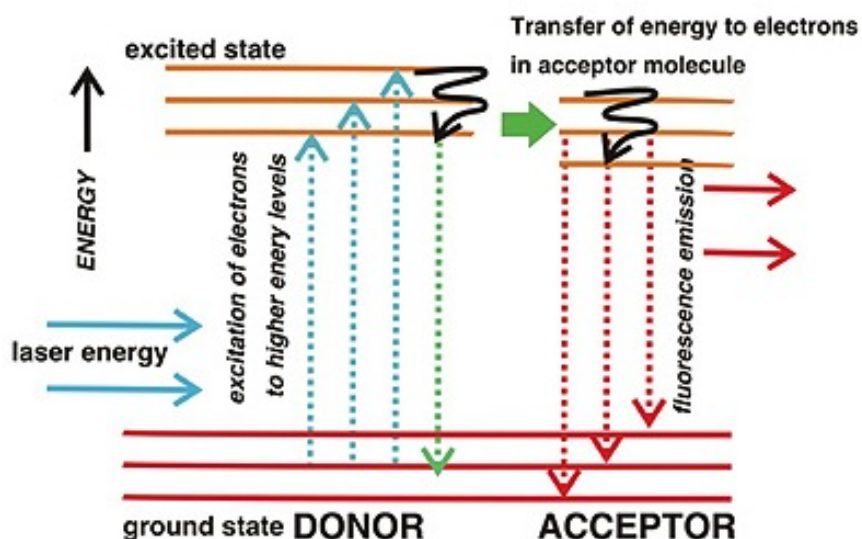


Figure 63 Förster Resonance Energy Transfer process
 (<http://www.ncl.ac.uk/bioimaging/techniques/fret/>)

In our case the quantum dot solutions are not monodisperse and they contain smaller and bigger particles relative to their average size. The smaller particles could behave as donors and the bigger as acceptors (see equation Figure 50). The amount of energy transfer (E_T) depends on the distance (R) between the donor and acceptor and according to theory (Dollefeld et al., 2002) the E_T follows the equation ($E_T \sim 1/R^6$). This means that the closer the molecules are, the bigger the energy transfer. This relationship is in agreement by our results since the green quantum dots are more closely packed (Figure 59c) than the red quantum dots (Figure 61c) and the shift is larger than the former. The templated arrangement may offer a way of controlling the photoluminescent properties of quantum dot nanofilms.

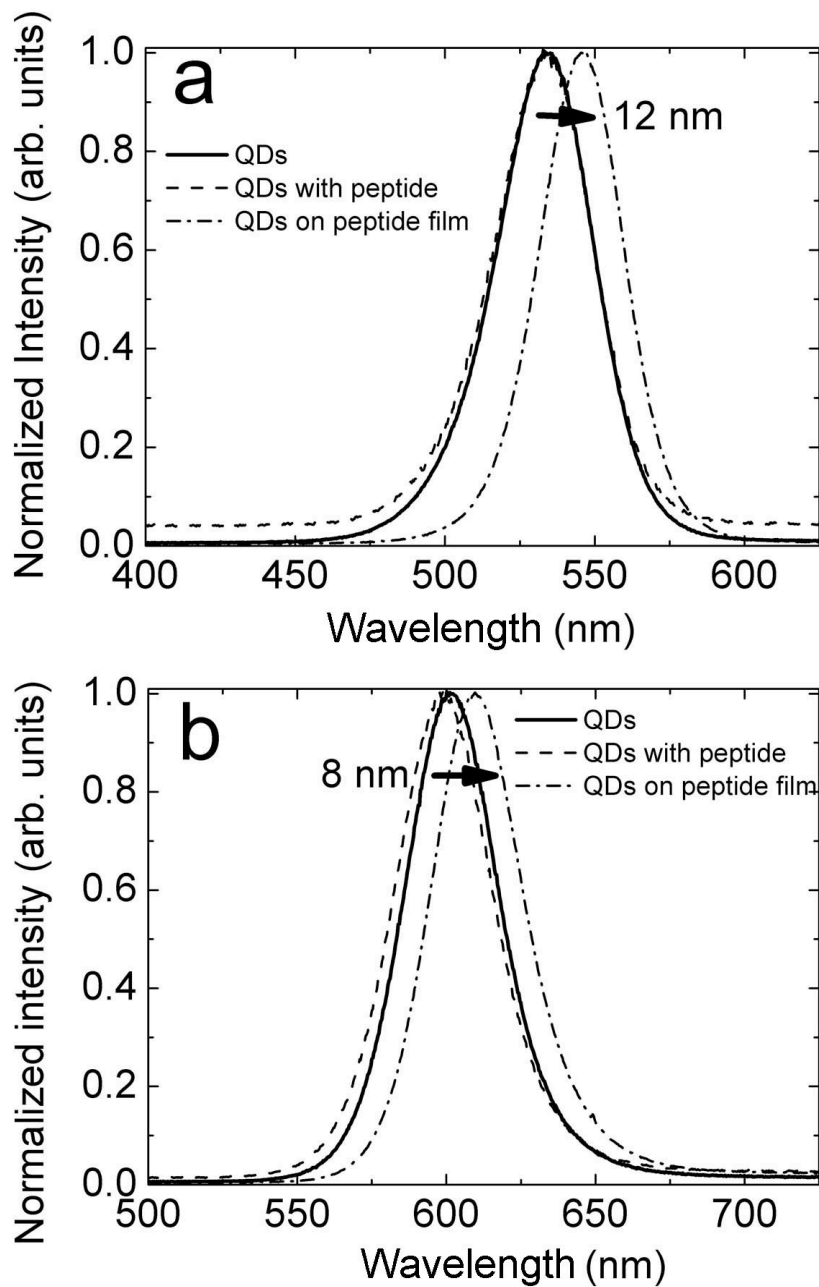


Figure 64 Photoluminescence experiments on the solid-state samples with a) Green and b) Red quantum dots. (Solid lines: Quantum dots, Dashed lines: Qdots with peptides, Dashed dot: Qdots on peptide film)

7.4 Conclusions

In summary, we have used the principles of self-assembly and thiol chemistry to achieve the fabrication of 2D quantum dots templated on fibril films. For this purpose we have used a self-assembling octapeptide, which is endowed with a cysteine that provides the thiol anchoring point. The peptide was studied in the interface between two non-miscible solvents, water and chloroform. It was found that the peptide forms well-ordered fibril films after the characterization with electron microscopy. The post-templating of preformed CdSe/ZnS quantum dots was achieved by mixing the peptide and the quantum nanoparticles in one phase, deposit the second solvent phase and letting the system to equilibrate.

The ordering of the Qdots on the surface of the fibrils induces a red shift in their emission peaks relative to their solution state. The importance of ordering and the changes in properties of the nanoparticles when they are into closed packed assembly has been addressed many years ago (Murray et al., 2000).

The properties of the final ensembled structures differ from the individual molecules and this new field is still unexplored. Focussing on quantum dot nanoparticles and their assemblies many groups have confirmed the changes in photoluminescent properties when the particles are arranged in close proximity (Galeotti et al., 2011) (Dollefeld et al., 2002) (Babayan et al., 2004) (Kumara et al., 2007a) (Gattas-Asfura et al., 2005). All these efforts to combine different interaction principles for the stability of the assembled nanocrystals have as an ultimate target the fabrication of novel materials for applications mainly in optoelectronics (by reducing the size of the devices), in light generation and optical switches, in data storage (through the assembly of ferromagnetic particles), in sensing purposes (through changes in physical properties such as photoluminescence or magnetic relaxation) and in imaging of biological components (Nie et al., 2010).

In this work an amphiphilic peptide was used both as ligand exchange element (via its cysteine residues) and at the same time as structural scaffold for the ordering of Qdots. The scaffolding properties are mediated by the ability of the amphiphilic peptide to self-assemble into films at the air-water interface. We believe that this protocol makes proof-of-principle for the 2D templating of Qdots on a self-assembled peptide film. It could be generally applied for other amphiphilic peptides with functional groups on their sequence and with various types of particles.

CHAPTER 8 CROSS-LINKING OF SELF-ASSEMBLING PEPTIDES

8.1 Background and state of the art

Fabricating complex structures with both stability and elasticity has been a challenging issue for biomaterials science. One of the strategies that Nature uses for the reinforcement of natural fibrous proteins is covalent crosslinking. In insects elastic proteins such as resilin are located at the joints and tendons and they are crosslinked with tyrosine residues creating dityrosine or trityrosine (Neff et al., 2000). Resilin gives a characteristic strong blue fluorescence under UV light with an emission maximum at 420nm, which is attributed to dityrosine. Tyrosine has an emission around 310nm (Figure 66c). This type of crosslinks confers to the material high rubber efficiency (resilience) and a very high fatigue lifetime. After the in vitro recombinant synthesis of resilin protein and insertion into a mold scientists formed dityrosine crosslinks through enzymatic process and finally created a rubber like material for biomedical applications (Figure 66) (Elvin et al., 2005).

Dityrosine crosslinks were identified approximately 50 years ago and they are located in proteins connected with age and oxidative stress (DiMarco and Giulivi, 2007). The dityrosine bond is not reversible, compared to the disulphide bond (Figure 65).

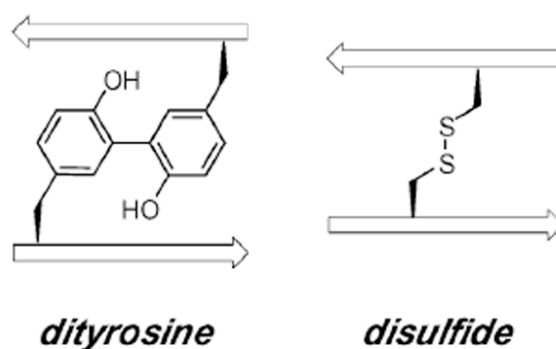


Figure 65 Dityrosine and Disulfide bridges (Yoburn et al., 2003).

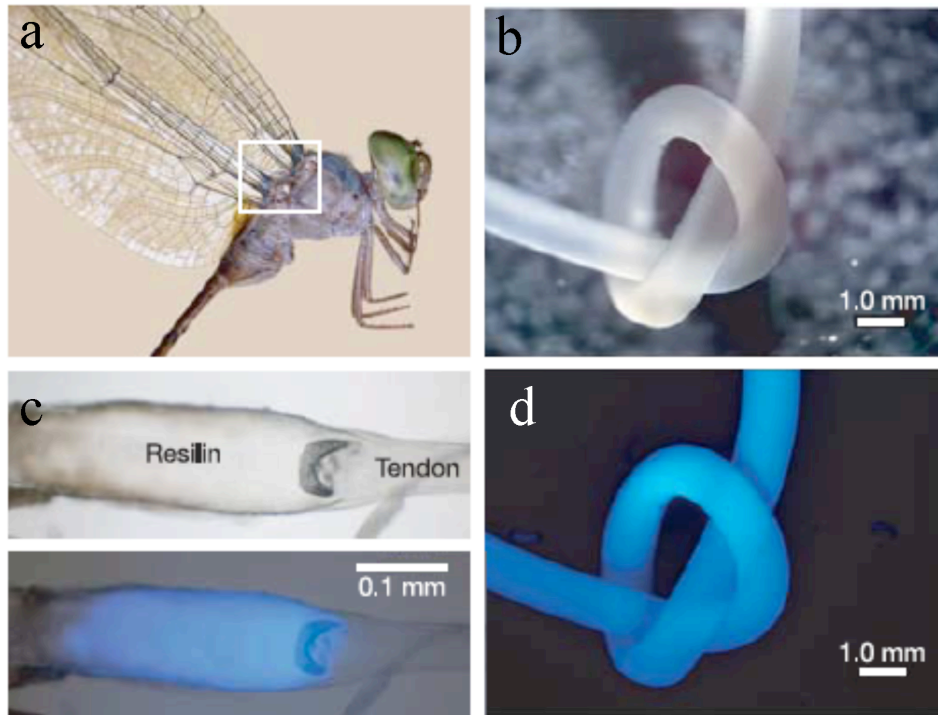


Figure 66 a) Part of the tendon from adult dragonfly (Zyxomma sp.) c) Fluorescence of resilin in the tendon wing under white light and ultraviolet light b) Fluorescence of a molded rod with recombinant resilin protein under white light and d) ultraviolet light (Elvin et al., 2005)

In vitro dityrosine crosslinks are created mainly by three methods. The first is through enzymatic process with peroxidase enzymes (Malencik and Anderson, 1996), the second is with photogenerated oxidants (Fancy and Kodadek, 1999) and the last using ultraviolet radiation of specific energy. The third method is more instant and it does not involve the presence of other molecules in the solution. The mechanism in both cases follows the path shown in Figure 67.

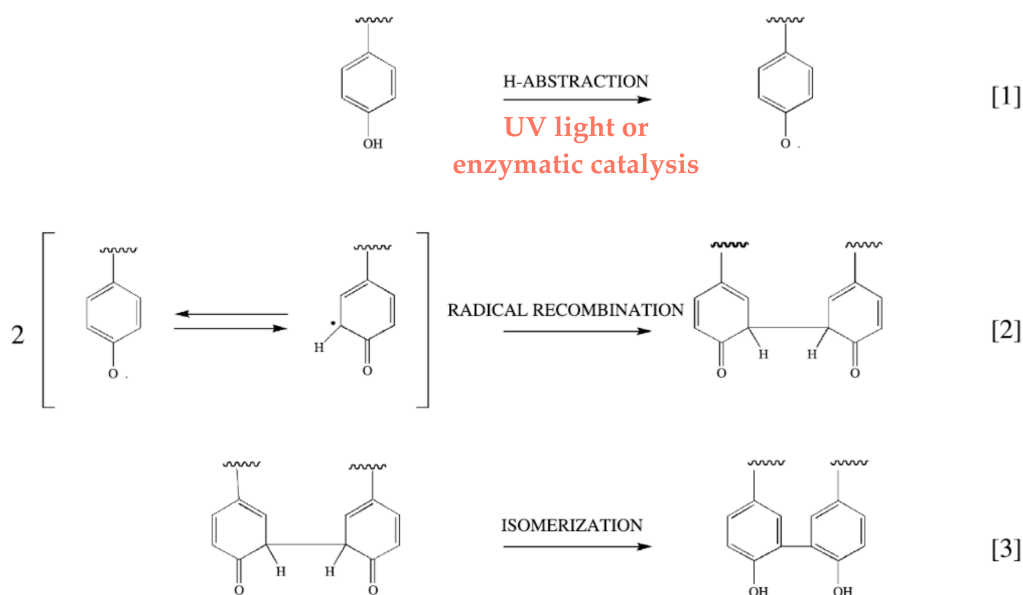


Figure 67 Dityrosine formation scheme: (1) Tyrosine and radical formation by UV (2) radical recombination (3) dityrosine isomerization and formation.

Initially the mechanism shows the formation of tyrosyl radicals after the UV light excitation. Then two of these radicals are combined together creating a dityrosine dimer. Finally after enolization the dityrosine crosslink is formed. Dityrosine can be detected by its fluorescent emission at 420nm upon excitation at 315nm (alkaline solutions) or 284nm (acidic solutions) (Giulivi et al., 2003). Lazare and colleagues reported for the first time the laser induced irradiation (Laser-Induced fluorescence (LIF)) of collagen matrix, with a specific energy, and the formation of a micro-foam structure (Lazare et al., 2005). After the spectroscopic study of the structure it was found that new type of cross-links were formed (Wisniewski et al., 2007). These cross-links were among tyrosine residues resulting in the formation of dityrosine. The same group developed nanofoaming structure by changing the frequency of the laser pulses and those scaffolds can be used for cell attachment and proliferation (Gaspard et al., 2007).

Self-assembling amyloid fibrils as described in previous chapters offer great advantages of templating their structures with materials after minor modifications to the native peptide sequence. In addition to templating with metal, quantum dot and silica nanoparticles, one more application that we can impose to the fibrous network is to create covalent crosslinks between the fibrils. The crosslinking enhances the stability of the structure and could provide new properties for cell and drug delivery applications to the material. Using the original building block as our starting model we substituted the

asparagine (Asn (N)) in the first position with a tyrosine (Tyr (Y)) residue and the resulting peptide was the NH₂-YSGAITIG-CONH₂. Following the self-assembly of the peptide in aqueous environment irradiation with specific energy was performed and dityrosine crosslinking was detected and analyzed.

8.2 Methodology

8.2.1 Stock solutions

Lyophilized peptide powder was dissolved in double distilled water at 10mg/ml concentration. 500 microliters were added in a quartz cuvette (Hellma 110-QS). For pumping and probing we used a fluence of $F_{\text{pump}}=66 \text{ mJ/cm}^2$ and $F_{\text{probe}}=5 \text{ mJ/cm}^2$ respectively.

Tyrosine amino acid, (purchased from Sigma) was dissolved into 0.34 mg/ml. 500 microliters were added in a quartz cuvette (Hellma 110-QS) and were irradiated with the same energies mentioned above.

8.2.2 Mass spectrometric analysis protocol

Non-irradiated and irradiated peptides were resuspended in H₂O at a final concentration of 10mg/ml. 1 μL of each were mixed with 4 μL of 50% ACN (acetonitrile, HPLC grade, Scharlau) in 0.1% TFA (trifluoroacetic acid, Merck, Germany), and equal volumes (0.5 μL) of peptide and matrix solution, consisted of 3 mg of alpha-cyano-4-hydroxycinnamic acid dissolved in 1 mL of 50% ACN in 0.1% TFA were deposited using thin layer method, onto a 384 Opti-TOF MALDI plate (Applied Biosystems, Framingham, MA). Mass spectrometric data were obtained using a 4800 MALDI-TOF/TOF analyzer (Applied Biosystems, Framingham, MA). MS spectra were acquired in reflector positive-ion mode with a Nd:YAG, 355nm wavelength laser, averaging 1000 laser shots and using a mix of peptides, bradykinin 1-7, angiotensin II, angiotensin I, substance P, bombesin, renin substrate, ACTH clip 1-17, ACTH clip 18-39, and somatostatin 28 (Bruker Daltonics, Bremen, Germany) as external calibration. The comparison of both samples was performed using the Data Explorer v4.9 software (Applied Biosystems, Framingham, MA).

8.3 Results and Discussion

Before any experimental trial for cross-linking of the peptide YSGAITIG peptide, the self-assembly amyloid fibril formation was checked. Transmission electron microscopy shows (Figure 68) that the peptide self-assembles into amyloid fibrils coexisting with tapes. The amyloid architecture was confirmed by X-ray fiber diffraction.

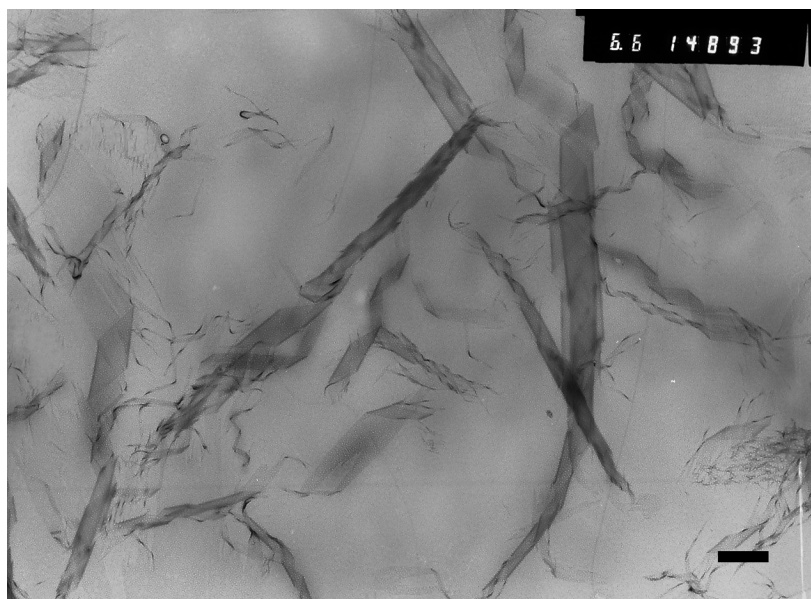


Figure 68 Self-assembling peptide ribbons (Scale bar: 140nm)

Following TEM characterization, irradiation of the solution using the LIF technique (described in Methods) was performed. The spectrum was acquired in real time and it is shown in Figure 69. The tyrosine residue fluoresces at 310nm and dityrosine molecule fluoresces at 420nm. It is clear that before any number of pulses (Probe method), tyrosine is detected. After a certain amount of pulses the tyrosine intensity is decreased while the dityrosine intensity is increased. As the sample continues to be irradiated with more pulses the intensity of dityrosine is increased.

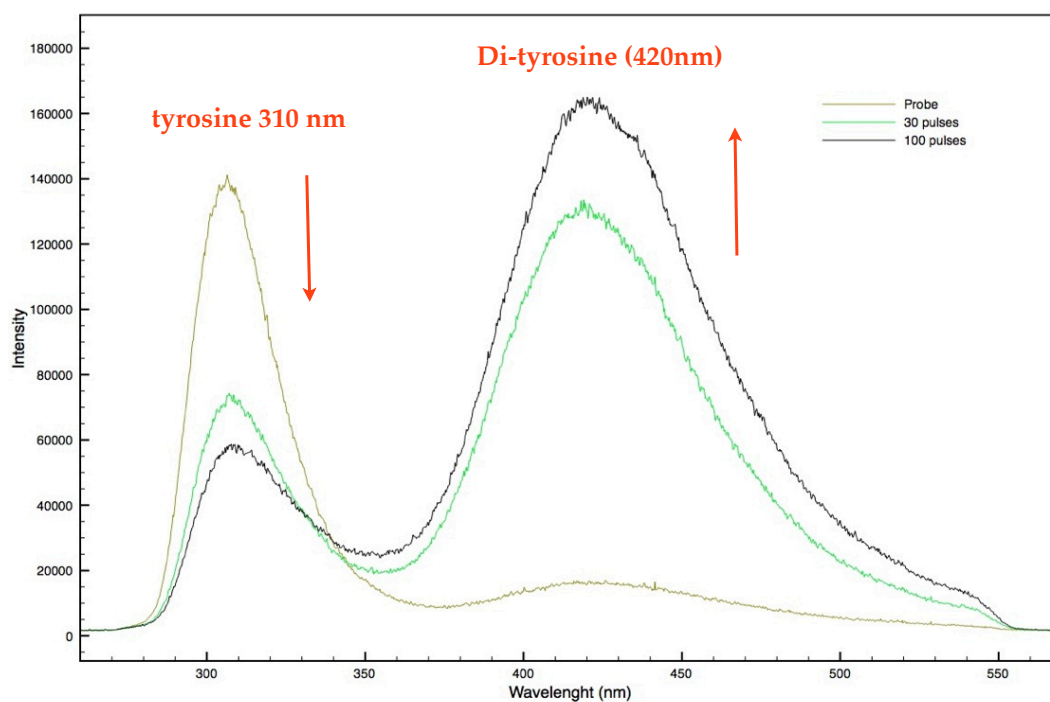


Figure 69 Fluorescence spectrum of dityrosine formation in the peptide solution

Observing the cuvette under a UV optical microscope the sample shows the characteristic blue color comparing with irradiated H₂O solution. This is an optical evidence for the dityrosine presence in the solution (Figure 70).

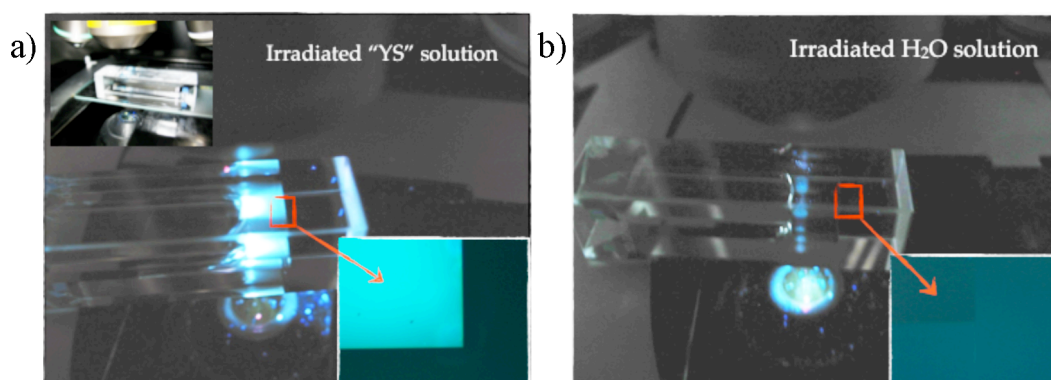


Figure 70 Cuvettes under the UV microscope of a) irradiated peptide solution and b) irradiated water solution

In order to test the non-destructive dityrosine formation in the isolated tyrosine amino acid, a single tyrosine solution was irradiated as well. The fluorescent spectrum shows the

absence of dityrosine before irradiation and the continuous formation of dityrosine due to the increased number of pulses (Figure 71).

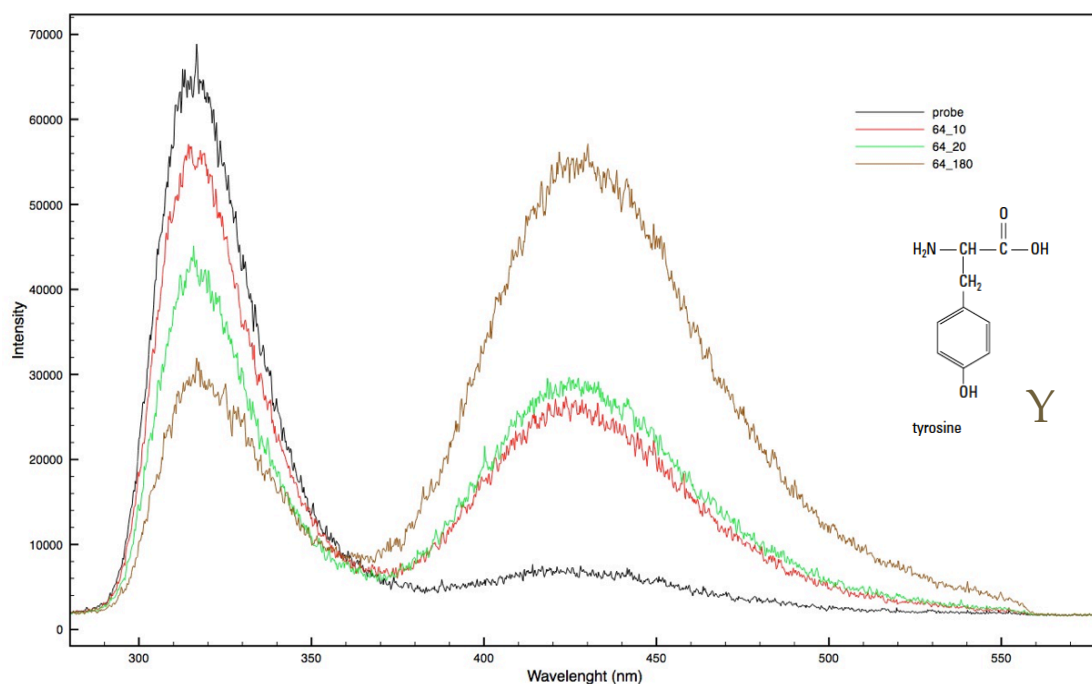


Figure 71 Fluorescent spectrum of dityrosine formation in the tyrosine residue solution

Mass spectrometry analysis was performed to the YSGAITIG, in the irradiated and non-irradiated peptide in order to detect the molecular weight of the product. The peptide has a molecular mass of 780 Da. In the first part of the mass spectrum (400-1000) (Figure 72), at the non-irradiated sample the peak of 780 is detected corresponding to the peptide monomer. After the irradiation of the sample the intensity of the peak at 780 in the spectrum (400-1000) is decreased and the dityrosine peptide dimer, which has a molecular mass of 1558, is detected in the second part of the spectrum (1400-1700) (Figure 73).

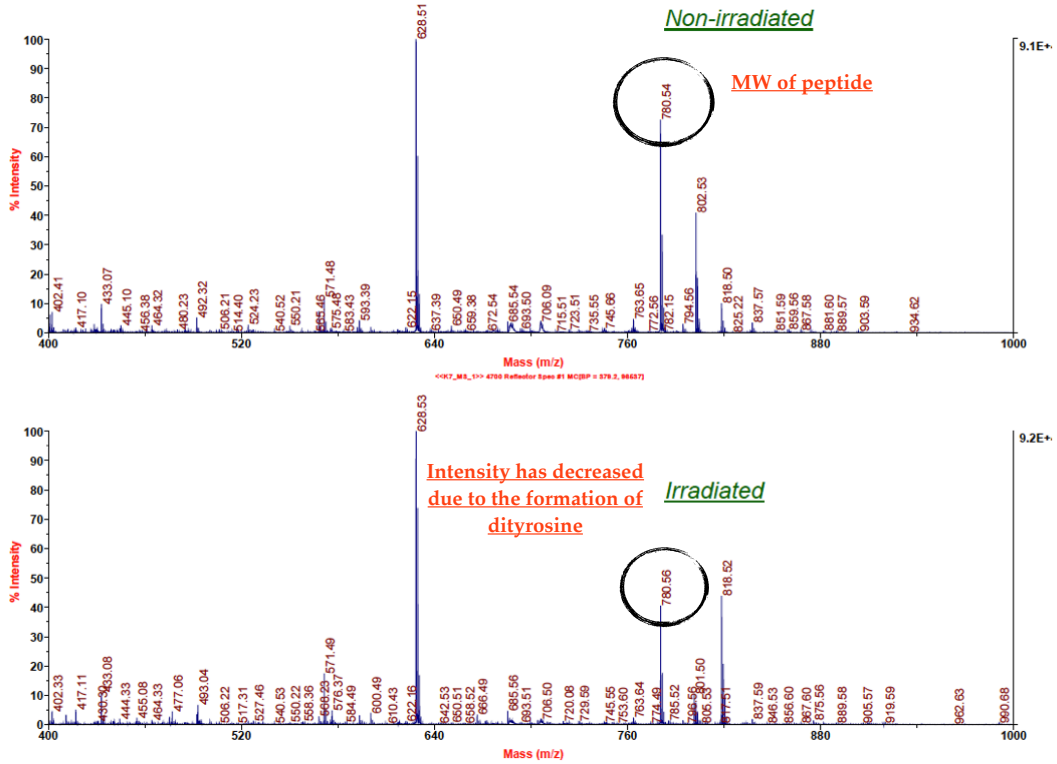


Figure 72 Mass Spectrum of non-irradiated and irradiated peptide Scale: 400-1000

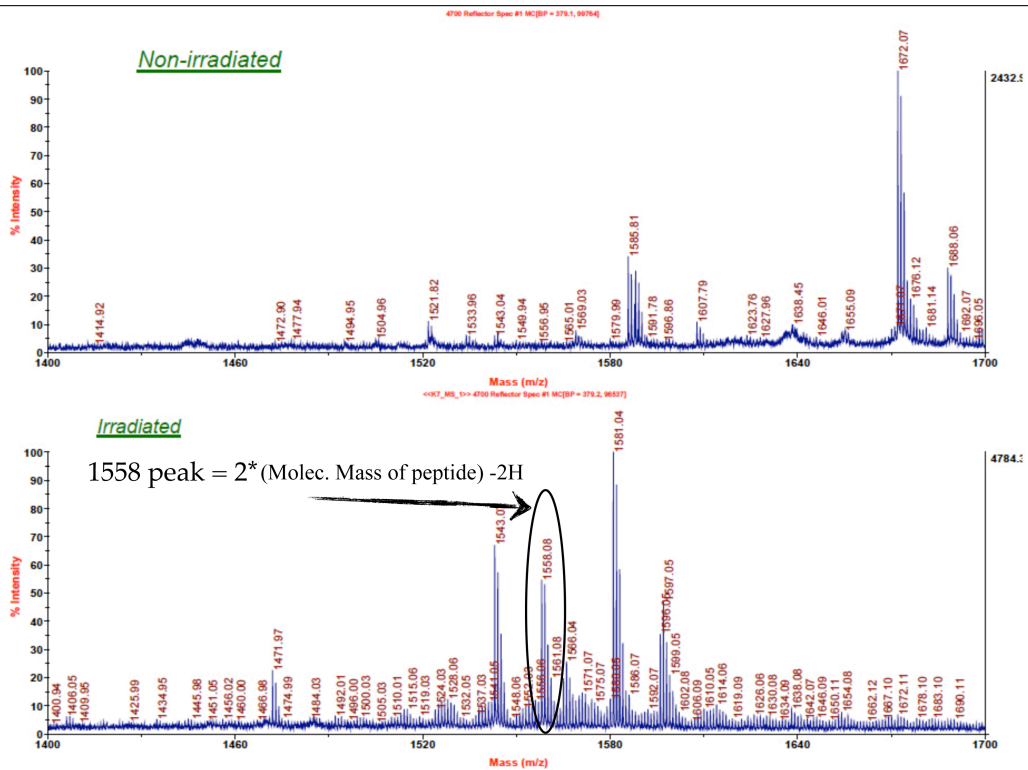


Figure 73 Mass Spectrum of non-irradiated and irradiated peptide Scale: 1400-1700

8.4 Conclusions

Cross-linking through laser-induced irradiation was successfully performed in the YSGAITIG self-assembling peptide system. The cross-linking network is attributed to dityrosine formation, which was confirmed with spectroscopy and mass analysis. This is therefore a direct technique allowing the creation of covalent crosslinks between amyloid fibrils network. This technique can be used for enhancing the elastic properties of self-assembling protein or peptide self-assembled materials without the addition of any other crosslinking factor. Of particular interest, is the possibility of hydrogel formation in higher peptide concentrations and various environments. Indeed, self-assembling peptide hydrogel matrices can be used as scaffolds for mineralization, drug delivery and cell attachment. (Branco et al., 2009). Creating covalent cross-links can confer improved physical properties to this type of self-assembling scaffolds.

CHAPTER 9 HYBRID PEPTIDE-PORPHYRIN SELF- ASSEMBLING MATERIALS

9.1 Background and state of the art

The novel synthesis of light-harvesting materials at the nanoscale has been the center of attention for energy conversion and storage devices. Nature with photosynthesis has already developed such systems and uses natural pigments (Caple et al., 1978) at certain intramolecular distances in order to optimize energy transfer, photon capture and electronic coupling. Materials Science has developed new hybrid materials for energy purposes, which consist of organic and inorganic (usually semiconducting) materials. Those materials are applied into the new type of solar cells, the Dye-sensitized solar cells (DSSCs) (Gratzel, 2003). In contrast to the common solar cells where the semiconductor has a double function of light absorption and charge carrier transport, in DSSCs systems light is absorbed by a specific dye that functions as a sensitizer, which is anchored in a semiconductor. This gives the ability to use dyes with a wide absorption spectrum and finally harvest more fraction of sunlight.

For the synthesis of new materials two important parameters have to be considered. First a synthetic analogue of natural pigments has to be used for converting sunlight into electric current and second a biological scaffold is prerequisite for the ordered intramolecular deposition of the pigment (Dunetz et al., 2005; Konovalova et al., 2001).

Porphyryns are natural organic aromatic compounds (Figure 74 c) that occur in Nature. A characteristic example is Heme (Figure 74 a), which facilitates in the oxygen transport in red blood cells. Porphyryns have been explored a lot as photosensitizers in different types of solar cells (Imahori et al., 2009) (Bessho et al., 2010).

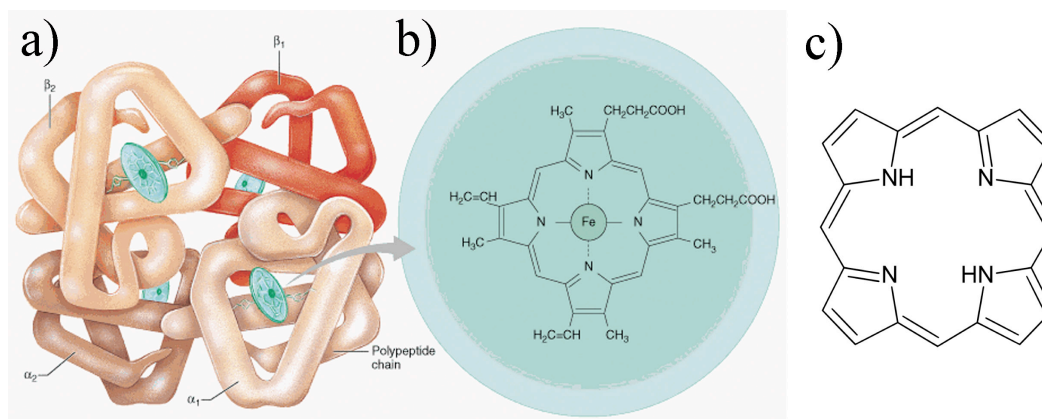


Figure 74 a) Hemoglobin b) Iron containing heme group c) Structure of the simplest porphyrin (<http://legacy.owensboro.kctcs.edu/gcaplan/anat2/notes/APIINotes6%20Blood%20RBC.htm>)

There are a number of reports on porphyrin molecules attached to self-assembling peptides. Kokona reported the non covalent interactions of a negatively charged porphyrin molecule with the basic residues of the peptide “Ac-Ile-Gln-Gln-Leu-Lys-Asn-Gln-Ile-Lys-Gln-Leu-Leu-Lys-Gln-CONH₂”, termed Cp3K-N (Kokona et al., 2009). The peptide self-assembles into a helical structure; it was found that the structure of the conjugate is retained as the peptide without the porphyrin molecule. Dunetz reported the attachment of two porphyrin molecules to the decapeptide CH₃CONH-Asn-Ala-Glu-Ala-Ser-Ala-Glu-Ser-Ala-Tyr-CONH₂ via amide coupling with the two negatively charged glutamic acid residues (Dunetz et al., 2005). The group was among the first that demonstrated such a hybrid system of self-assembly. The new building block has been studied among various parameters such as pH, concentration and temperature and has been found that it self-assembles into a helix.

The previously adopted strategy for the design of novel functional nano materials, as we mentioned in all chapters, consisted in the predesign of the building block with functional groups and the post templating/modification of it. An alternative strategy consists in the chemical pre-functionalization of the peptide followed by the self-assembly of the hybrid building block. In this chapter, we describe the covalent attachment of porphyrin molecules to a peptide building block and the study of its self-assembling properties.

Within the framework of the functionalization of adenovirus-derived self-assembling peptides (Ad-SAPs), we sought to form conjugates with porphyrin molecules for the fabrication of hybrid amyloid fibrils with photoelectronic properties. However, the quantities of the peptides needed for this type of experiments imposed a severe limitation since Ad-SAPs are not a commercially available system. Another limitation was that the adenovirus peptides have side chains, which can interfere when the chemical coupling of the porphyrin

molecule at one unique position is wanted. Keeping our experimental idea intact, another well-studied self-assembling system was selected for creating hybrid peptide-porphyrins, testing their self-assembling ability, and subsequently their photoelectronic properties

Gazit's diphenylalanine self-assembling peptide system was selected since this system is commercially available in large quantities, has two non-reactive side chains and offers many possibilities of modifications (Reches and Gazit, 2003). The diphenylalanine peptide self-assembles into well-structured nanotubes. Upon changing the protection group on the N-terminus of the peptide with a Boc or Fmoc group and using binary solvent systems, the peptides can form nanospheres or hydrogels instead of nanotubes (Adler-Abramovich and Gazit, 2008) (Mahler et al., 2006). The original hypothesis was to decorate the nanotubes with well-ordered porphyrin molecules. If the FF peptides nanotubes could maintain the ability to self-assemble into nanotubes within the hybrid construct, then they could guide the nanoscale organization of the porphyrin moiety.

9.2 Methodology

This work was carried out in collaboration with Prof. Athanassios Coutsolelos, Dr. Georgios Charalambidis and Dr. Theodore Lazaridis from the Department of Chemistry and was recently published. My contribution consisted in the study of the self-assembling properties of all the conjugates synthesized by the Chemistry group. In addition, they carried out the spectroscopic and electrochemical characterization of the conjugates (Charalambidis et al., 2011).

The diphenylalanine (F-F) peptide is known to self-assemble into nanotubes after dissolving in 1,1,1,3,3,3-hexafluoro-2-propanol (HFIP) and subsequent dilution in water (Reches and Gazit, 2003). Five different hybrid derivatives were synthesized: monoaminoporphyrin conjugated with F-F, unprotected and protected with Boc and Fmoc groups and, for comparison, the single phenylalanine-porphyrin hybrid compound with and without Fmoc protection (Figure 75). The phenylalanine amino acid by itself has not been reported to form any self-assembled structures.

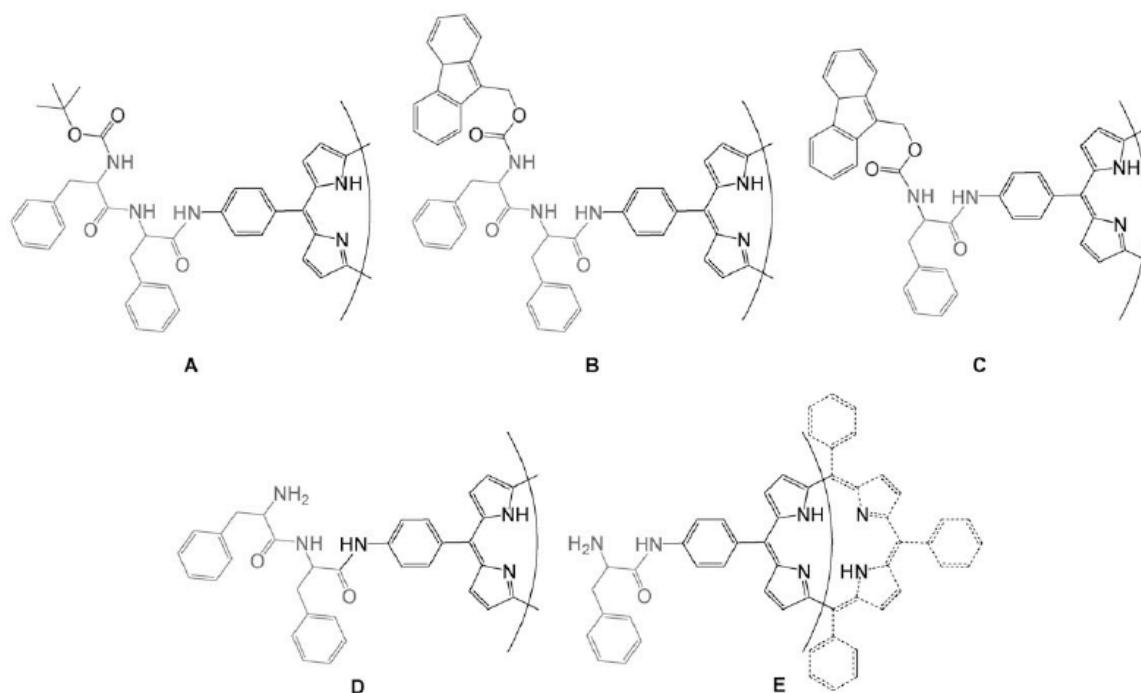


Figure 75 The five hybrid coupled derivatives: monoaminoporphyrin-FF-Boc (Boc-FF-P) (A), monoaminoporphyrin-FF-Fmoc (Fmoc-FF-P) (B), monoaminoporphyrin-F-Fmoc (Fmoc-F-P) (C), monoaminoporphyrin-FF (FF-P) (D) and monoaminoporphyrin-F (F-P) (E).

All the hybrid peptides were studied following a similar protocol to the F-F nanotube formation and the solvents used were water, methanol, ethanol, acetonitrile and THF. The proportion of solvent to HFIP was 80/20 and the concentration was kept constant at 7mM. All the peptides (protected or not) and the monoaminoporphyrin molecule were tested as well as control samples. Only the studies with methanol and THF are shown extensively in the following chapters.

9.2.1 Peptide-porphyrin hybrids studied in methanol

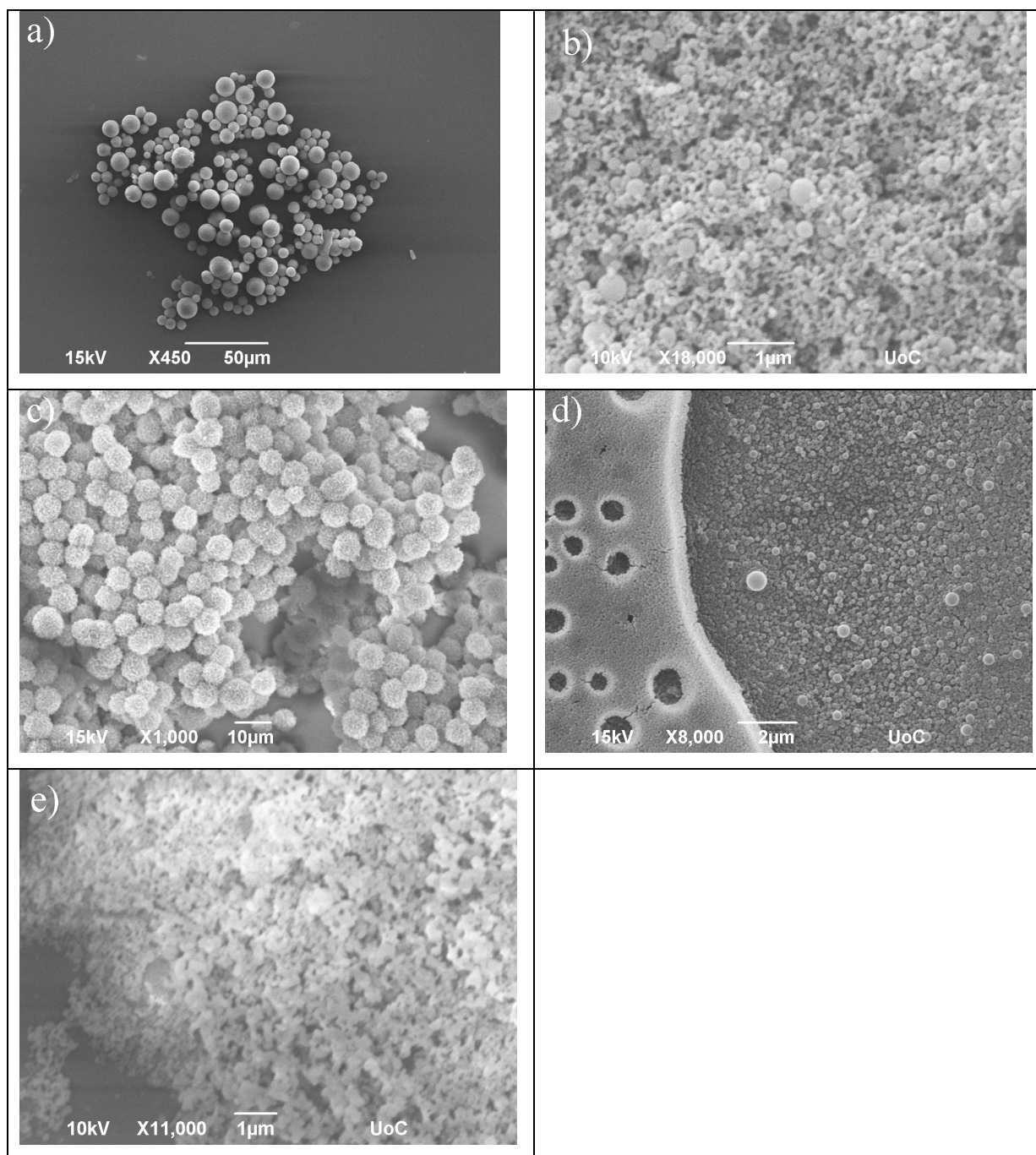


Figure 76 Scanning electron microscopy analysis of the peptide-porphyrin conjugates (7mM concentration), prepared in 20% HFIP and 80% methanol and subsequent dried on glass slides after one day of incubation a) Boc-FF-P, b) Fmoc-FF-P, c) FF-P, d) Fmoc-F-P, e) F-P

9.2.2 Peptide controls studied in methanol

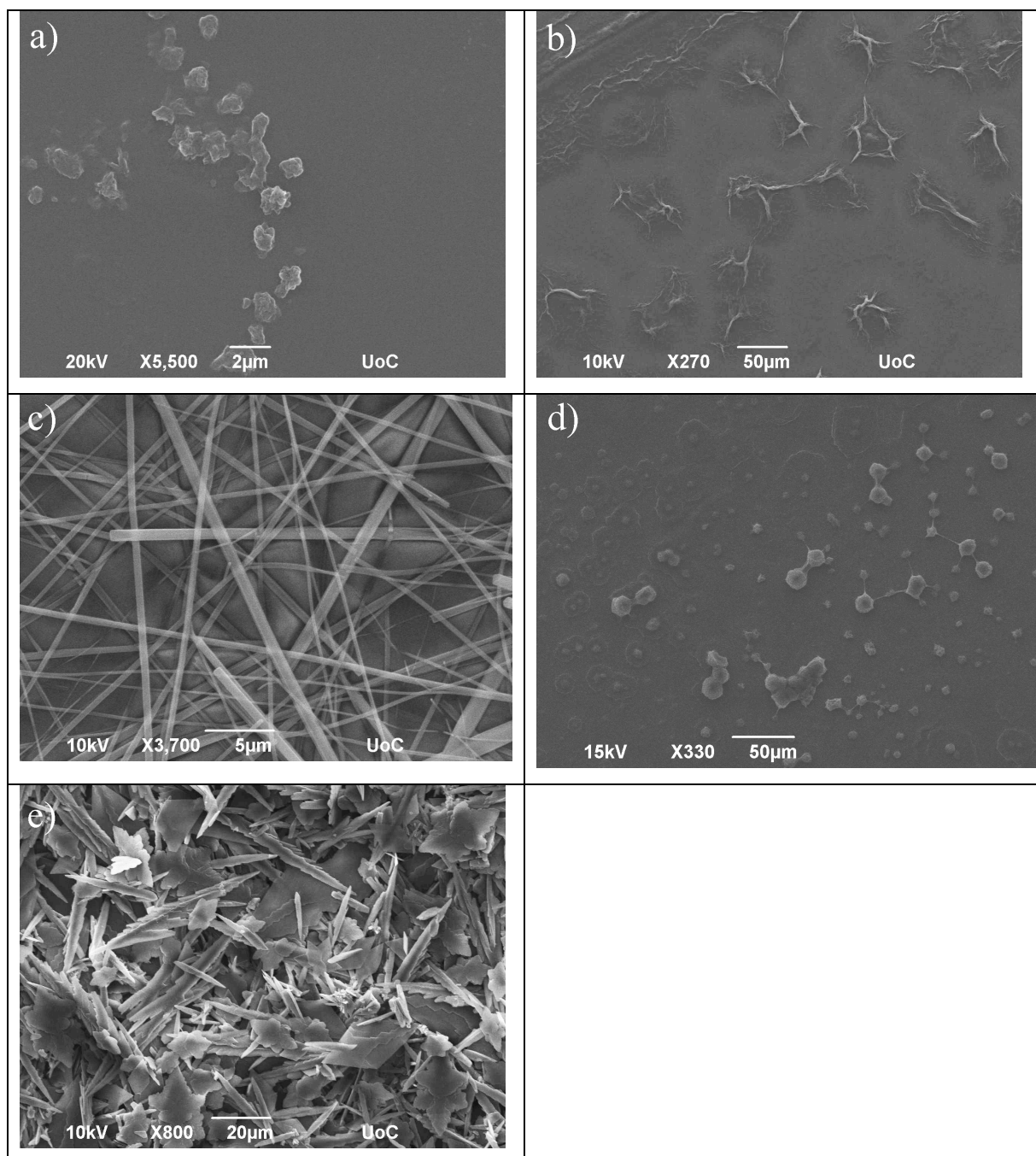


Figure 77 Scanning electron microscopy analysis of the control peptides and the porphyrin molecule (7mM concentration), prepared in 20% HFIP and 80% methanol and subsequent dried on glass slides after one day of incubation. a) Boc-FF, b) Fmoc-FF, c) FF, d) Fmoc-F, e) Porphyrin molecule

9.2.3 Peptide-porphyrin hybrids studied in THF

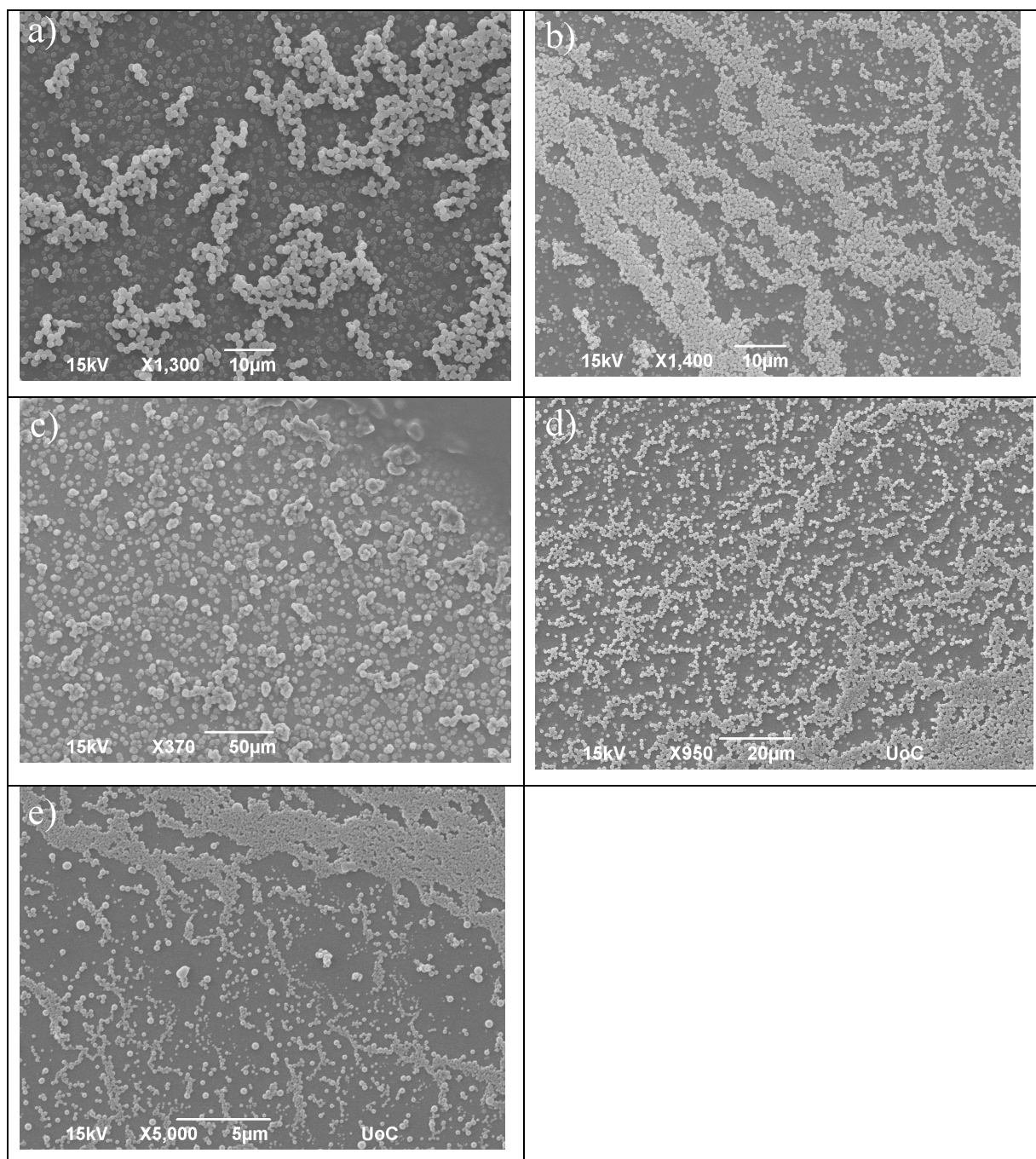


Figure 78 Scanning electron microscopy analysis of the peptide-porphyrin conjugates (7mM concentration), prepared in 20% HFIP and 80% THF and subsequent dried on glass slides after one day of incubation. a) Boc-FF-P, b) Fmoc-FF-P, c) FF-P, d) Fmoc-F-P, e) F-P

9.2.4 Peptide controls studied in THF

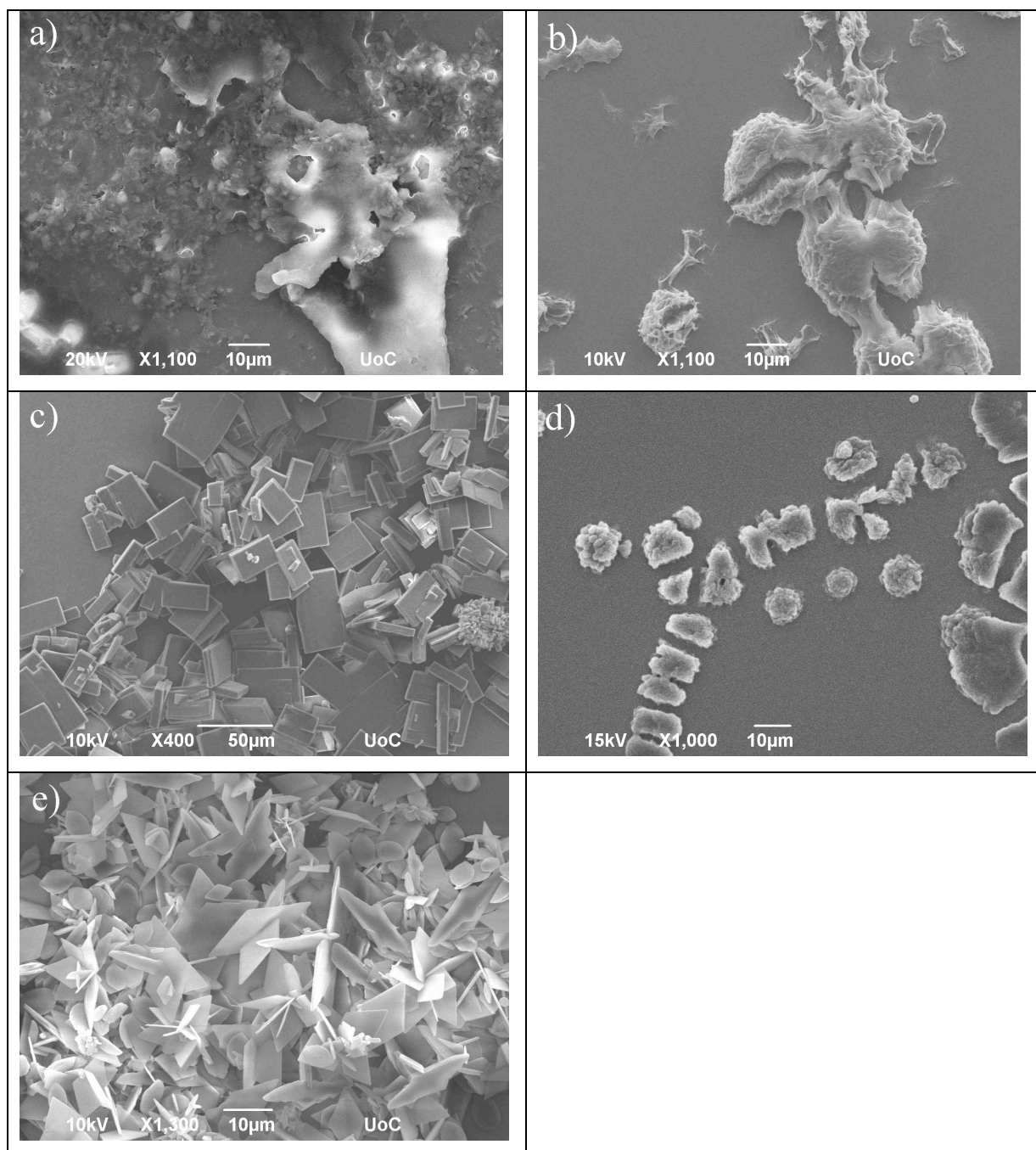


Figure 79 Scanning electron microscopy analysis of the control peptides and porphyrin molecule, (7mM concentration), prepared in 20% HFIP and 80% THF and subsequent dried on glass slides after one day of incubation a) Boc-FF, b) Fmoc-FF, c) FF, d) Fmoc-F, e) Porphyrin molecule

9.3 Results and Discussion

After dissolving in methanol and THF solvents the samples were let for incubation for 24h and then 8 microliters were dried on glass slides. After sputtering with 10nm gold the samples were viewed in Scanning Electron Microscope using a JEOL JSM-6390LV operating at 10 and 15 kV (Department of Biology of the University of Crete).

The hybrids afforded regular spherical shapes with solvent- and time-dependent sizes. Sphere formation was not observed in all the control samples. In the case of methanol the spheres were polydisperse and their diameter was ranging from 3 to 20 micrometers. In the case of THF the spheres are less polydisperse with a diameter around one micrometer.

The nanotube formation from the peptide F-F in methanol (Figure 77c) is eliminated when the monoaminoporphyrin molecule is attached to the peptide (Figure 76c). The difference in the structure comparing to the nanotubes can be attributed to the stacking interactions, which are considered to be a major driving force in the assembly of these aromatic dipeptides, in addition to the hydrogen bonding between the peptide backbone and other weak interactions. (Gazit, 2002). For the dipeptide-porphyrin and even the phenylalanine-porphyrin conjugates, stacking interactions between the porphyrin ring and the dipeptide (or amino acid) side-chain may also play a critical role in determining the outcome of the self-assembly.

Closer examination of the surfaces of the sphere in Scanning Electron Microscopy (SEM) revealed a rough texture, which suggests a porous nature. To gain further insight into the structures of the spheres, we examined thin sections by TEM after embedding a pellet of the sample in resin. The sections confirmed a porous architecture (Figure 80). This result is even more interesting given that the self-assembly of the porphyrin-peptide hybrids is completely reversible when they are dissolved in common solvents.

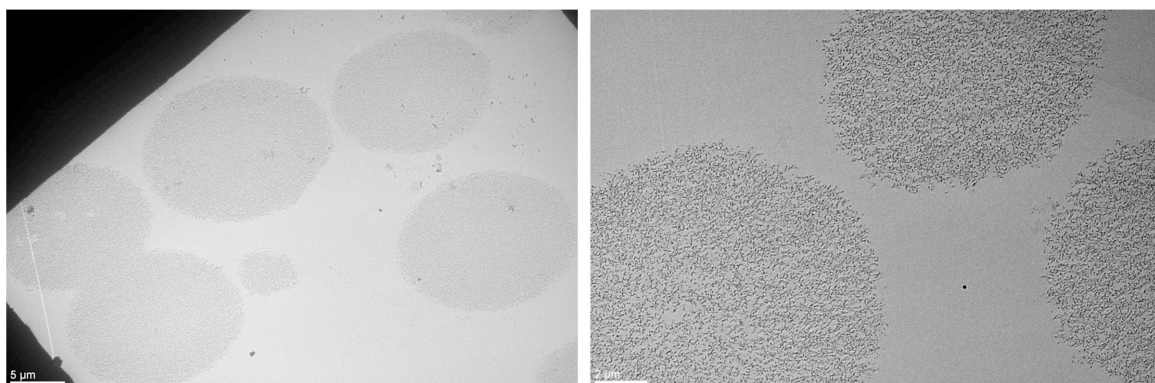


Figure 80 High-Resolution TEM (HRTEM) of sections of the spheres embedded in resin

For structural and mass characterization the samples were examined with Nuclear Magnetic Resonance spectroscopy (NMR) and MALDI-TOF mass spectroscopy. A comparative study of the samples in liquid and solid state was performed with fluorescence spectroscopy. The indications showed that the porphyrin units are involved in excited-state interactions in the solid state. Additionally UV/Vis spectroscopy has allowed to further confirm a regular arrangement due to the self-assembling and supramolecular structure of the dipeptide-porphyrin conjugates. Finally in order to assess the potential importance of a hybrid material as a sensitizer in a TiO₂-based DSSC, it is essential to study its electrochemical behavior. For this reason the redox properties of all the samples were studied by cyclic and squarewave voltammetry. According to the oxidation potentials the hybrid materials record values that are favorable for electron transfer to the conduction band of TiO₂.

Summarizing the properties of the above mentioned novel hybrid complexes; it is obvious that they are categorized as mesoporous materials that combine high surface area with optically and electrochemically active molecules. These materials are the subject of intense research for application in optoelectronic devices (Hauser and Zhang, 2010) and also can contribute to the fabrication of photovoltaic and photo-therapeutical devices, molecular sensors and biosensors (Filatov et al., 2010) (Sol et al., 1997).

Self-Assembly Into Spheres of a Hybrid Diphenylalanine–Porphyrin: Increased Fluorescence Lifetime and Conserved Electronic Properties

Georgios Charalambidis,^[a] Emmanouil Kasotakis,^[b] Theodore Lazarides,^[a]
Anna Mitraki,^{*,[b]} and Athanassios G. Coutsolelos^{*,[a]}

Abstract: A series of protected phenylalanine and diphenylalanine derivatives have been coupled through a peptide bond to a monoaminoporphyrin to form new materials. A comparative study in solution and in the solid state has been performed and confirmed new and interesting properties for the self-assembled hybrid materials while conserving the electronic properties of the chromophore. Thus, they are powerful candidates for use in dye-sensitized solar cells.

Keywords: amino acids · electronic properties · fluorescence · porphyrinoids · self-assembly

Introduction

The most efficient energy-harvesting mechanism in nature is the conversion of solar photons into electrons and further into chemical energy through photosynthesis.^[1] Harnessing the energy produced by the sun is therefore a promising avenue for the development of novel energy sources.^[2] Functional hybrid materials consisting of semiconductors and organic components form an exciting new area of research in modern materials science.^[3] The finest application of such hybrid materials is the conversion of sunlight into electric current. Since the development of dye-sensitized solar cells (DSSCs),^[4] research into organic–inorganic photovoltaic devices has increased enormously. In addition, porphyrin molecules have long been explored for use as photosensitizers in different types of solar cell.^[5]

Self-assembled biological structures (viruses, proteins, peptides) can serve as templates guiding the nanoscale organization of porphyrins to facilitate long-range electron and energy transfer in solution.^[6] Furthermore, they offer the advantage of precise spatial control by introduction of site-specific changes at the sequence level. Covalent coupling of porphyrins to form a short decapeptide designed to fold into a helical structure has been previously reported to

result in extended self-assembled arrays.^[7] α -Helical peptides can also be designed to form extended coil structures and to bind porphyrins through noncovalent interactions.^[8b] However, a fundamental question remains: could these supramolecular structures also serve as solid-state electronic conductors? Answering this question requires simple methods to study the conductivity of the “dry” system (which can only contain an oligopeptide scaffold with structured electron donors) sandwiched between two electronic conductors in a solid-state-type configuration. If successful, such systems could serve as the basis for future, bioinspired electronic device technology for dye sensitizer solar cells. Short peptide building blocks that self-assemble into fibers, tubes, or spheres are resistant to harsh conditions and coupling porphyrins to them can be a beneficial approach. It has recently been shown that organic solar cells composed of a series of porphyrin–peptide oligomers show enhanced photoelectrochemical performance.^[8] Among self-assembling peptide systems, diphenylalanine peptides (FF) have recently emerged as a well-studied system with open-ended applications, for example, as templates for casting metals and inorganic compounds, for integration into nanofabricated devices, or as biosensing platforms.^[9] These peptides self-assemble into hollow tubes after dissolving in 1,1,1,3,3,3-hexafluoro-2-propanol (HFIP) and subsequent dilution in water. Furthermore, upon evaporation of HFIP on siliconized glass surfaces they form nanoforests of vertically aligned nanotubes.^[10] The FF nanotubes can withstand extreme conditions, such as standard autoclaving conditions and dry heat up to 150 °C. The FF peptide powders can even withstand vapor deposition conditions; heating on a 200 °C stage and subsequent evaporation on a surface placed 2 cm above the heating stage results in coating of the surface with vertically aligned nanotubes.^[11] Given the physical strength and chemical resistance of the peptide nanotubes (PNTs), the possibility of using them as supports functionalized with porphyrin moieties seemed very attractive. We therefore sought to couple porphyrin moieties to FF peptides and to study the

[a] G. Charalambidis, T. Lazarides, Prof. A. G. Coutsolelos
Chemistry Department, University of Crete, Voutes Campus
PO Box 2208, 71003 Heraklion, Crete (Greece)
Fax: (+30)28105455161
E-mail: coutsole@chemistry.uoc.gr

[b] E. Kasotakis, Prof. A. Mitraki
Department of Materials Science and Technology
University of Crete and IESL-FORTH
Voutes Campus, 71003, Heraklion, Crete (Greece)
Fax: (+30)2810394408
E-mail: mitraki@materials.uoc.gr

[*] These authors contributed equally to this work

Supporting information for this article is available on the WWW under <http://dx.doi.org/10.1002/chem.201100362>.

self-assembly properties of the hybrids. If the FF peptides could maintain the ability to self-assemble into nanotubes within the hybrid construct, then they could template the nanoscale organization of the porphyrin moiety.

Results and Discussion

We therefore proceeded to synthesize five different hybrid derivatives of monoaminoporphyrin by using FF protected with Boc and Fmoc or unprotected in various solvents. For comparison, the single phenylalanine–porphyrin hybrid compound (the phenylalanine amino acid by itself has not been reported to form any self-assembled structures) was synthesized (Scheme 1).

We report herein the unanticipated formation of spheres by the hybrid derivatives. After dissolving in various solvents and drying on glass slides, the hybrids afforded regular spherical shapes with solvent- and time-dependent sizes. We also report on their electrochemical behavior and fluorescence emission properties in the dry state.

Studies in solution: In our design, the 5-(4-aminophenyl)-10,15,20-triphenylporphyrin is covalently attached in an amide coupling reaction to the free carboxylate terminal of Boc-diphenylalanine, Fmoc-diphenylalanine, and Fmoc-phenylalanine, giving rise to derivatives **A**, **B**, and **C** in very high yields ($\approx 98\%$). The deprotection of the Fmoc groups in **B** and **C** after the addition of piperidine gave rise, respectively, to derivatives **D** and **E** quantitatively (Scheme 2).

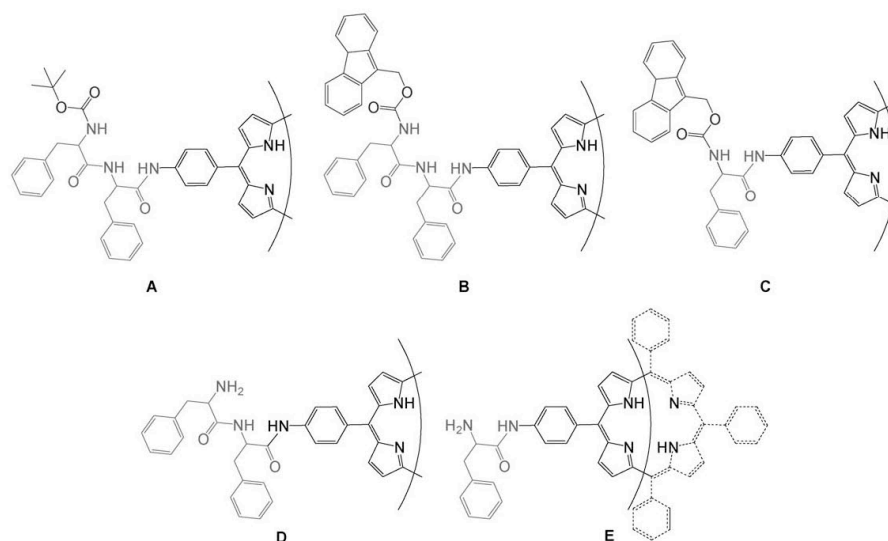
The UV/Vis spectrum of the initial monoaminoporphyrin was not affected by the coupling, and the hybrid materials

presented characteristic UV/Vis spectra that correspond to the porphyrin ring in respect of the wavelengths of the Soret bands, as well as the annex bands. The molecular ions $[M+H]^+$ were detected for all of the hybrid materials by MALDI-TOF mass spectroscopy and this clearly confirms the expected molecular formulae. A complete and comparative study was performed by ^1H and ^{13}C NMR spectroscopy and two-dimensional experiments on the five hybrids and their precursors to complete the study in solution. All of the signals have been attributed to the corresponding protons in each material (see the Supporting Information for the ^1H and ^{13}C NMR spectra of all five derivatives).

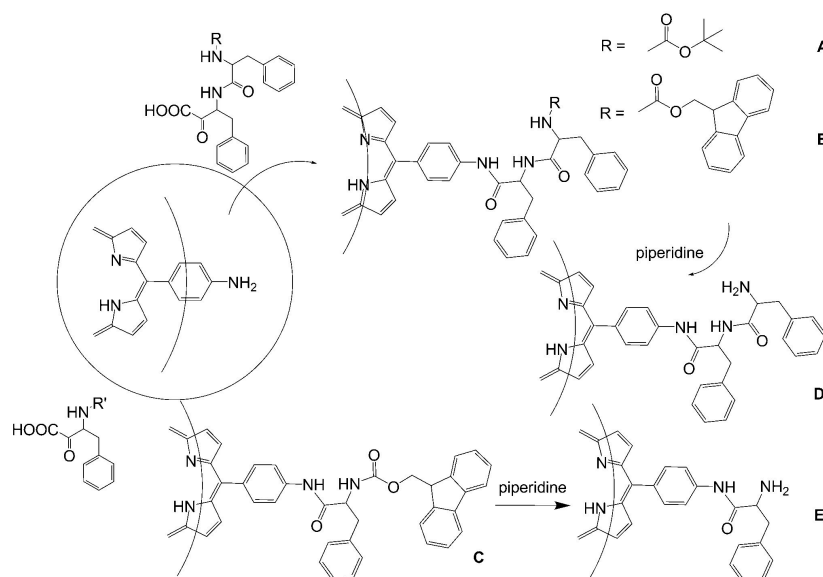
A study by fluorescence spectroscopy was also performed. For experiments in solution, a typical spectrum, which corresponds to the monoaminoporphyrin, was observed for all the studied hybrid derivatives. However, this was not the case in the solid state, as will be discussed below.

In a TiO_2 -based DSSC, the oxidation potential of the first excited state of the photosensitizer has to be favorable for the injection of electrons into the conduction band of the semiconductor. Therefore, to assess the potential importance of a hybrid material as a sensitizer in a DSSC, it is essential to study its electrochemical behavior. For this reason the redox properties of **A–E** were studied by cyclic and square-wave voltammetry in dichloromethane by using ferrocene as the internal standard.

The redox data for **A–E** versus Fc/Fc^+ are shown in Table 1. All of the compounds show two sequential reversible oxidation processes and two reversible reductions, as expected for porphyrin derivatives.^[12] The first excited state oxidation potentials, E_{ox}^{0*} , for **A–E** can be estimated by using Equation (1), in which E_{ox}^0 is the potential of the first oxida-



Scheme 1. The five hybrid coupled derivatives: monoaminoporphyrin-FF-Boc (**A**), monoaminoporphyrin-FF-Fmoc (**B**), monoaminoporphyrin-F-Fmoc (**C**), monoaminoporphyrin-FF (**D**) and monoaminoporphyrin-F (**E**).



Scheme 2. Synthetic approach to the various FF moieties.

Table 1. Redox data for compounds **A–E** in dichloromethane versus Fc/Fc^+ .

Compound	Reduction E [V] ^[a]		Oxidation E [V] ^[a]	
A	−2.08	−1.70	0.83	0.52
B	−2.04	−1.67	0.82	0.51
C	−2.06	−1.68	0.83	0.52
D	−2.09	−1.70	0.81	0.51
E	−2.08	−1.68	0.82	0.51

[a] All redox potentials are quoted vs. Fc/Fc^+ .

tion (ca. 0.51 V from Table 1) and E_{00} is the energy of either the first excited singlet or the first triplet state (1.92 and 1.43 eV, respectively, for TPP derivatives^[13]). According to the above, the oxidation potentials of the first singlet excited states and the first triplet states are approximately −1.41 and −0.92 V versus Fc/Fc^+ , respectively, in both cases favorable for electron transfer to the conduction band of TiO_2 .^[4,5]

$$E_{\text{ox}}^{0*} = E_{\text{ox}}^0 - E_{00} \quad (1)$$

Studies in the solid state: The diphenylalanine–porphyrin and phenylalanine–porphyrin conjugates were dissolved in various solvents, as described in the Experimental Section, dried on glass slides, and studied by scanning electron microscopy (SEM). Sphere formation was a consistent pattern observed for the conjugates in almost all of the solvents (Figure 1a and Figures S2 and S4 of the Supporting Information show two of the five solvent conditions studied: methanol and THF).

Tubes or other high aspect ratio morphologies were not observed. Sphere formation was not observed in the control

samples, that is, the dipeptide (protected or not), the phenylalanine amino acid, and the porphyrin moiety alone (Fig-

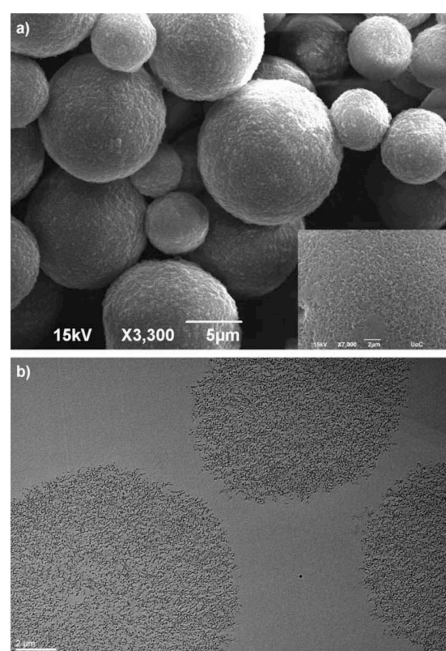


Figure 1. SEM and TEM analyses of sections of the Boc-FF-P peptide–porphyrin complex. a) SEM of the spheres (scale bar = 5 μm). Insert: Close-up image of the spheres (scale bar = 2 μm). b) HRTEM of sections of the spheres embedded in resin (scale bar = 2 μm).

ures S3 and S5 of the Supporting Information). Under some conditions, dipeptide nanotubes were observed, for example, the FF peptide forms nanotubes in 20% HFIP/80% methanol (Figure S3c). The same peptide forms microscale plate-like structures in 20% HFIP/80% THF (Figure S5c). Under these two conditions, the porphyrin moiety forms plate- or needle-like structures on the microscale (Figure S3e and S5e). However, the corresponding conjugate (FFP) forms spheres under both conditions (Figure S2c and S4c). This suggests that the self-assembly properties are inherent to the peptide-porphyrin conjugates and not a sum of the assembly properties of both constituents. Closer examination of the surfaces of the sphere in SEM revealed a rough texture (Figure 1a, insert), which suggests a porous nature. To gain further insight into the structures of the spheres, we examined thin sections by TEM after embedding a pellet of the sample in resin. The sections confirm an intricate, yet porous architecture (Figure 1b).

The emission properties of the spherical assemblies were studied by steady-state and time-resolved luminescence spectroscopy under ambient conditions and compared with those of regular microcrystalline samples and with the luminescence shown by TPP derivatives in dichloromethane. As shown in Figure 2a, the fluorescence of a dry sample of spheres of **A**, assembled from a mixture of ethanol and HFIP, is slightly broadened and redshifted compared with that of a microcrystalline sample, prepared from the evaporation of a solution of **A** in dichloromethane. Both solid-state emission spectra are broadened and redshifted relative to the emission spectrum of **A** in dichloromethane. This observation is consistent with the results of Hasobe and co-workers^[14] in their study of porphyrin-based nanoassemblies and indicates that the porphyrin units are involved in excited-state interactions in the solid state.^[14]

The UV/Vis spectrum of the spheres in the solid state was recorded to compare their properties with the ground solid form. Hydrosoluble TPPS porphyrin is a well-investigated dye due to its ability to self-aggregate noncovalently to form H-aggregates (face-to-face) or J-aggregates (side-by-side) under certain concentrations, pH, and ionic strength^[15] depending on the electronic and stereochemical properties of the porphyrin. J- and H-aggregation is indicated by the appearance of sharp and narrow absorption bands that are shifted to the red or blue, respectively, with respect to the monomeric Soret band. In our case, a comparison was made between the self-assembled spheres of the hybrid derivatives and the ground solid. As we can observe in Figure 2b, the self-assembling derivative presents a blueshift of 5 nm compared with the ground solid, which is a characteristic of H-aggregation and suggests a face-to-face arrangement of the porphyrin rings. Furthermore, in the Q-band region several changes can be observed for all four bands in addition to the blueshift: relative to the spectrum of the ground solid sample (which is similar to the one in solution), the spectrum of the spheres possesses much broader Q-bands with a different relative absorbance between them. Thus, UV/Vis spectroscopy has allowed us to further confirm a regular ar-

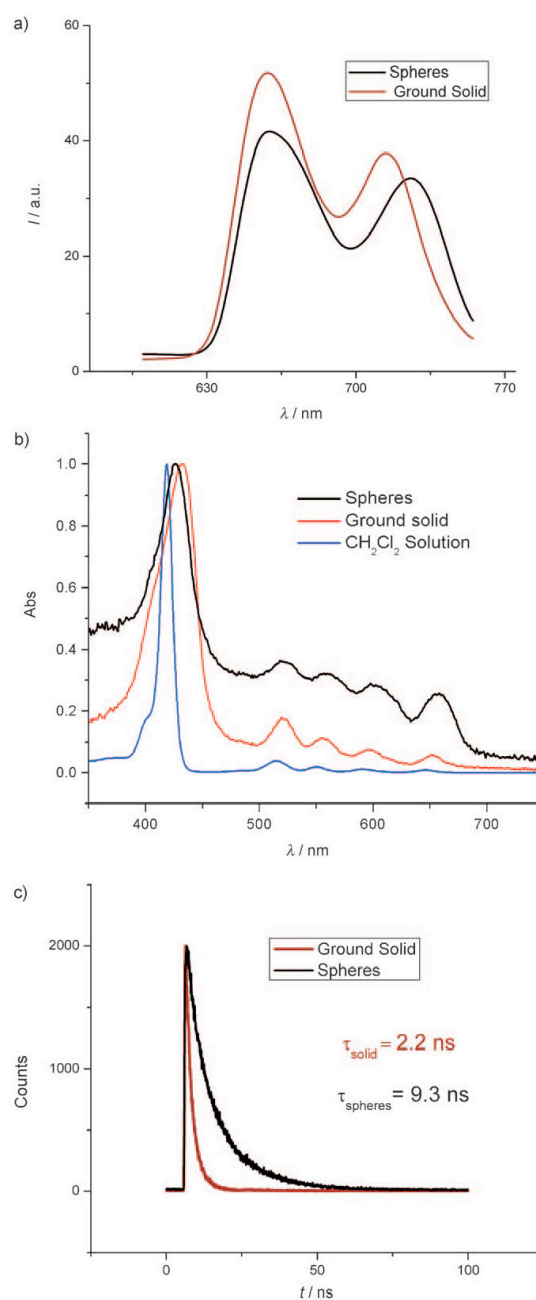


Figure 2. a) Emission spectrum, b) UV/Vis transmission behavior, and c) the corresponding lifetimes of spheres and the ground solid of compound **A**.

rangement due to the self-assembling and supramolecular structure of the dipeptide-porphyrin conjugates.

A time-resolved emission measurement of the microcrystalline sample of **A** revealed a fluorescence lifetime τ_{solid} of 2.2 ns, whereas the self-assembled spheres have a lifetime τ_{spheres} of 9.3 ns (Figure 2c), which is comparable to the lifetime of **A** in dichloromethane. The short lifetime of the microcrystalline sample is a result of quenching due to intermolecular interactions between porphyrin units giving rise to energy transfer and singlet-singlet annihilation.^[14] The relatively long lifetime measured for the self-assembled sample further supports that within the spheres, the porphyrin units mainly exist either as H aggregates^[15] or isolated monomers arranged in a way that prevents interactions between them. These results are consistent with the results of all the self-assembled spheres regardless of the protecting group. Thus, in the solid state the spherical assemblies provide structural control of the porphyrin-diphenylalanine hybrid material and consequently of their lifetime.

Thus, the conjugation of a porphyrin moiety to diphenylalanine dipeptides, protected or not, and to the single amino acid phenylalanine has been achieved. The conjugates were structurally and electrochemically characterized. Also, the conjugates self-assembled into microscale spheres upon drying from a variety of solvents, such as methanol, ethanol, acetonitrile, and THF.

Under the same conditions, none of the constituent parts of the conjugates were found to adopt a spherical morphology. Stacking interactions are considered to be a major driving force in the assembly of these aromatic dipeptides,^[16] in addition to the hydrogen bonding between the peptide backbone and other weak interactions. For the dipeptide-porphyrin and even the phenylalanine-porphyrin conjugates, stacking interactions between the porphyrin ring and the dipeptide (or amino acid) side-chain may also play a critical role in determining the outcome of the self-assembly. From the solvent conditions studied, the most homogeneous spheres, with diameters on the microscale, are formed in THF. The spheres formed are porous, as revealed by TEM examination of thin sections of the samples embedded in resin. This result is even more interesting given that the self-assembly of the porphyrin-peptide hybrids is completely reversible when they are dissolved in common solvents. Mesoporous materials that combine high surface area with optically and electrochemically active molecules are the subject of intense research for application in optoelectronic devices.^[17] Photovoltaic devices, molecular sensors, and biosensors are some of the very recent examples,^[18] and finally, photodynamic therapy may be another area of application for these porous spherical materials.^[19]

Conclusion

We have reported herein peptide-porphyrin and amino acid-porphyrin conjugates that self-assemble upon drying into porous spheres with tunable size dependent on the solvent conditions. Within the spherical self-assemblies, the porphyrin units change their fluorescence behavior and their

lifetime values; however, they maintain their ability for electron transfer. These novel hybrid materials may find uses in solar cell technologies and biomedical applications.

Experimental Section

¹H NMR spectra were recorded on Bruker AMX-500 MHz and Bruker DPX-300 MHz spectrometers as solutions in deuteriochloroform by using the solvent peak as the internal standard. UV/Vis spectra were recorded on a Shimadzu UV-1700 PharmaSpec instrument. High-resolution mass spectra were performed on a Bruker ultrafleXtreme MALDI-TOF/TOF spectrometer. Redox potentials were determined by cyclic voltammetry on a EG&G potentiostat PGSTA20 Autolab instrument at room temperature in dry and deoxygenated CH₂Cl₂ containing 0.1 M tetrabutylammonium hexafluorophosphate as the supporting electrolyte with a solute concentration in the range of 1.5×10^{-5} M. A saturated calomel electrode (SCE) was used as the reference. Under these conditions, the reversible oxidation of ferrocene was $E_{\text{Fc}} = +0.47$ V. The error in the reported potentials is ± 0.01 V. Lifetime measurements were performed on a mini τ (Edinburgh Instruments) equipped with an EPL 405 nm laser. The emission spectra were measured on a JASCO FP-6500 fluorescence spectrophotometer equipped with a red-sensitive WRE-343 photomultiplier tube (wavelength range: 200–850 nm).

Peptides and amino acids were purchased from Bachem. Following the conjugation reactions of peptides with the porphyrin moieties the products were dried and resuspended in chloroform as stock solutions. Aliquots of the stock solution were dried in Eppendorf tubes in air. They were then redissolved in 1,1,1,3,3,3-hexafluoro-2-propanol (HFIP) and water, methanol, ethanol, acetonitrile, or THF were added to give a solvent mixture of 20% HFIP/80% solvent. The final concentration of each conjugate was kept constant at 7 mM.

All samples were observed by scanning electron microscopy following incubation for 24 h. A sample solution (8 μ L) was deposited on a glass slide and left to dry in air. Samples were subsequently covered with 10 nm gold sputtering and observed directly. SEM experiments were performed at the Department of Biology of the University of Crete by using a JEOL JSM-6390LV microscope operating at 10 and 15 kV. For TEM analysis of sections, the sample was centrifuged and the supernatant liquid was removed. The pellet was embedded directly in the epoxy resin DurcupanTM (ACM Fluka) for 48 h. Sections were cut with a microtome and deposited on a 300 mesh carbon-coated copper grid for TEM analysis. TEM experiments were performed at the Department of Biology of the University of Crete by using a JEOL HR-TEM JEM-2100 microscope operating at 80 kV.

General procedure for the coupling of the peptides with the porphyrin: The Boc- or Fmoc-protected diphenylalanine (1 equiv) or the Fmoc-protected phenylalanine (1 equiv) was dissolved in dichloromethane. The solution was cooled to 0°C in an ice bath and *N,N*-dicyclohexylcarbodiimide (DCC; 1.2 equiv) and 1-hydroxybenzotriazole hydrate (HOBt; 1.2 equiv) were added. The reaction mixture was stirred at 0°C for 30 min and the monoaminoporphyrin (1 equiv) was added. The resulting solution was stirred at 5°C for 48 h, after which time CH₂Cl₂ was added and the solution washed once with water. The organic layer was dried with Na₂SO₄, filtered, concentrated, and the residue was purified by chromatography on a silica gel column.

Monoaminoporphyrin-Fmoc (A): The general procedure was used to couple monoaminoporphyrin (61 mg, 0.097 mmol) with Boc-diphenylalanine (40 mg, 0.097 mmol) by using DCC (24 mg, 0.12 mmol) and HOBt (16 mg, 0.12 mmol) in CH₂Cl₂ (5 mL). The title compound was isolated by column chromatography (silica gel, CH₂Cl₂/EtOH, 100:1 v/v) as a purple solid (94 mg, 95%). ¹H NMR (500 MHz, CDCl₃): δ = 8.87 (m, 8H), 8.61 (brs, 1H), 8.22 (d, J = 6.5 Hz, 6H), 8.16 (d, J = 8.5 Hz, 2H), 7.99 (m, 2H), 7.77 (m, 9H), 7.36 (m, 6H), 7.26 (m, 2H), 7.16 (brs, 2H), 6.49 (m, 1H), 5.01 (m, 1H), 4.90 (brs, 1H), 4.41 (m, 1H), 3.52 (m, 1H), 3.15 (m, 3H), 1.28 (s, 9H), -2.76 ppm (s, 2H); ¹³C NMR (75 MHz, CDCl₃): δ = 171.3, 169.2, 156.2, 142.3, 138.3, 137.6, 136.3, 135.9, 135.1,

134.7, 131.2, 129.5, 129.4, 129.2, 129.1, 127.8, 127.7, 127.5, 126.8, 120.3, 119.9, 118.5, 81.5, 56.7, 54.2, 37.5, 37.2, 28.3 ppm; UV/Vis (CH_2Cl_2): λ_{max} (ϵ)=418 (503.4), 515 (18.9), 550 (9.2), 590 (5.6), 646 nm ($4.5\text{ m}^{-1}\text{ cm}^{-1}$); HRMS (MALDI-TOF): m/z calcd for $\text{C}_{67}\text{H}_{58}\text{N}_7\text{O}_4$: 1024.4550 $[\text{M}+\text{H}]^+$; found: 1024.4562.

Monoaminoporphyrin-FF-Fmoc (B): The general procedure was used to couple monoaminoporphyrin (100 mg, 0.16 mmol) with Fmoc-diphenylalanine (85 mg, 0.16 mmol) by using DCC (39 mg, 0.19 mmol) and HOBT (26 mg, 0.19 mmol) in CH_2Cl_2 (10 mL). The title compound was isolated by column chromatography (silica gel, $\text{CH}_2\text{Cl}_2/\text{EtOH}$, 100:4 v/v) as a purple solid (175 mg, 95%). $^1\text{H NMR}$ (500 MHz, CDCl_3): δ =8.85 (s, 8H), 8.36 (brs, 1H), 8.22 (m, 6H), 8.15 (d, J =8.0 Hz, 2H), 7.89 (brs, 2H), 7.77 (m, 11H), 7.51 (m, 2H), 7.34 (m, 10H), 7.23 (m, 4H), 6.54 (brs, 1H), 5.17 (brs, 1H), 4.94 (brs, 1H), 4.47 (m, 2H), 4.39 (brs, 1H), 4.17 (t, J =6.5 Hz, 1H), 3.29 (m, 2H), 3.17 (brs, 1H), 2.99 (brs, 1H), -2.77 ppm (s, 2H); $^{13}\text{C NMR}$ (75 MHz, CDCl_3): δ =171.3, 169.0, 156.6, 143.6, 142.3, 141.4, 138.4, 137.4, 136.5, 135.9, 135.2, 134.7, 131.2, 129.4, 129.3, 129.2, 129.1, 128.0, 127.8, 127.6, 127.4, 127.3, 126.8, 125.1, 125.0, 120.3, 120.2, 119.7, 118.4, 67.5, 56.8, 55.2, 47.2, 38.0, 37.6 ppm; UV/Vis (CH_2Cl_2): λ_{max} (ϵ)=418 (525.9), 515 (19.3), 550 (9.3), 590 (5.8), 646 nm ($4.8\text{ m}^{-1}\text{ cm}^{-1}$); HRMS (MALDI-TOF): m/z calcd for $\text{C}_{77}\text{H}_{60}\text{N}_7\text{O}_4$: 1146.4707 $[\text{M}+\text{H}]^+$; found: 1146.4718.

Monoaminoporphyrin-F-Fmoc (C): The general procedure was used to couple monoaminoporphyrin (44 mg, 0.07 mmol) with Fmoc-phenylalanine (27 mg, 0.07 mmol) by using DCC (17 mg, 0.08 mmol) and HOBT (11 mg, 0.08 mmol) in CH_2Cl_2 (4 mL). The title compound was isolated by column chromatography (silica gel, $\text{CH}_2\text{Cl}_2/\text{EtOH}$, 100:1 v/v) as a purple solid (65 mg, 93%). $^1\text{H NMR}$ (500 MHz, CDCl_3): δ =8.85 (s, 8H), 8.22 (m, 6H), 8.15 (d, J =8.0 Hz, 2H), 8.06 (brs, 1H), 7.76 (m, 13H), 7.61 (t, J =8.0 Hz, 2H), 7.40 (m, 9H), 5.61 (brs, 1H), 4.73 (brs, 1H), 4.54 (m, 2H), 4.28 (t, J =6.5 Hz, 1H), 3.32 (brs, 2H), -2.77 ppm (s, 2H); $^{13}\text{C NMR}$ (75 MHz, CDCl_3): δ =169.5, 156.5, 143.8, 142.3, 141.5, 138.7, 137.0, 136.5, 135.2, 134.7, 131.3, 129.6, 129.2, 128.0, 127.9, 127.6, 127.3, 126.8, 125.1, 120.3, 120.2, 119.5, 118.5, 67.5, 57.5, 47.3, 38.7 ppm; UV/Vis (CH_2Cl_2): λ_{max} (ϵ)=418 (516.1), 514 (19.0), 550 (9.0), 590 (5.7), 645 nm ($4.5\text{ m}^{-1}\text{ cm}^{-1}$); HRMS (MALDI-TOF): m/z calcd for $\text{C}_{66}\text{H}_{51}\text{N}_7\text{O}_3$: 999.4023 $[\text{M}+\text{H}]^+$; found: 999.4018.

Monoaminoporphyrin-FF (D): Piperidine (0.6 mL, 6.0 mmol) was added to a solution of porphyrin A (55 mg, 0.05 mmol) in DMF (3 mL) and the solution was stirred at room temperature for 2 h. The solvent was then removed under vacuum and the solid was dissolved in CH_2Cl_2 (50 mL) and extracted with water (2×50 mL), dried with Na_2SO_4 , filtered, and concentrated under vacuum. The title compound was isolated by column chromatography (silica gel, $\text{CH}_2\text{Cl}_2/\text{EtOH}$, 100:6 v/v) as a purple solid (43 mg, 93%). $^1\text{H NMR}$ (500 MHz, CDCl_3): δ =8.83 (s, 8H), 8.18 (m, 9H), 7.87 (d, J =7.5 Hz, 2H), 7.74 (m, 9H), 7.34 (m, 7H), 7.23 (m, 3H), 4.96 (d, J =7.0 Hz, 1H), 4.05 (m, 1H), 3.91 (brs, 1H), 3.47 (m, 1H), 3.39 (m, 1H), 3.24 (m, 2H), 2.64 (brs, 2H), -2.78 ppm (s, 2H); $^{13}\text{C NMR}$ (75 MHz, CDCl_3): δ =169.5, 142.3, 138.4, 137.5, 137.2, 136.9, 135.2, 134.7, 131.2, 129.6, 129.4, 129.0, 127.8, 127.3, 126.8, 120.3, 119.6, 118.4, 56.4, 55.7, 40.5, 37.5 ppm; UV/Vis (CH_2Cl_2): λ_{max} (ϵ)=418 (458.2), 515 (17.4), 550 (8.4), 590 (5.2), 646 ppm ($4.2\text{ m}^{-1}\text{ cm}^{-1}$); HRMS (MALDI-TOF): m/z calcd for $\text{C}_{62}\text{H}_{40}\text{N}_7\text{O}_2$: 924.4026 $[\text{M}+\text{H}]^+$; found: 924.4031.

Monoaminoporphyrin-F (E): Piperidine (0.3 mL, 3.0 mmol) was added to a solution of porphyrin C (25 mg, 0.025 mmol) in DMF (1.5 mL) and the solution was stirred at room temperature for 2 h. The solvent was then removed under vacuum and the solid was dissolved in CH_2Cl_2 (30 mL) and extracted with water (2×30 mL), dried with Na_2SO_4 , filtered, and concentrated under vacuum. The title compound was isolated by column chromatography (silica gel, $\text{CH}_2\text{Cl}_2/\text{EtOH}$, 100:2 v/v) as a purple solid (18 mg, 93%). $^1\text{H NMR}$ (500 MHz, CDCl_3): δ =9.86 (brs, 1H), 8.86 (m, 8H), 8.21 (m, 8H), 8.01 (d, J =8.0 Hz, 2H), 7.76 (m, 9H), 7.37 (m, 5H), 3.97 (brs, 1H), 3.55 (d, J =13.5 Hz, 1H), 2.98 (m, 2H), -2.76 ppm (s, 2H); $^{13}\text{C NMR}$ (75 MHz, CDCl_3): δ =172.7, 142.3, 138.2, 137.6, 135.3, 134.7, 131.3, 129.6, 129.1, 127.8, 127.3, 126.8, 120.3, 119.8, 117.9, 57.1, 40.8 ppm; UV/Vis (CH_2Cl_2): λ_{max} (ϵ)=418 (497.0), 514 (18.9), 550 (9.1), 590 (5.6), 646 nm ($4.6\text{ m}^{-1}\text{ cm}^{-1}$); HRMS (MALDI-TOF): m/z calcd for $\text{C}_{53}\text{H}_{41}\text{N}_7\text{O}$: 777.3342 $[\text{M}+\text{H}]^+$; found: 777.3350.

Acknowledgements

This research was funded by the European Commission (FP7-REGPOT-2008-1 Project BIOSOLENUTI No. 229927), a Heraklitos grant from the Ministry of Education, and GSRT. Technical support with E.M by A. Sialkoulis Gallanopoulou and E. Papadogiorgaki is gratefully acknowledged.

- a) G. McDermott, S.M. Prince, A.A. Freer, A.M. Hawthornthwaite-Lawless, M.Z. Papiz, R.J. Cogdell, N.W. Isaacs, *Nature* **1995**, *374*, 517–521; b) S. Karrasch, P.A. Bullough, R. Ghosh, *EMBO J.* **1995**, *14*, 631–638; c) J. Barber, *Chem. Soc. Rev.* **2009**, *38*, 185–196; d) L. Hammarstrom, S. Hammes-Schiffer, *Acc. Chem. Res.* **2009**, *42*, 1859–1860.
- a) M.R. Wasielewski, *Acc. Chem. Res.* **2009**, *42*, 1910–1921; b) N. Aratani, D. Kim, A. Osuka, *Acc. Chem. Res.* **2009**, *42*, 1922–1934, and references therein.
- a) E. Coronado, E. Palomares, *J. Mater. Chem.* **2005**, *15*, 3593–3597; b) M.-S. Choi, T. Yamazaki, I. Yamazaki, T. Aida, *Angew. Chem.* **2004**, *116*, 152–160; *Angew. Chem. Int. Ed.* **2004**, *43*, 150–158; c) B. Tian, T. J. Kempa, C. M. Lieber, *Chem. Soc. Rev.* **2009**, *38*, 16–24; d) M. Wang, S.-J. Moon, M. Xu, K. Chittibabu, P. Wang, N.-L. Cevey-Ha, R. Humphry-Baker, S. M. Zakeeruddin, M. Grätzel, *Small* **2010**, *6*, 319–324; e) R. Das, P. J. Kiley, M. Segal, J. Norville, A. A. Yu, L. Wang, S. A. Trammell, L. E. Reddick, R. Kumar, F. Stellacci, N. Lebedev, J. Schnur, B. D. Bruce, S. Zhang, M. Baldo, *Nano Lett.* **2004**, *4*, 1079–1083.
- B. O'Regan, M. Grätzel, *Nature* **1991**, *353*, 737–740.
- a) T. Hasobe, S. Fukuzumi, P. V. Kamat, *Interface* **2006**, *15*, 47–51; b) C. Y. Lee, J. T. Hupp, *Langmuir* **2010**, *26*, 3760–3765; c) J. K. Park, J. Chen, H. R. Lee, S. W. Park, H. Shinokubo, A. Osuka, D. Kim, *J. Phys. Chem. C* **2009**, *113*, 21956–21963; d) T. D. Santos, A. Morandeira, S. Koops, A. J. Mozer, G. Tsekouras, Y. Dong, P. Wagner, G. Wallace, J. C. Earles, K. C. Gordon, D. Officer, J. R. Durrant, *J. Phys. Chem. C* **2010**, *114*, 3276–3279; e) E. Maligaspe, N. V. Tkachenko, N. K. Subbaiyan, R. Chitta, M. E. Zandler, H. Lemmetyinen, F. D'Souza, *J. Phys. Chem. A* **2009**, *113*, 8478–8489; f) J. Rochford, D. Chu, A. Hagfeldt, E. Galoppini, *J. Am. Chem. Soc.* **2007**, *129*, 4655–4665; g) M. Tao, L. Liu, D. Liu, X. Zhou, *Dyes Pigm.* **2010**, *85*, 21–26; h) A. Hagfeldt, G. Boschloo, L. Sun, L. Kloo, H. Pettersson, *Chem. Rev.* **2010**, *110*, 6595–6663; i) H. Imahori, T. Umeyama, S. Ito, *Acc. Chem. Res.* **2009**, *42*, 1809–1818; j) T. Bessho, S. M. Zakeeruddin, C.-Y. Yeh, E. W.-G. Diau, M. Grätzel, *Angew. Chem.* **2010**, *122*, 6796–6799; *Angew. Chem. Int. Ed.* **2010**, *49*, 6646–6649.
- a) B. C. Kovaric, B. Kokona, A. D. Schwab, M. A. Twomey, J. C. de Paula, R. Fairman, *J. Am. Chem. Soc.* **2006**, *128*, 4166–4167; b) B. Kokona, A. M. Kim, R. C. Roden, J. P. Daniels, B. J. Pepe-Mooney, B. C. Kovaric, J. C. de Paula, K. A. Johnson, R. Fairman, *Biomacromolecules* **2009**, *10*, 1454–1459; c) Y. S. Nam, T. Shin, H. Park, A. P. Magyar, K. Choi, G. Fantner, K. A. Nelson, A. M. Belcher, *J. Am. Chem. Soc.* **2010**, *132*, 1462–1463; d) C. J. Medforth, Z. Wang, K. Ewing Martin, Y. Song, J. L. Jacobsen, J. A. Shelmutt, *Chem. Commun.* **2009**, 7261–7277.
- J. R. Dunetz, C. Sandstrom, E. R. Young, P. Baker, S. A. Van Name, T. Cathopolous, R. Fairman, J. C. de Paula, K. S. Åkerfeldt, *Org. Lett.* **2005**, *7*, 2559–2561.
- T. Hasobe, K. Saito, P. V. Kamat, V. Troiani, H. Qiu, N. Solladié, K. S. Kim, J. K. Park, D. Kim, F. D'Souza, S. Fukuzumi, *J. Mater. Chem.* **2007**, *17*, 4160–4170.
- a) M. Reches, E. Gazit, *Science* **2003**, *300*, 625–627; b) E. Gazit, *FEBS J.* **2007**, *274*, 317–322; c) M. Yemini, M. Reches, E. Gazit, J. Rishpon, *Anal. Chem.* **2005**, *77*, 5155–5159; d) M. Yemini, M. Reches, J. Rishpon, E. Gazit, *Nano Lett.* **2005**, *5*, 183–186.
- M. Reches, E. Gazit, *Nat. Nanotechnol.* **2006**, *1*, 195–200.
- a) L. Adler-Abramovich, M. Reches, V. L. Sedman, S. Allen, S. J. B. Tendler, E. Gazit, *Langmuir* **2006**, *22*, 1313–1320; b) L. Adler-Abramovich, D. Aronov, P. Beker, M. Yevnin, S. Stempler, L. Buzhansky, G. Rosenman, E. Gazit, *Nat. Nanotechnol.* **2009**, *4*, 849–854.

- [12] *The Porphyrin Handbook* (Eds.: K. Kadish, K. Smith, R. Guilard), Academic, New York, **2000**.
- [13] a) J. R. Darwent, P. Douglas, A. Harriman, G. Porter, M. C. Richoux, *Coord. Chem. Rev.* **1982**, *44*, 83–126; b) K. M. Kadish, E. V. Caemelbecke, *J. Solid State Electrochem.* **2003**, *7*, 254–258.
- [14] A. S. D. Sandanayaka, Y. Araki, T. Wada, T. Hasobe, *J. Phys. Chem. C* **2008**, *112*, 19209–19216.
- [15] a) O. Ohno, Y. Kaizu, H. Kobayashi, *J. Chem. Phys.* **1993**, *99*, 4128–4139; b) N. C. Maiti, S. Mazumdar, N. Periasamy, *J. Phys. Chem. B* **1998**, *102*, 1528–1538; c) D. L. Akins, H.-R. Zhu, C. Guo, *J. Phys. Chem.* **1994**, *98*, 3612–3618; d) L. Zhao, R. Ma, J. Li, Y. Li, Y. An, L. Shi, *Biomacromolecules* **2008**, *9*, 2601–2608.
- [16] a) E. Gazit, *FASEB J.* **2002**, *16*, 77–83; b) C. A. Hunter, J. K. M. Sanders, *J. Am. Chem. Soc.* **1990**, *112*, 5525–5534.
- [17] C. A. E. Hauser, S. Zhang, *Nature* **2010**, *468*, 516–517.
- [18] M. A. Filatov, F. Laquai, D. Fortin, R. Guilard, P. Harvey, *Chem. Commun.* **2010**, *46*, 9176–9178.
- [19] V. Sol, J. C. Blais, G. Bolbach, V. Carre, R. Granet, M. Guilloton, M. Spiro, P. Krausz, *Tetrahedron Lett.* **1997**, *38*, 6391–6394.

Received: February 1, 2011
Published online: May 26, 2011

CHAPTER 10 GENERAL CONCLUSIONS AND OUTLOOK

The present study demonstrated the possibility of construction of a minimal self-assembling system with various and tunable functionalities. The first part of the design consisted in choosing the minimal self-assembly peptide sequence for obtaining amyloid type fibrils. The second part consisted in the choice of the environment where the assembly of the peptide will be initiated (single or binary solvent system). Each of the two gives fibrils or fibril films respectively. Both cases are based on “bottom up” approach since they start from single peptide building blocks. The third part consisted in the proper choice of the functional residue that will be incorporated in the sequence.

Within the framework of this thesis the following steps were taken:

1) The original, serine-containing octapeptide was found to template the formation of silica nanoparticles starting from the TEOS precursor. The mechanism of silica templating was deciphered and was attributed to the serine (Ser (S)) residue that is rendered nucleophilic by the N-terminal amino group of the peptide. The *in vitro* silification reaction and the templating of silica on amyloid fibrils can be further used for the fabrication of silica nanotubes of variable sizes, depending of the internal biological template and the reaction time. The silica nanotubes can be further used not only for drug delivery and controlled release but also for hydrogen storage and catalysis. Moreover, the role of the nucleophilic serine (Ser (S)) can be exploited further for the templating of non-biogenic oxides and the participation in reactions such as ring opening polymerization (Curnow et al., 2006).

2) When thiols are inserted in the peptide sequence through Cysteine residues, the peptide is capable to attach to metallic particles and quantum dot particles. It was found that this peptide forms well-ordered fibril films at the water- chloroform interface, inducing 2D ordering of the Qdots and a red shift in their emission peaks relative to their solution state. This method might be used as general strategy for the fabrication of peptide films templated with Qdots. Examining the quantum dot deposition and the difference in their properties upon spacing between them, it is possible to manipulate those distances. One approach is to use various types of sizes of quantum dots or to vary the length/composition of the template peptide to provide variable spacing between the quantum dots. Finally apart from quantum dot nanoparticles, there is a wide variety of nanoparticles (Nie et al., 2010), which can be

used according to the desired application in optoelectronic, data storage, sensing, and biological labeling. For example, bifunctional peptides could be designed containing both cysteine residues and cell attachment motifs for specific targeting of Q-dots into cells. One such motif is the Arginine-Glycine-Aspartic acid (RGD) that has been applied so far in many cell attachment applications (Chow et al., 2008).

3) The photo-crosslinking of self-assembling peptides opens future possibilities for improving stability in this class of materials. The previously mentioned fibril films can be irradiated before the attachment of particles in order to enhance their stability. The LIF technique is a non-destructive and instant method of photo crosslinking, without any interference in the chemical environment of the cross-linking peptide.

4) Finally the synthesis of a peptide-porphyrin conjugate and its self-assembly into uniform and monodisperse spheres opens an avenue for the construction of hybrid materials for solar cell applications. The same synthesis protocol can be followed with other self-assembling systems as well in order to fabricate scaffolds with photoelectronic properties.

In summary, the bottom up fabrication of peptide-based biomaterials is a powerful technique that allows us to drive self-assembly from the nanoscale to millimetre scale in one, two or three dimensions. In the future, other varieties of peptides could be investigated and their functionalization with various types of nanoparticles can lead to further applications. A very important concern that has to be taken into account is the limitations of peptide-based materials such as thermal instability (compared to materials such as carbon nanotubes) and the (still) high costs of production. However their numerous advantages, namely their environmental-friendly synthesis, and their biocompatible and biodegradable character, make the self-assembling peptide field a promising one for the years to come.

CHAPTER 11 REFERENCES

Acar, H., Garifullin, R., Guler, M.O., 2011. Self-Assembled Template-Directed Synthesis of One-Dimensional Silica and Titania Nanostructures. *Langmuir* 27, 1079.

Adamson, D.H., Dabbs, D.M., Pacheco, C.R., Giotto, M.V., Morse, D.E., Aksay, I.A., 2007. Non-peptide polymeric silicatein alpha mimic for neutral pH catalysis in the formation of silica. *Macromolecules* 40, 5710.

Adler-Abramovich, L., Gazit, E., 2008. Controlled patterning of peptide nanotubes and nanospheres using inkjet printing technology. *Journal of Peptide Science* 14, 217.

Aggeli, A., Bell, M., Boden, N., Keen, J.N., Knowles, P.F., McLeish, T.C., Pitkeathly, M., Radford, S.E., 1997a. Responsive gels formed by the spontaneous self-assembly of peptides into polymeric beta-sheet tapes. *Nature* 386, 259.

Aggeli, A., Bell, M., Boden, N., Keen, J.N., Knowles, P.F., McLeish, T.C.B., Pitkeathly, M., Radford, S.E., 1997b. Responsive gels formed by the spontaneous self-assembly of peptides into polymeric beta-sheet tapes. *Nature* 386, 259.

Altunbas, A., Sharma, N., Lamm, M.S., Yan, C.Q., Nagarkar, R.P., Schneider, J.P., Pochan, D.J., 2010. Peptide-Silica Hybrid Networks: Biomimetic Control of Network Mechanical Behavior. *Acs Nano* 4, 181.

Babayyan, Y., Barton, J.E., Greyson, E.C., Odom, T.W., 2004. Templated and hierarchical assembly of CdSe/ZnS quantum dots. *Advanced Materials* 16, 1341.

Bean, J.W., Kopple, K.D., Peishoff, C.E., 1992. Conformational - Analysis of cyclic hexapeptides containing the D-Pro-L-Pro sequence to fix beta-turn positions. *Journal of The American Chemical Society* 114, 5328.

Beaulac, R., Archer, P.I., Ochsenein, S.T., Gamelin, D.R., 2008. Mn(2+)-Doped CdSe Quantum Dots: New Inorganic Materials for Spin-Electronics and Spin-Photonics. *Advanced Functional Materials* 18, 3873.

Bessho, T., Zakeeruddin, S.M., Yeh, C.Y., Diau, E.W.G., Gratzel, M., 2010. Highly Efficient Mesoscopic Dye-Sensitized Solar Cells Based on Donor-Acceptor-Substituted Porphyrins. *Angewandte Chemie-International Edition* 49, 6646.

Bounos, G., Selimis, A., Georgiou, S., Rebollar, E., Castillejo, M., Bityurin, N., 2006. Dependence of ultraviolet nanosecond laser polymer ablation on polymer molecular weight: Poly(methyl methacrylate) at 248 nm. *Journal of Applied Physics* 100.

Branco, M.C., Pochan, D.J., Wagner, N.J., Schneider, J.P., 2009. Macromolecular diffusion and release from self-assembled beta-hairpin peptide hydrogels. *Biomaterials* 30, 1339.

Brannigan, J.A., Dodson, G., Duggleby, H.J., Moody, P.C.E., Smith, J.L., Tomchick, D.R., Murzin, A.G., 1995. A protein catalytic framework with an N-terminal nucleophile is capable of self-activation. *Nature* 378, 416.

- Brinker, C.J., 1988. Hydrolysis and condensation of silicates - effects on structure. *Journal of Non-Crystalline Solids* 100, 31.
- Brutchev, R.L., Morse, D.E., 2008. Silicatein and the Translation of its Molecular Mechanism of Biosilicification into Low Temperature Nanomaterial Synthesis. *Chemical Reviews* 108, 4915.
- Bui, H., Onodera, C., Kidwell, C., Tan, Y., Graugnard, E., Kuang, W., Lee, J., Knowlton, W.B., Yurke, B., Hughes, W.L., 2010. Programmable Periodicity of Quantum Dot Arrays with DNA Origami Nanotubes. *Nano Letters* 10, 3367.
- Caple, M.B., Chow, H., Strouse, C.E., 1978. Photosynthetic pigments of green sulfur bacteria- esterifying alcohols of bacteriochlorophylls-c from chlorobium-limicola. *Journal of Biological Chemistry* 253, 6730.
- Carny, O., Shalev, D.E., Gazit, E., 2006. Fabrication of coaxial metal nanocables using a self-assembled peptide nanotube scaffold. *Nano Letters* 6, 1594.
- Cha, J.N., Shimizu, K., Zhou, Y., Christiansen, S.C., Chmelka, B.F., Stucky, G.D., Morse, D.E., 1999. Silicatein filaments and subunits from a marine sponge direct the polymerization of silica and silicones in vitro. *Proceedings of the National Academy of Sciences of the United States of America* 96, 361.
- Chan, W.C.W., Maxwell, D.J., Gao, X.H., Bailey, R.E., Han, M.Y., Nie, S.M., 2002. Luminescent quantum dots for multiplexed biological detection and imaging. *Current Opinion in Biotechnology* 13, 40.
- Charalambidis, G., Kasotakis, E., Lazarides, T., Mitraki, A., Coutsolelos, A.G., 2011. Self-Assembly Into Spheres of a Hybrid Diphenylalanine-Porphyrin: Increased Fluorescence Lifetime and Conserved Electronic Properties. *Chemistry-a European Journal* 17, 7213.
- Chen, C.L., Rosi, N.L., 2010. Peptide-Based Methods for the Preparation of Nanostructured Inorganic Materials. *Angewandte Chemie-International Edition* 49, 1924.
- Chiang, C.Y., Mello, C.M., Gu, J.J., Silva, E., Van Vliet, K.J., Belcher, A.M., 2007. Weaving genetically engineered functionality into mechanically robust virus fibers. *Advanced Materials* 19, 826.
- Chilov, G.G., Sidorova, A.V., Svedas, V.K., 2007. Quantum chemical studies of the catalytic mechanism of N-terminal nucleophile hydrolase. *Biochemistry-Moscow* 72, 495.
- Chow, D., Nunalee, M.L., Lim, D.W., Simnick, A.J., Chilkoti, A., 2008. Peptide-based biopolymers in biomedicine and biotechnology. *Materials Science & Engineering R-Reports* 62, 125.
- Coradin, T., Lopez, P.J., 2003. Biogenic silica patterning: Simple chemistry or subtle biology? *ChemBiochem* 4, 251.
- Curnow, P., Kisailus, D., Morse, D.E., 2006. Biocatalytic synthesis of poly(L-lactide) by native and recombinant forms of the silicatein enzymes. *Angewandte Chemie-International Edition* 45, 613.

- Dabbousi, B.O., RodriguezViejo, J., Mikulec, F.V., Heine, J.R., Mattoussi, H., Ober, R., Jensen, K.F., Bawendi, M.G., 1997. (CdSe)ZnS core-shell quantum dots: Synthesis and characterization of a size series of highly luminescent nanocrystallites. *Journal of Physical Chemistry B* 101, 9463.
- Dickerson, M.B., Naik, R.R., Stone, M.O., Cai, Y., Sandhage, K.H., 2004. Identification of peptides that promote the rapid precipitation of germania nanoparticle networks via use of a peptide display library. *Chemical Communications*, 1776.
- Dickerson, M.B., Sandhage, K.H., Naik, R.R., 2008. Protein- and Peptide-Directed Syntheses of Inorganic Materials. *Chemical Reviews* 108, 4935.
- DiMarco, T., Giulivi, C., 2007. Current analytical methods for the detection of dityrosine, a biomarker of oxidative stress, in biological samples. *Mass Spectrometry Reviews* 26, 108.
- Dollefeld, H., Weller, H., Eychmuller, A., 2002. Semiconductor nanocrystal assemblies: Experimental pitfalls and a simple model of particle-particle interaction. *Journal of Physical Chemistry B* 106, 5604.
- Dong, A.G., Chen, J., Vora, P.M., Kikkawa, J.M., Murray, C.B., 2010. Binary nanocrystal superlattice membranes self-assembled at the liquid-air interface. *Nature* 466, 474.
- Drexler, K.E., 1981. Molecular engineering - an approach to the development of general capabilities for molecular manipulation. *Proceedings of the National Academy of Sciences of the United States of America-Physical Sciences* 78, 5275.
- Drexler, K.E., 1986. *Engines of Creation: The coming Era of Nanotechnology*. anchor Books.
- Dunetz, J.R., Sandstrom, C., Young, E.R., Baker, P., Van Name, S.A., Cathopolous, T., Fairman, R., de Paula, J.C., Akerfeldt, K.S., 2005. Self-assembling porphyrin-modified peptides. *Organic Letters* 7, 2559.
- Elvin, C.M., Carr, A.G., Huson, M.G., Maxwell, J.M., Pearson, R.D., Vuocolo, T., Liyou, N.E., Wong, D.C.C., Merritt, D.J., Dixon, N.E., 2005. Synthesis and properties of crosslinked recombinant pro-resilin. *Nature* 437, 999.
- Erhardt, M., Namba, K., Hughes, K.T., 2010. *Bacterial Nanomachines: The Flagellum and Type III Injectisome*. Cold Spring Harbor Perspectives in Biology 2.
- Espinosa, H.D., Rim, J.E., Barthelat, F., Buehler, M.J., 2009. Merger of structure and material in nacre and bone - Perspectives on de novo biomimetic materials. *Progress in Materials Science* 54, 1059.
- Fairhead, M., Johnson, K.A., Kowatz, T., McMahon, S.A., Carter, L.G., Oke, M., Liu, H., Naismith, J.H., van der Walle, C.F., 2008. Crystal structure and silica condensing activities of silicatein alpha-cathepsin L chimeras. *Chemical Communications*, 1765.
- Fancy, D.A., Kodadek, T., 1999. Chemistry for the analysis of protein-protein interactions: Rapid and efficient cross-linking triggered by long wavelength light. *Proceedings of the National Academy of Sciences of the United States of America* 96, 6020.

- Filatov, M.A., Laquai, F., Fortin, D., Guillard, R., Harvey, P.D., 2010. Strong donor-acceptor couplings in a special pair-antenna model. *Chemical Communications* 46, 9176.
- Foo, C.W.P., Huang, J., Kaplan, D.L., 2004. Lessons from seashells: silica mineralization via protein templating. *Trends in Biotechnology* 22, 577.
- Galeotti, F., Mroz, W., Bolognesi, A., 2011. CdTe nanocrystal assemblies guided by breath figure templates. *Soft Matter* 7, 3832.
- Gaspard, S., Oujja, M., de Nalda, R., Abrusci, C., Catalina, F., Banares, L., Lazare, S., Castillejo, M., 2007. Nanofoaming in the surface of biopolymers by femtosecond pulsed laser irradiation. *Applied Surface Science* 254, 1179.
- Gattas-Asfura, K.M., Constantine, C.A., Lynn, M.J., Thimann, D.A., Ji, X.J., Leblanc, R.M., 2005. Characterization and 2D self-assembly of CdSe quantum dots at the air-water interface. *Journal of The American Chemical Society* 127, 14640.
- Gazit, E., 2002. A possible role for pi-stacking in the self-assembly of amyloid fibrils. *Federation of American Societies for Experimental Biology Journal* 16, 77.
- Gazit, E., 2005. Mechanisms of amyloid fibril self-assembly and inhibition. *Federation of the Societies of Biochemistry Journal* 272, 5971.
- Gazit, E., 2007. *Plenty of Room for Biology at the Bottom: An Introduction to Bionanotechnology*. Imperial College Press.
- Giulivi, C., Traaseth, N.J., Davies, K.J.A., 2003. Tyrosine oxidation products: analysis and biological relevance. *Amino Acids* 25, 227.
- Gratzel, M., 2003. Dye-sensitized solar cells. *Journal of Photochemistry and Photobiology C-Photochemistry Reviews* 4, 145.
- Grelet, E., Moreno, A., Backov, R., 2011. Hybrid Macroscopic Fibers from the Synergistic Assembly Between Silica and Filamentous Viruses. *Langmuir* 27, 4334.
- Hauser, C.A.E., Zhang, S.G., 2010. Nanotechnology Peptides as biological semiconductors. *Nature* 468, 516.
- Henry, E., Dif, A., Schmutz, M., Legoff, L., Amblard, F., Marchi-Artzner, V., Artzner, F., 2011. Crystallization of Fluorescent Quantum Dots within a Three-Dimensional Bio-Organic Template of Actin Filaments and Lipid Membranes. *Nano Letters* 11, 5443.
- Imahori, H., Umeyama, T., Ito, S., 2009. Large pi-Aromatic Molecules as Potential Sensitizers for Highly Efficient Dye-Sensitized Solar Cells. *Accounts of Chemical Research* 42, 1809.
- Ithurria, S., Bousquet, G., Dubertret, B., 2011. Continuous Transition from 3D to 1D Confinement Observed during the Formation of CdSe Nanoplatelets. *Journal of The American Chemical Society* 133, 3070.

- Ji, X.J., Wang, C.S., Xu, J.M., Zheng, J.Y., Gattas-Asfura, K.M., Leblanc, R.M., 2005. Surface chemistry studies of (CdSe)ZnS quantum dots at the air-water interface. *Langmuir* 21, 5377.
- Juzenas, P., Chen, W., Sun, Y.P., Coelho, M.A.N., Generalov, R., Generalova, N., Christensen, I.L., 2008. Quantum dots and nanoparticles for photodynamic and radiation therapies of cancer. *Advanced Drug Delivery Reviews* 60, 1600.
- Kagan, C.R., Murray, C.B., Bawendi, M.G., 1996. Long-range resonance transfer of electronic excitations in close-packed CdSe quantum-dot solids. *Physical Review B* 54, 8633.
- Kasotakis, E., Mossou, E., Adler-Abramovich, L., Mitchell, E.P., Forsyth, V.T., Gazit, E., Mitraki, A., 2009. Design of Metal-Binding Sites Onto Self-Assembled Peptide Fibrils. *Biopolymers* 92, 164.
- Kim, M., Hong, J., Lee, J., Hong, C.K., Shim, S.E., 2008. Fabrication of silica nanotubes using silica coated multi-walled carbon nanotubes as the template. *Journal of Colloid and Interface Science* 322, 321.
- Kisailus, D., Choi, J.H., Weaver, J.C., Yang, W.J., Morse, D.E., 2005. Enzymatic synthesis and nanostructural control of gallium oxide at low temperature. *Advanced Materials* 17, 314.
- Klimov, V.I., 2003. Nanocrystal Quantum Dots From fundamental photophysics to multicolor lasing. *Los Alamos Science* 28 214.
- Klostranec, J.M., Chan, W.C.W., 2006. Quantum dots in biological and biomedical research: Recent progress and present challenges. *Advanced Materials* 18, 1953.
- Knecht, M.R., Wright, D.W., 2003. Functional analysis of the biomimetic silica precipitating activity of the R5 peptide from *Cylindrotheca fusiformis*. *Chemical Communications*, 3038.
- Kokona, B., Kim, A.M., Roden, R.C., Daniels, J.P., Pepe-Mooney, B.J., Kovaric, B.C., de Paula, J.C., Johnson, K.A., Fairman, R., 2009. Self Assembly of Coiled-Coil Peptide-Porphyrin Complexes. *Biomacromolecules* 10, 1454.
- Konovalova, N.V., Evstigneeva, R.P., Luzgina, V.N., 2001. Synthetic molecular systems based on porphyrins as models for study of energy transfer in photosynthesis. *Uspekhi Khimii* 70, 1059.
- Kroger, N., Deutzmann, R., Bergsdorf, C., Sumper, M., 2000. Species-specific polyamines from diatoms control silica morphology. *Proceedings of the National Academy of Sciences of the United States of America* 97, 14133.
- Kroger, N., Deutzmann, R., Sumper, M., 1999. Polycationic peptides from diatom biosilica that direct silica nanosphere formation. *Science* 286, 1129.
- Kroger, N., Lorenz, S., Brunner, E., Sumper, M., 2002. Self-assembly of highly phosphorylated silaffins and their function in biosilica morphogenesis. *Science* 298, 584.
- Kumara, M.T., Tripp, B.C., Muralidharan, S., 2007a. Exciton energy transfer in self-assembled quantum dots on bioengineered bacterial flagella nanotubes. *Journal of Physical Chemistry C* 111, 5276.

- Kumara, M.T., Tripp, B.C., Muralidharan, S., 2007b. Self-assembly of metal nanoparticles and nanotubes on bioengineered flagella scaffolds. *Chemistry of Materials* 19, 2056.
- Lamm, M.S., Sharma, N., Rajagopal, K., Beyer, F.L., Schneider, J.P., Pochan, D.J., 2008. Laterally spaced linear nanoparticle arrays templated by laminated beta-sheet fibrils. *Advanced Materials* 20, 447.
- Lazare, S., Tokarev, V., Sionkowska, A., Wisniewski, M., 2005. Surface foaming of collagen, chitosan and other biopolymer films by KrF excimer laser ablation in the photomechanical regime. *Applied Physics a-Materials Science & Processing* 81, 465.
- Lee, S.Y., Royston, E., Culver, J.N., Harris, M.T., 2005. Improved metal cluster deposition on a genetically engineered tobacco mosaic virus template. *Nanotechnology* 16, S435.
- Lepere, M., Chevillard, C., Hernandez, J.F., Mitraki, A., Guenoun, P., 2007. Multiscale surface self-assembly of an amyloid-like peptide. *Langmuir* 23, 8150.
- Luckey, M., Hernandez, J., Arlaud, G., Forsyth, V.T., Ruigrok, R.W., Mitraki, A., 2000. A peptide from the adenovirus fiber shaft forms amyloid-type fibrils. *Federation of the Societies of Biochemistry Letters* 468, 23.
- Mahler, A., Reches, M., Rechter, M., Cohen, S., Gazit, E., 2006. Rigid, self-assembled hydrogel composed of a modified aromatic dipeptide. *Advanced Materials* 18, 1365.
- Malencik, D.A., Anderson, S.R., 1996. Dityrosine formation in calmodulin: Cross-linking and polymerization catalyzed by Arthromyces peroxidase. *Biochemistry* 35, 4375.
- Medintz, I.L., Uyeda, H.T., Goldman, E.R., Mattoussi, H., 2005. Quantum dot bioconjugates for imaging, labelling and sensing. *Nature Materials* 4, 435.
- Meegan, J.E., Aggeli, A., Boden, N., Brydson, R., Brown, A.P., Carrick, L., Brough, A.R., Hussain, A., Ansell, R.J., 2004. Designed self-assembled beta-sheet peptide fibrils as templates for silica nanotubes. *Advanced Functional Materials* 14, 31.
- Meyers, M.A., Lin, A.Y.M., Seki, Y., Chen, P.Y., Kad, B.K., Bodde, S., 2006. Structural biological composites: An overview. *Journal of the Minerals, Metals and Materials Society* 58, 35.
- Minones, J., Conde, O., Gomezulla, A., 1984. Interactions in films spread at the air water interface - a study of protein monolayers spread on silicic-acid substrates. *Colloids and Surfaces* 10, 85.
- Murray, C.B., Kagan, C.R., Bawendi, M.G., 2000. Synthesis and characterization of monodisperse nanocrystals and close-packed nanocrystal assemblies. *Annual Review of Materials Science* 30, 545.
- Neff, D., Frazier, S.F., Quimby, L., Wang, R.T., Zill, S., 2000. Identification of resilin in the leg of cockroach, *Periplaneta americana*: confirmation by a simple method using pH dependence of UV fluorescence. *Arthropod Structure & Development* 29, 75.
- Nie, Z.H., Petukhova, A., Kumacheva, E., 2010. Properties and emerging applications of self-assembled structures made from inorganic nanoparticles. *Nature Nanotechnology* 5, 15.

- Oinonen, C., Rouvinen, J., 2000. Structural comparison of Ntn-hydrolases. *Protein Science* 9, 2329.
- Pace, C.N., Grimsley, G.R., Scholtz, J.M., 2009. Protein Ionizable Groups: pK Values and Their Contribution to Protein Stability and Solubility. *Journal of Biological Chemistry* 284, 13285.
- Papanikolopoulou, K., Schoehn, G., Forge, V., Forsyth, V.T., Riekkel, C., Hernandez, J.F., Ruigrok, R.W.H., Mitraki, A., 2005. Amyloid fibril formation from sequences of a natural beta-structured fibrous protein, the adenovirus fiber. *Journal of Biological Chemistry* 280, 2481.
- Piston, D.W., Rizzo, M.A., 2008. FRET by fluorescence polarization microscopy, in: Sullivan, K.F. (Ed.), *Fluorescent Proteins, Second Edition*, 415
- Pouget, E., Dujardin, E., Cavalier, A., Moreac, A., Valery, C., Marchi-Artzner, V., Weiss, T., Renault, A., Paternostre, M., Artzner, F., 2007. Hierarchical architectures by synergy between dynamical template self-assembly and biomineralization. *Nature Materials* 6, 434.
- Ratanatawanate, C., Tao, Y., Balkus, K.J., 2009. Photocatalytic Activity of PbS Quantum Dot/TiO₂ Nanotube Composites. *Journal of Physical Chemistry C* 113, 10755.
- Reches, M., Gazit, E., 2003. Casting metal nanowires within discrete self-assembled peptide nanotubes. *Science* 300, 625.
- Reches, M., Gazit, E., 2006. Designed aromatic homo-dipeptides: formation of ordered nanostructures and potential nanotechnological applications. *Physical Biology* 3, S10.
- Reis, A.V., Fajardo, A.R., Schuquel, I.T.A., Guilherme, M.R., Vidotti, G.J., Rubira, A.F., Muniz, E.C., 2009. Reaction of Glycidyl Methacrylate at the Hydroxyl and Carboxylic Groups of Poly(vinyl alcohol) and Poly(acrylic acid): Is This Reaction Mechanism Still Unclear? *Journal of Organic Chemistry* 74, 3750.
- Reiss, P., Protiere, M., Li, L., 2009. Core/Shell Semiconductor Nanocrystals. *Small* 5, 154.
- Roth, K.M., Zhou, Y., Yang, W.J., Morse, D.E., 2005. Bifunctional small molecules are biomimetic catalysts for silica synthesis at neutral pH. *Journal of The American Chemical Society* 127, 325.
- Royston, E., Lee, S.Y., Culver, J.N., Harris, M.T., 2006. Characterization of silica-coated tobacco mosaic virus. *Journal of Colloid and Interface Science* 298, 706.
- Schlick, T.L., Ding, Z.B., Kovacs, E.W., Francis, M.B., 2005. Dual-surface modification of the tobacco mosaic virus. *Journal of The American Chemical Society* 127, 3718.
- Schneider, J.P., Pochan, D.J., Ozbas, B., Rajagopal, K., Pakstis, L., Kretsinger, J., 2002. Responsive hydrogels from the intramolecular folding and self-assembly of a designed peptide. *Journal of The American Chemical Society* 124, 15030.
- Sedman, V.L., Kasotakis, E., Chen, X.Y., Allen, S., Roberts, C.J., Mitraki, A., Tandler, S.J.B., 2011. Surface-Templated Fibril Growth of Peptide Fragments from the Shaft Domain of the Adenovirus Fibre Protein. *Protein and Peptide Letters* 18, 268.

- Sengul, H., Theis, T.L., 2011. An environmental impact assessment of quantum dot photovoltaics (QDPV) from raw material acquisition through use. *Journal of Cleaner Production* 19, 21.
- Serpell, L.C., Smith, J.M., 2000. Direct visualisation of the beta-sheet structure of synthetic Alzheimer's amyloid. *Journal of Molecular Biology* 299, 225.
- Sewell, S.L., Wright, D.W., 2006. Biomimetic synthesis of titanium dioxide utilizing the R5 peptide derived from *Cylindrotheca fusiformis*. *Chemistry of Materials* 18, 3108.
- Shenton, W., Douglas, T., Young, M., Stubbs, G., Mann, S., 1999. Inorganic-organic nanotube composites from template mineralization of tobacco mosaic virus. *Advanced Materials* 11, 253.
- Shevchenko, E.V., Talapin, D.V., Murray, C.B., O'Brien, S., 2006. Structural characterization of self-assembled multifunctional binary nanoparticle superlattices. *Journal of The American Chemical Society* 128, 3620.
- Shimizu, K., Cha, J., Stucky, G.D., Morse, D.E., 1998. Silicatein alpha: Cathepsin L-like protein in sponge biosilica. *Proceedings of the National Academy of Sciences of the United States of America* 95, 6234.
- Smith, K.H., Tejada-Montes, E., Poch, M., Mata, A., 2011. Integrating top-down and self-assembly in the fabrication of peptide and protein-based biomedical materials. *Chemical Society Reviews* 40, 4563.
- Sol, V., Blais, J.C., Bolbach, G., Carre, V., Granet, R., Guilloton, M., Spiro, M., Krausz, P., 1997. Toward glycosylated peptidic porphyrins: a new strategy for PDT? *Tetrahedron Letters* 38, 6391.
- Sone, E.D., Stupp, S.I., 2004. Semiconductor-encapsulated peptide-amphiphile nanofibers. *Journal of The American Chemical Society* 126, 12756.
- Sumerel, J.L., Yang, W.J., Kisailus, D., Weaver, J.C., Choi, J.H., Morse, D.E., 2003. Biocatalytically templated synthesis of titanium dioxide. *Chemistry of Materials* 15, 4804.
- Tamamis, P., Kasotakis, E., Mitraki, A., Archontis, G., 2009. Amyloid-Like Self-Assembly of Peptide Sequences from the Adenovirus Fiber Shaft: Insights from Molecular Dynamics Simulations. *Journal of Physical Chemistry B* 113, 15639.
- Tanford, C., 1962. The Interpretation Of Hydrogen Ion Titration Curves Of Proteins. *Advanced Protein Chemistry* 17, 69.
- Tang, Z.Y., Zhang, Z.L., Wang, Y., Glotzer, S.C., Kotov, N.A., 2006. Self-assembly of CdTe nanocrystals into free-floating sheets. *Science* 314, 274.
- Thurlkill, R.L., Grimsley, G.R., Scholtz, J.M., Pace, C.N., 2006. pK values of the ionizable groups of proteins. *Protein Science* 15, 1214.
- Toksoz, S., Guler, M.O., 2009. Self-assembled peptidic nanostructures. *Nano Today* 4, 458.

Toroz, D., Corni, S., 2011. Peptide Synthesis of Gold Nanoparticles: The Early Steps of Gold Reduction Investigated by Density Functional Theory. *Nano Letters* 11, 1313.

Valery, C., Paternostre, M., Robert, B., Gulik-Krzywicki, T., Narayanan, T., Dedieu, J.C., Keller, G., Torres, M.L., Cherif-Cheikh, R., Calvo, P., Artzner, F., 2003. Biomimetic organization: Octapeptide self-assembly into nanotubes of viral capsid-like dimension. *Proceedings of the National Academy of Sciences of the United States of America* 100, 10258.

van Raaij, M.J., Mittraki, A., Lavigne, G., Cusack, S., 1999. A triple beta-spiral in the adenovirus fibre shaft reveals a new structural motif for a fibrous protein. *Nature* 401, 935.

Wang, S.J., Ge, X., Xue, J.Y., Fan, H.M., Mu, L.J., Li, Y.P., Xu, H., Lu, J.R., 2011. Mechanistic Processes Underlying Biomimetic Synthesis of Silica Nanotubes from Self-Assembled Ultrashort Peptide Templates. *Chemistry of Materials* 23, 2466.

Weaver, J.C., Morse, D.E., 2003. Molecular biology of demosponge axial filaments and their roles in biosilicification. *Microscopy Research and Technique* 62, 356.

Wisniewski, M., Sionkowska, A., Kaczmarek, H., Lazare, S., Tokarev, V., Belin, C., 2007. Spectroscopic study of a KrF excimer laser treated surface of the thin collagen films. *Journal of Photochemistry and Photobiology a-Chemistry* 188, 192.

Yang, S.Y., Wang, C.F., Chen, S., 2011a. Interface-Directed Assembly of One-Dimensional Ordered Architecture from Quantum Dots Guest and Polymer Host. *Journal of The American Chemical Society* 133, 8412.

Yang, X.F., Tang, H., Cao, K.S., Song, H.J., Sheng, W.C., Wu, Q.O., 2011b. Templated-assisted one-dimensional silica nanotubes: synthesis and applications. *Journal of Materials Chemistry* 21, 6122.

Yang, Y.L., Khoe, U., Wang, X.M., Horii, A., Yokoi, H., Zhang, S.G., 2009. Designer self-assembling peptide nanomaterials. *Nano Today* 4, 193.

Yoburn, J.C., Tian, W.Q., Brower, J.O., Nowick, J.S., Glabe, C.G., Van Vranken, D.L., 2003. Dityrosine cross-linked A beta peptides: Fibrillar beta-structure in A beta(1-40) is conducive to formation of dityrosine cross-links but a dityrosine cross-link in alpha beta(8-14) does not induce beta-structure. *Chemical Research in Toxicology* 16, 531.

Yu, W.W., Peng, X.G., 2002. Formation of high-quality CdS and other II-VI semiconductor nanocrystals in noncoordinating solvents: Tunable reactivity of monomers. *Angewandte Chemie-International Edition* 41, 2368.

Yu, W.W., Qu, L.H., Guo, W.Z., Peng, X.G., 2003. Experimental determination of the extinction coefficient of CdTe, CdSe, and CdS nanocrystals. *Chemistry of Materials* 15, 2854.

Yuwono, V.M., Hartgerink, J.D., 2007. Peptide amphiphile nanofibers template and catalyze silica nanotube formation. *Langmuir* 23, 5033.

Zhang, S.G., 2002. Emerging biological materials through molecular self-assembly. *Biotechnology Advances* 20, 321.

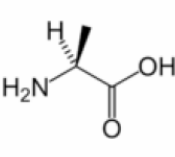
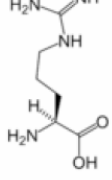
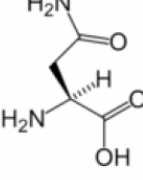
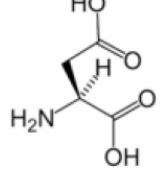
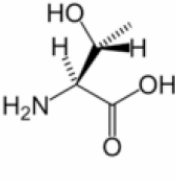
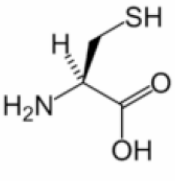
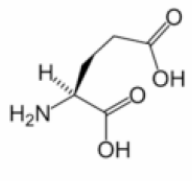
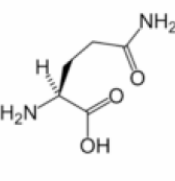
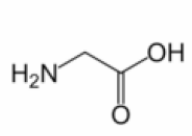
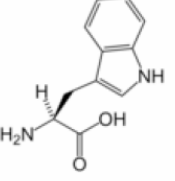
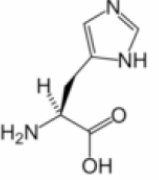
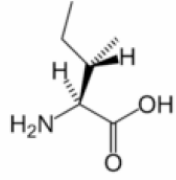
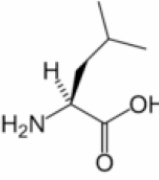
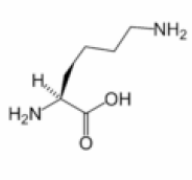
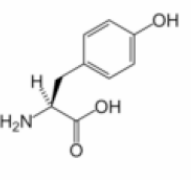
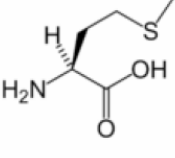
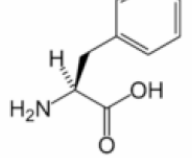
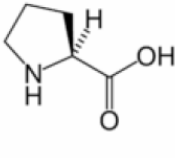
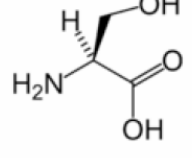
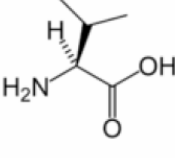
Zhang, S.G., 2003. Fabrication of novel biomaterials through molecular self-assembly. *Nature Biotechnology* 21, 1171.

Zhang, S.G., Holmes, T., Lockshin, C., Rich, A., 1993. Spontaneous assembly of a self-complementary oligopeptide to form a stable macroscopic membrane. *Proceedings of the National Academy of Sciences of the United States of America* 90, 3334.

Zhao, X.B., Pan, F., Xu, H., Yaseen, M., Shan, H.H., Hauser, C.A.E., Zhang, S.G., Lu, J.R., 2010. Molecular self-assembly and applications of designer peptide amphiphiles. *Chemical Society Reviews* 39, 3480.

Appendix

Structures and symbols of the 20 amino acids, which are directly encoded for protein synthesis by the standard genetic code.

 <p>L-Alanine (Ala / A)</p>	 <p>L-Arginine (Arg / R)</p>	 <p>L-Asparagine (Asn / N)</p>	 <p>L-Aspartic acid (Asp / D)</p>	 <p>L-Threonine (Thr / T)</p>
 <p>L-Cysteine (Cys / C)</p>	 <p>L-Glutamic acid (Glu / E)</p>	 <p>L-Glutamine (Gln / Q)</p>	 <p>Glycine (Gly / G)</p>	 <p>L-Tryptophan (Trp / W)</p>
 <p>L-Histidine (His / H)</p>	 <p>L-Isoleucine (Ile / I)</p>	 <p>L-Leucine (Leu / L)</p>	 <p>L-Lysine (Lys / K)</p>	 <p>L-Tyrosine (Tyr / Y)</p>
 <p>L-Methionine (Met / M)</p>	 <p>L-Phenylalanine (Phe / F)</p>	 <p>L-Proline (Pro / P)</p>	 <p>L-Serine (Ser / S)</p>	 <p>L-Valine (Val / V)</p>

CURRICULUM VITAE

EMMANOUIL KASOTAKIS

PERSONAL INFORMATION:

Date of birth: 25-05-1983
Place of Birth: Thessaloniki
Nationality: Greek
Marital Status: Single
Military Service: Unaccomplished
Home Address: Erganis 33, Heraklion Crete, Greece
Professional Address: Department of Materials Science and Technology
University of Crete
710 03 Heraklion, Crete, Greece
Telephone: +30 2810 39 40 96 fax: +30 2810 39 44 08

EDUCATION:

- 2001 Greek High School Diploma
- 2001-2005 B.Sc. Materials Science, Department of Materials Science and Technology, University of Crete
- 2006-2008 M.Sc Biomaterials, Department of Materials Science and Technology, University of Crete, *Title of Master's thesis subject:* "Design and study of composite biomaterials based on self-assembling peptides from natural fibrous proteins". Under the supervision of Assoc. Prof. Anna Mitraki
- 2008-2012 Ph.D, Department of Materials Science and Technology, University of Crete. *Title of PhD thesis:* "Design and study of peptide composite biomaterials". Under the supervision of Assoc. Prof. Anna Mitraki

LANGUAGES:

- Greek (mother)
- English (MICHIGAN PROFICIENCY level)

PUBLICATIONS IN PEER-REVIEWED JOURNALS:

1. Dinca V., Kasotakis E., Catherine J., Mourka A., Mitraki A., Popescu A., Dinescu M., Farsari M., and Fotakis C. (2007) “Development of peptide-based patterns by laser transfer” **Applied Surface Science**, 154: 1160-1163
2. Dinca V., Kasotakis E., Catherine J., Mourka A., Ranella A., Ovsianikov A, Chichkov B., Farsari M., Mitraki A., and Fotakis C. (2008) “Directed three-dimensional patterning of self-assembled peptide fibrils” **Nanoletters**, 8: 538-543
3. Dinca V., Kasotakis E., Mourka A., Ranella A., Farsari M., Mitraki A., and Fotakis C. (2008) “Fabrication of amyloid peptide micro-arrays using laser-induced forward transfer and avidin-biotin mediated assembly” **Phys. Stat. Sol. (c)** 5, 12: 3576–3579
4. Kasotakis E., Mossou E., Adler-Abramovich L., Mitchell EP, Forsyth VT, Gazit E, Mitraki A. (2009) “Design of Metal-Binding Sites Onto Self-Assembled Peptide Fibrils” **Biopolymers – Peptide science**, 92, 3: 164-172
5. Tamamis, P., Kasotakis, E., Mitraki, A., and Archontis, G. (2009) “Amyloid-like self-assembly of peptide sequences from the adenovirus fiber shaft: insights from molecular dynamics simulations” **J. Phys. Chem. B.** 113: 15639-15647
6. Sedman, VL., Kasotakis, E., Chen, X., Allen, S., Roberts, CJ., Mitraki A., and Tendler SJ. (2010) “Surface-Templated Fibril Growth of Peptide Fragments from the Shaft Domain of the Adenovirus Fibre” **Protein Pept. Lett.** , 268-274
7. Charalambidis G., Kasotakis E., Lazarides Th., Mitraki A., Coutsolelos A. G. (2011) “Self-assembly into spheres of a hybrid diphenylalanine-porphyrin: increased fluorescence lifetime, conserved electronic properties” **Chemistry - A European Journal**, 17, Issue 26, 7213–7219
8. Viguier B., Zor K., Kasotakis E., Mitraki A., Clausen C.H., Svendsen W.E., and Castillo-Leon J. (2011) “Development of an electrochemical metal-ion biosensor using self-assembled peptide nanofibrils” **ACS Appl. Mater. Interfaces**, 3 (5), 1594–1600
9. Clausen C.H., Dimaki M., Panagos S.P., Kasotakis E., Mitraki A., Svendsen W.E., Castillo-León J. (2011) “Electrostatic Force Microscopy of Self Assembled Peptide Structures” **Scanning** 32, 1–7

PUBLICATIONS IN PREPARATION:

10. Kasotakis E., Mitraki A. Silica biotemplating by self-assembling peptides via serine residues activated by the peptide amino group.
11. Kasotakis E., Kostopoulou A., Spuch-Calvar M., Andoulidaki M., Lappas A., Mitraki A. Fabrication of Two-Dimensional quantum dot arrays on peptide fibril films at the water-chloroform interface.
12. Kasotakis E., Sygletou M., Alonso J., Selimis A., Fotakis C., Mitraki A. Cross-linking of tyrosine containing self-assembled peptide fibrils using Laser-Induced Fluorescence (LIF).

BOOK CHAPTERS

- 1) Kasotakis E. and Mitraki A. (2011) “Design of metal-binding sites onto self-assembled peptides” In: *Protein Nanotechnology: Protocols, Instrumentation, Applications*; Second, completely revised edition, edited by Juliette Gerrard, in: Methods in Molecular Biology series, Humana Press, Totowa, NJ. (To appear in 2012)
- 2) Mitraki A. and Kasotakis E. (2011) “Natural and designed self – assembling peptides and their applications in bionanotechnology” In: *Self-Assembled peptide nanostructures: Advantages and challenges for their use in nanobiotechnology* edited by Jaime Castillo-Leon , Pan Stanford Publishing Pte Ltd

SCIENTIFIC AND LABORATORY EXPERIENCE:

- **06/2003 - 08/2003** Collaboration in thermoelectric materials experiments
- **06/2004 - 08/ 2004** Measurement Techniques of thermoelectric materials
Both projects took place in Magnetic and Superconducting materials Laboratory under the supervision of Prof. J. Giapintzakis.
- **09/2004 – 08/2005** Diploma thesis in Magnetic and Superconducting materials. Laboratory of Prof. J. Giapintzakis (**University of Crete**) [Grade: 9.5/10]. *Title of Diploma thesis subject:* “Synthesis and Characterization of Thermoelectric materials”.
- **07/2006 – 10/2006** Collaboration with Prof. Kelly Velonia in the University of Chemistry in Geneva. *Title of project:* “Synthesis of novel Biohybrid materials from self-assembling peptides and polymers”.
- **02/05/11-02/06/11** Collaboration with Dr. Patrick Guenoun (e-mail: Patrick.Guenoun@cea.fr) at CEA (COMISSARIAT A L’ ENERGIE ATOMIQUE) Laboratoire Interdisciplinaire sur l’Organisation Nanométrique et Supramoléculaire (LIONS). *Title of project:* Formation and metallization of peptide films in the air/water interface.

FELLOWSHIPS - HONOURS:

- Awarded three fellowships from IKY (the Greek Government Foundation of Fellowships) (1st of the class 2001-2004)
- Awarded a Master’s fellowship from “Manasaki” foundation from University of Crete (2005 –2006)
- Awarded a three months fellowship from FEBS (Federation of European Biochemical Societies) for collaboration with Prof. Kelly Velonia in the University of Chemistry in Geneva (07/2006 – 10/2006)

SCIENTIFIC SCHOOLS:

- 1) Methods in Micro-Nano Technology & Nanobiotechnology Summer School, National Center for Scientific Research “Demokritos” July 11-22, 2006 Athens, Greece
- 2) 10th Advanced Summer Course in Cell-Materials Interactions - Self-assembly: from nature to clinics, June 22-27, 2009, Porto, Portugal
- 3) EMMI Intensive Programme "Design and Validation of Imaging Probe", September 9-18, 2009, Turin, Italy
- 4) EMAT Winter Workshop on Transmission Electron Microscopy 2011, January 17-28, 2011, University of Antwerp, Belgium

PARTICIPATION IN RESEARCH PROJECTS:

1) **Title:** BeNatural: Bioengineered nanomaterials for research and applications

Financial entity: European Union

2007-2009

Responsible Researcher: Assoc Prof. Mitraki Anna

PATENT:

US Patent Applications Title: Method and system for manipulating organic nanostructures
Pub. No.: US 2011/0156109 A1, Pub. Date: Jun. 30, 2011

CONFERENCES:

1. Protein Assembly in Materials Biology and Medicine Meeting, Crete, Greece, 8-11 June 2007

-Poster presentation: “**Construction and surface functionalization of 3D structures using biomolecules**” Dinca V., Kasotakis E., Catherine J., Mourka A., Mitraki A., Farsari M., Fotakis C.

-Poster presentation: “**Construction of peptide micro-arrays by laser-induced forward transfer**” Dinca V., Kasotakis E., Catherine J., Mourka A., Mitraki A., Farsari M., Fotakis C.
2. Biomolecular Self-Assembly Workshop, School of Pharmacy, University of Nottingham, United Kingdom, 28 November 2007

-Poster presentation: “**Surface functionalization of 3D Structures using biomolecules**” Dinca V., Kasotakis E., Catherine J., Mourka A., Ranella A., Ovsianikov A, Chichkov B.N., Mitraki A., Farsari M., Fotakis C.

3. European Materials Research Society (EMRS), Strasbourg, France, 26-30 May 2008
 -Poster presentation: **“Directed 3D patterning of amyloid peptide fibers using multi-photon polymerization and avidin-biotin mediated assembly”** Dinca V., Kasotakis E., Catherine J., Mourka A., Ranella A, Ovsianikov A, Chichkov B.N., Mitraki A., Farsari M., Fotakis C.
4. Nano²Life Annual Meeting Crete, Greece, 25-27 June 2008
 -Poster presentation: **“Self-assembling peptides as scaffolds for nanowire fabrication and tissue engineering”** Kasotakis E., Kalloudi E., Mossou E., Adler-Abramovich L., V. Forsyth T., Gazit E., Mitraki A.
5. European Materials Research Society (EMRS), Strasbourg, France, 08-12 June 2009
 -Poster presentation: **“Self-assembling peptides as scaffolds for binding of metal nanoparticles”** Kasotakis E., Kalloudi E., Mossou E., Adler-Abramovich L., Mitchell E. P., V. Forsyth T., Gazit E., Mitraki A.
6. 10th Advanced Summer Course in Cell-Materials Interactions - Self-assembly: from nature to clinics, Porto, Portugal, June 22-27, 2009
 -Poster presentation: **“Self-assembling peptides as scaffolds for nanowire fabrication and tissue engineering”** Kasotakis E., Kalloudi E., Mossou E., Adler-Abramovich L., V. Forsyth T., Gazit E., Mitraki A.
7. 3rd International Conference from Nanoparticles and Nanomaterials to Nanodevices and Nanosystems (IC4N). Crete, Greece, June 26-29, 2011
 -Poster presentation: **‘Design and study of composite self-assembled peptides’** Kasotakis E., Spuch-Calvar M., Lappas A., Mitraki A.
8. 8th International Conference on Nanosciences & Nanotechnologies – NN11 'Ioannis Vellidis' Congress Centre, 12-15 July 2011 Thessaloniki, Greece
 -Oral presentation: **‘Design and study of composite self-assembled peptides’**
Kasotakis E., M. Sigletou, A. Selimis, C. Fotakis and A. Mitraki